A lift-off investigation of next-generation offshore wind turbine generator components for feedering in the U.S.

Creating understanding in the release stage of a tower segment

Offshore and Dredging Engineering - MSc Thesis

Marius Smorenberg

TU Delft Van Oord

Marine ingenuity

A lift-off investigation of next-generation offshore wind turbine generator components for feedering in the U.S.

Master thesis submitted to Delft University of Technology

in partial fulfilment of the requirements for the degree of

MASTER OF SCIENCE

In **Offshore and Dredging Engineering**

Faculty of Mechanical, Maritime and Materials Engineering

by

Marius Smorenberg

Student number: 4700899

To be defended in public on July 5th 2022

Graduation committee

Chairman	: Dr.-Ing. S. Schreier, Maritime and Transport Technology
First Supervisor	: Dr.-Ing. S. Schreier, Maritime and Transport Technology
Second Supervisor	: Dr. O. J. Colomes Gene, Hydraulic Engineering
Third Supervisor	: Dr. S. Fazi, Engineering Systems and Services
Fourth Supervisor	: Dr. ir. Antonini, Hydraulic Engineering
External Supervisor	: Ir. W. de Wildt, Van Oord, OW OFF EE Sub Sea

Certain values, texts and appendices in this public version have been altered or removed due to confidential information

Executive summary

Climate change is triggering an ever-growing demand for renewable energy. The U.S. is still far behind Europe when it comes to offshore wind energy. They have made ambitious plans to reach 30 GW in offshore wind energy by 2030 while currently 42 MW is installed. One of the main challenges in the U.S. is the installation method since a legislation called the Jones act prevents the usage of European installation vessels for shuttling (the conventional method). Building a Jones act. compliant installation vessel is a large investment which comes with risks and long lead times. Feedering is an alternative strategy, but barely any research on it is available. Here, a feeder vessel sails back and forth from the storage port to the (non-Jones act. compliant) installation vessel to supply Wind Turbine Generator (WTG) components. These components need to be lifted from the floating feeder in order to be installed. In the literature, this step is deemed to be the riskiest. However, barely any technical research is available with regards to the lift-off.

In the first thesis of this double degree program, a lift/installation sequence called the direct installation method is deemed to be highly interesting with respect to the logistics and costs. Here, the tower segments and nacelle are lifted and installed directly (one by one). Nothing is allowed to be attached to the bottom of the components so they can be installed immediately after lift-off. However, this research misses a technical study in order to understand if it is technically reachable to directly install these components.

In this research, barges are used as the allocated feeder vessel based on a market study of suitable available vessels. The tower segment of a 20 MW WTG is chosen to be lifted since this component is deemed to be the most challenging. A heave compensator in the crane is used to decouple the motions between the tower segment and the crane as much as possible. The scope is also set to beam and regular waves due to time constraints of the project. This research focuses on the pre-tension phase before the lift-off. This contains the steps where the crane of the installation vessel is already attached to the tower segment, pre-tension is building up and the release of the sea-fastening. Here, pre-tension is a percentage of the load that is taken in the crane before the lift-off. This research aims to increase the understanding of whether a tower segment can be released safely on the floating barge and what can be done in order to realise the idea of a direct installation method.

Frequency, as well as time-domain simulations, are used to investigate the problem. In regular waves, the results show that snap loads occur for pre-tensions up to 10%. From 30% and higher, the tower segment will start toppling. Toppling is initiated due to the inertia of the large tower segment when it is released from its sea-fastening. This means that when the barge starts rotating back from the maximum roll displacement after the tower segment is released, the tower segment keeps on rotating. Toppling the tower segment is not allowed since this could damage the tower segment itself, the sea-fastening and/or other components on the feeder. The limiting wave heights (in regular waves) for 90-degree incoming waves are extremely low, especially for the higher pre-tensions.

Increasing the limiting wave height is a must in order to make the direct installation method practicable. This can firstly be done by using more tower segments. Therefore, reducing the size of each segment. However, this is logistically less interesting due to the extra steps that need to be taken. Another option is to implement a motion compensation tool that decouples the motions of the feeder and the tower segment. The third option is to design a seafastening system that reduces the moment after the release, by for example spring-loaded clamps, to counter-act the toppling motion of the tower segment. All in all, can be stated that safely releasing a 20 MW tower segment on a floating barge is highly challenging and more research is required to solve the issues that are found in this research. This is necessary to allow the direct feeder method to be used for future wind installation projects in the U.S.

This page is intentionally left blank

Acknowledgements

This thesis is part of the Master of Science program 'Offshore and Dredging Engineering' at the faculty of Mechanical, Maritime and Materials Engineering (Delft University of Technology). This research is sponsored and hosted by Van Oord, Gorinchem. This is the second thesis of my double degree program for the masters Management of Technology and Offshore and Dredging Engineering.

I am really grateful to have worked on an upcoming hot topic in the offshore wind industry together with many experts in various fields during my thesis. Their support was essential to realise this thesis and I would like to thank everybody for their contribution. COVID-19 forced everyone to work at home in the beginning of the project. Later, more was allowed and the office opened up. Despite this, communication has been great since everyone was really helpful at Van Oord and the TU Delft.

First and foremost, I would like to give special recognition and thanks to Wouter de Wildt as my daily supervisor at Van Oord. He had a crucial role in the process to successfully complete my final thesis. He was always available to provide good feedback, new ideas and connected me with other people and companies to have brainstorming sessions. Many thanks to Wouter Dirks for helping me find this topic and welcoming me at Van Oord.

I would also like to thank Dr.-ing. Sebastian Schreier from the 3ME faculty for guiding and supporting me during my thesis being the first supervisor and chairman of the graduation committee. I would also like to thank Dr.ir. Sape Miedema for his input. Unfortunately, he retired during the project. Next, I would like to thank Dr. Stefano Fazi and Dr. Roland Ortt, from the TPM faculty for their support and input from the MOT perspective that helped me to improve this 'technical' thesis.

I would like to give recognition and thanks to the E&E hydro team as well as other colleagues at Van Oord who supported me and answered all my questions during my thesis.

Last but not least, I would like to thank my parents Harry and Nely, and brother Pieter for their infinite support and motivation. You were always there for me and made this possible.

Marius Smorenberg
Delft, June 2022

This page is intentionally left blank

Contents

List of Figures

List of Tables

Acronyms

AHC Active Heave Compensator. 20

COB Centre of Buoyancy. 11, 12

COG Centre of Gravity. 3, 4, 7, 8, 11, 12, 21, 26, 28, 34, 56, 57, 62

DAF Dynamic Amplification Factor. 4, 19, 59, 62

DOF Degrees of Freedom. 2, 21, 22, 26, 28–30, 32, 42

DP Dynamic Positioning. 19, 59

GW Gigawatt. 1

MW Megawatt. 1, 4, 6, 8, 25, 57, 60–62

OWF Offshore Wind Farm. 1, 14

PHC Passive Heave Compensator. 20

PSV Platform Supply Vessel. 11, 12, 57, 59, 61

RAO Response Amplitude Operator. 14, 15, 25, 30–33, 35–40, 42, 57, 58

WTG Wind Turbine Generator. vii, 1–6, 8, 11, 12, 25, 56, 57, 59, 60, 62, A-I, B-I

Nomenclature

heave A vessel motion along the vertical axis (up and down). 14, 20–22, 25, 32, 41–44, 47–49, 51, 58

hub The component that holds the rotor blades together and connects the rotational movement to the drive train in the nacelle. 7

jack-up vessel A vessel that can be elevated above the waves using legs when in position so it will not interact with the waves. 3

nacelle The housing for the drive train of the wind turbine. vii, 1, 4, 6–12, 19, 56, 59, 60

pitch A motion where a vessel's bow moves up and the stern down or the other way around and goes back and forth. 9, 21, 25, 28, 39, 57, 58

roll A motion where a vessel tilts to the port and starboard side or goes back and forth. 9, 11, 12, 15, 21, 22, 25, 31, 33, 38, 39, 44, 49, 58, 62

rotor blade The component that harnesses wind energy and creates the rotational movement. 1, 6, 7

snap loads High loads due to slack lines suddenly becoming taut. 3, 4, 20, 22, 44, 56, 57, 61, 62

surge A vessel motion along the horizontal x-axis. 21, 25, 28

sway A vessel motion along the horizontal y-axis. 21, 25, 31, 33

tower The vertical component that holds the other components at the correct height. vii, 1, 4, 6–12, 17–23, 26, 28, 34–37, 39, 40, 42–49, 51, 53, 56–63

workability The percentage of time a vessel can operate under environmental conditions depending on its workable limits. 3, 8, 15, 56, 59, 60, 63

yaw A motion where a vessel rotates around its z-axis. 21, 25, 28

This page is intentionally left blank

Chapter 1: Introduction

Climate change has become a major issue on a global scale and throughout the years, several initiatives have been promoted with the goal of reducing CO_2 emissions (UNCCC, 2020). For example, the 2015 Paris Agreement triggered a large demand for renewable energy. To cope with such growth, the renewable energy sector has been growing and developing over the years. Wind energy projects became in high demand, especially offshore, due to their higher capabilities in terms of efficiency and energy production and the limited visual and noise pollution (IEA, 2018). In Europe, after roughly 30 years, over 25 GW of offshore wind energy is installed (Wind Europe, 2021). On the contrary, to date, the offshore wind market in the U.S. consists only of two Offshore Wind Farms OWFs of 42 MW combined (U.S. Department of Energy, 2021). However, the current government wants to move to a 'clean energy revolution' and to 'jump start' the offshore wind market (The White House, 2021). The U.S. offshore wind target is set to reach 30 GW by 2030. This 'new' offshore wind market leads to opportunities as well as challenges for foreign companies (contractors) who are specialized in installing OWFs.

One of the main challenges for these contractors is to comply with the rules and regulations in the U.S. There is a federal legislation, called the Jones Act, that has four main requirements which apply to the installation process of OWFs (Transportation Institute, 2020);

- Transportation vessels must be owned by U.S. companies that are controlled by U.S. citizens with at least 75% U.S. percent ownership
- Transportation vessels must at least be 75% crewed by U.S. citizens
- Transportation vessels must be built (or rebuilt) in the U.S.
- Transportation vessels must be registered (flagged) in the U.S.

For contractors with a non-Jones act compliant installation vessel, this legislation prohibits the use of the conventional method. for this method, an installation vessel loads multiple full sets of WTG components on deck in the port. Then it sails to the OWF to install all carried components at the allocated locations. Next, it sails back to the port to repeat the process. This method is also depicted and explained stepwise in Appendix A. This is the most common installation strategy for Wind Turbine Generator (WTG) components (tower, nacelle and rotor blades). Investing in a Jones act compliant installation vessel is a high and risky investment and has a long lead time. Therefore, another installation method called feedering is currently investigated by multiple non-U.S.-based companies. This strategy uses Jones act compliant feeder vessels to transport/supply the WTG components to the non-Jones act compliant installation vessel which stays offshore. This is explained in more detail in Appendix B.

Feedering WTG components offshore is new for the offshore wind market. Ait Alla et al. (2017) and Oelker et al. (2018) were the first to investigate different feeder strategies. Rippel et al. (2019) criticised their work on the basis that they only used one configuration in their simulation. The investigation continued in the first thesis of this double degree program with multiple configurations/strategies, as well as the implantation of practical knowledge of Van Oord, being a marine contractor with OWF installation experience (Smorenberg, 2021). The first thesis results in the conclusion that shuttling (the conventional method) would be better than feedering. However, shuttling is not allowed in the U.S. with the current European (non-Jones act) installation vessels. All these studies were mostly focused on the best logistic configuration as well as the economics of the installation process. A technical investigation of the feeder process for WTG components has not yet been investigated in the literature.

In the paper of Haselsteiner et al. (2019), the riskiest step during the feeder installation process is deemed to be the WTG component lift-off from the floating feeder. Here, the crane of the jacked-up installation vessel needs to be connected to the component while it is still sea-fastened to the feeder. The component moves with the motions of the feeder (caused by the environment) due to the sea-fastening. When the sea-fastening is released, the component will have more Degrees of Freedom (DOF) and potentially slide or topple while still placed on the feeder deck. An (unwanted) accidental lift-off (and set/slam down) could also occur if the crane takes the full load of the component by accident. These are some of the potential risks during the release stage for a lift-off, of which very limited knowledge is available. During the lift-off itself, there are many unknowns, such as how the component will respond when lifted from a feeder while it rolls and translates due to the waves and if there would be a re-hit between the feeder and component when lifted. On top of this, WTGs are rapidly increasing in size and weight, which potentially increases the risks even further.

Damaging a component is unacceptable since this would (most likely) delay the entire installation project. Therefore, a clear understanding of what happens with the component during the release of sea-fastening and lift-off is key to avoiding and/or decreasing the risks in the field. Haselsteiner et al. (2019) suggest a deeper study where hydrodynamic simulations are used to learn more about the motions of the component. This deeper study is undertaken in this thesis.

The next chapter explains the problem in more detail and provides the research questions. Chapter 3 explains the methodology of how the main research question is being answered. Here hydrodynamic frequency and time-domain simulations are used as suggested by Haselsteiner et al. (2019). In Chapter 4, the results are shown and evaluated. This is followed by a discussion of the project in Chapter 5. The last chapter, Chapter 6, draws conclusions and answers the research questions.

Chapter 2: Problem description

This chapter firstly provides the problem statement that includes the goal, scope and knowledge gap. Next, the main research question, as well as sub-questions, are stated. Lastly, the problem is analysed on a deeper level by stating all the influencing elements during the process. This includes assumptions to narrow down the scope of the problem.

2.1 Problem statement

The goal of this research is to increase understanding of the lift-off operation for WTG components from a floating feeder. A jack-up vessel is set to be the installation vessel. The complete lift-off operation starts when the feeder vessel is positioned next to the jacked-up installation vessel and it has to maintain this position. Secondly, the crane of the installation vessel needs to connect to the WTG component that will be lifted. The individual components are temporarily fixed to the feeder vessel by sea-fastening. The sea-fastening needs to be released during the next step. The release can be before or during the process as the tension in the crane is building up. The component can be lifted from the feeder only when the sea-fastening is released. This is the complete lifting procedure in short and will need to be repeated for all components.

As described in Chapter 1, the release and lift-off itself have the highest risk of damages. Therefore, the phase where the crane is being connected to the component is left out of the scope of this research. This leaves two main parts, the release and the lift-off itself, which are two sequential parts. It is important to understand that a lift-off can only happen when the component can be released safely. During a project for a marine contractor such as Van Oord, both parts need to be investigated in sequential order and iterative loops are required to find the best solution for that particular project. However, this research does not offer the best solution. So more technical understanding of the process is needed to create insight for a workable solution. On top of this, there is limited time for this research, and only one phase can be investigated thoroughly. Therefore, as a result of the above-mentioned reasons, the focus of this research is at the release stage. The scope will not include an investigation of the actual lift-off itself. However, this will be included in the overall picture.

Very little is known when it comes to lifting WTG components from a floating feeder offshore since this has not been done in the past. Haselsteiner et al. (2019) described the state-of-the-art tools that would reduce the risk and increase the workability during the lift-off procedure. However, they only investigated this on a qualitative level. They suggested that hydrodynamic simulations are necessary to evaluate their ideas, such as the usage of motion compensation tools, as well as gaining knowledge of this process.

In fact, Zhu et al. (2017), did a lift-off simulation of a WTG tripod foundation as shown in Figure 2.1a. This figure shows an installation vessel that lifts a tripod from a floating (feeder) vessel. They briefly investigate the lift-off where a barge is used as well as a jacked-up installation vessel. They found that a lift-off from a floating barge is much more demanding than from a steady ground (like from a jacked-up vessel). However, they mainly looked at the lift itself since the tripod has a very wide base and relatively low Centre of Gravity (COG) making it relatively stable on top of the moving barge. This size comparison is depicted in Figure 2.1b. This figure shows the foundation being a tripod as well as the WTG which is installed on top of the foundation. They found that one of the issues are the crane wire snap loads during the phase before the lift. These snap loads are unwanted sudden peak loads in the lines caused when a line is slack and becomes taut. It could even be that the tripod is accidentally lifted (and set back) due to the barge excitations. This is called an accidental lift-off and should be avoided due to the risk of damages.

Next, they found that a re-hit is also a risk when the actual lift-off is started. This occurs when the component is lifted with intent but the barge slams against it due to the excitations. The last risk is just after the lift-off. The tripod is accelerated when it is lifted. This creates a dynamic effect on top of the static load causing a peak load in the crane (cable). The dynamic effect is called the Dynamic Amplification Factor (DAF) which is a percentage of the static load. During the lift, the crane takes 100% of the load plus for example 5% (DAF) due to the accelerations. All these risks are shown in the two time-domain simulations in Figure 2.2. The two lines in this figure represent different seeds. Each seed represents a wave train (in irregular waves) where only the phase of the waves is different for each seed.

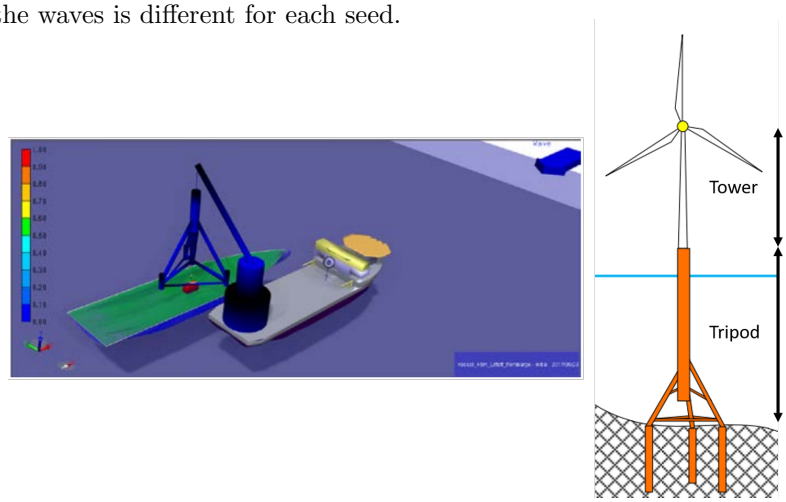

Figure 2.1: a) Tripod on a barge for a lift-off (Zhu et al., 2017), b) Fully installed WTG on a tripod (Pasin et al., 2019) - not to scale

In the current research, snap loads and accidental lift-offs remain an important part of the problem since the focus is on the release phase. The DAF and re-hit probability play a smaller part in the problem since they must be considered as a follow-up issue for when this research is extended (with a lift-off). On top of these issues, the stability of the components does play an important role since the components can topple and be damaged when the sea-fastening is released. For example, one of the components are tower segments. These have a much smaller base and higher COG in comparison with a tripod, especially for the next-generation (20 MW) WTGs. This makes the tower segments more unstable on deck of the moving feeder when the sea-fastening is released.

When toppling occurs, all the loads rest on one pressure point on, for example, the connection flange, potentially damaging it. In addition, the component will slam back against its sea-fastening when it is rotated back again. Therefore, toppling is not allowed. To solve this, a wide base frame could be attached to the bottom of the tower segment which increases the stability when the sea-fastening is released. When the tower is lifted from the feeder, the base frame will still be attached. This implies the requirement that the tower has to be placed on deck of the installation vessel before installation to remove the base frame.

In the first part of this double degree program, Smorenberg (2021) called this strategy the 'indirect installation method' since the components are lifted from the feeder to the installation vessel before installation. Smorenberg (2021) also found that it would be beneficial to install WTG components, tower segments and/or nacelle, directly from the feeder, instead of placing them on the installation vessel first. This is the so-called 'direct installation method'. In order to do so, nothing can be attached to the bottom of the component during the lift-off. Thus, a base frame cannot be used to increase stability. This creates a very interesting knowledge gap which is the understanding of the behaviour of a WTG component when its sea-fastening is released without a support frame. The technical challenges need to be identified and investigated in order to increase the possibility for the market to use the direct feeder installation strategy.

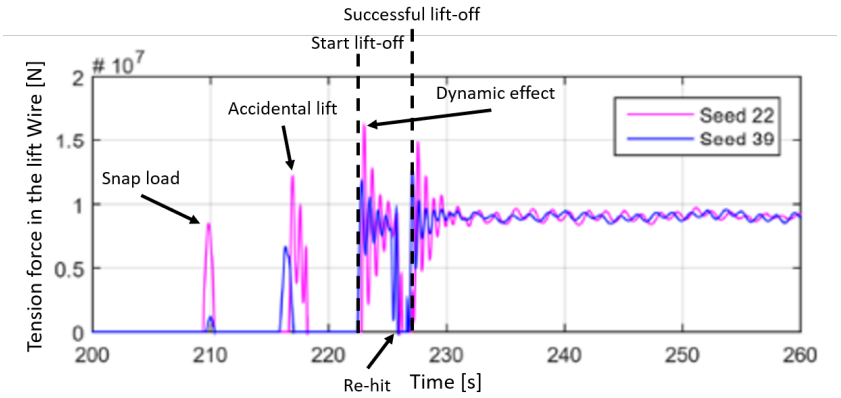

Figure 2.2: Time series of a tripod lift-off from a feeder, based on (Zhu et al., 2017)

2.2 Research questions

The goal of this research is to increase understanding in the release phase for a direct installation method of WTG components from a feeder vessel. This is also the scientific contribution as there is very limited knowledge available of for example the responses of a component when released. It is never been done before since the global market did not have the need to do so. However, since the U.S. market is growing, feedering will become a must due to the Jones Act as long as there are too few Jones Act compliant installation vessels available to fulfil the demand. The U.S. market will contain next-generation WTGs to increase their sprint to more sustainable energy. This leads to the main research question:

What are the reactions of a next-generation WTG component when released from its sea-fastening on a feeder vessel in the U.S. offshore wind market?

1. What elements are key to understanding the release of the WTG component?
2. What is the suitable approach to determine the reactions?
   (a) How can the key elements/aspects be included in a time-domain simulation?
3. How will the model be verified and validated?
4. What are the parameters that can be used in a sensitivity analysis?
5. What parameters is the system most sensitive to?

The first sub-question is answered in this chapter next since the key elements define the scope of the problem. The other sub-questions are answered in the following chapters.

2.3 Influencing elements

In this section, all elements that could contribute to the problem are discussed and assumptions are made to reduce the size of the problem. The elements are subdivided into component types, feeder types, environment, positioning system, crane, cable and compensation, and sea-fastening and feeder interface.

2.3.1 Component types

One of the most important elements in the problem is the component that is lifted from the feeder and in which order. A WTG contains three types of components; rotor blades, nacelle and a tower. The length of these rotor blades, the height of the tower and the weight of the nacelle increase as the WTG size increases as shown in Figure 2.3. This research focuses on the future of offshore wind energy. Therefore, 20 MW WTGs are used in this research. When a component is released from its sea-fastening, it could potentially start sliding over deck or toppling due to the motions of the feeder. Each component type is described as why or why not they are fit to be used further in this research.

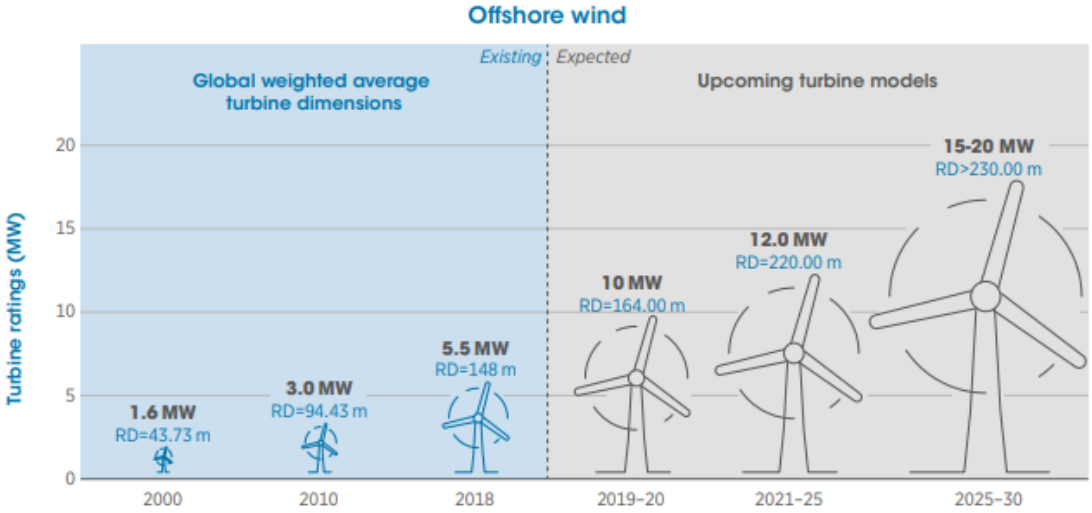

Figure 2.3: Expected increase in size of offshore WTG over the years (IRENA, 2019)

Rotor blades

The blades are transported horizontally. Two support frames are needed to be able to lift a long and flexible blade. These support frames are called blade racks. To increase space as well as lifting efficiency, all three blade racks are stacked on top of each other as shown in Figure 2.4. The blades combined are estimated to weigh roughly [redacted] tonnes and each blade has a length of [redacted] meters. Lifting the blade out of the rack is a very precise task since the blade is most likely to be damaged if it hits the blade rack. This is normally done on a steady platform such as the deck of the installation vessel when jacked up. This means that lifting the blades out of the rack and installing them straight after the lift would be too risky. Therefore, the blade rack needs to be lifted from the feeder to the installation vessel before installation. This is out of the focus of the knowledge gap where components need to be installed straight from the feeder and will not be looked into.

Figure 2.4: Example of a blade rack lift(Snieckus, 2020)

Nacelle

In this research, the assembled nacelle and hub is referred to as the 'nacelle'. The nacelle contains all components for the rotor blades to be connected, a housing and the drive train to generate electricity. The nacelle has an estimated weight of roughly [redacted] tonnes and a rough dimension of [redacted] meters. There are two main types of drive trains that are used in the market. The first option is the direct drive where the rotor is directly linked to the generator as depicted in Figure 2.5. The COG of the nacelle is within the circumference of the flange that connects to the tower due to heavy parts (rotor and generator) in the front. The second one is the nacelle with the conventional drive train of which the rotor is attached to a gearbox. The gearbox is connected to a generator as depicted in Figure 2.5. The COG of this option would be more or less straight above the flange (within its circumference) that is used to connect the nacelle to the tower.

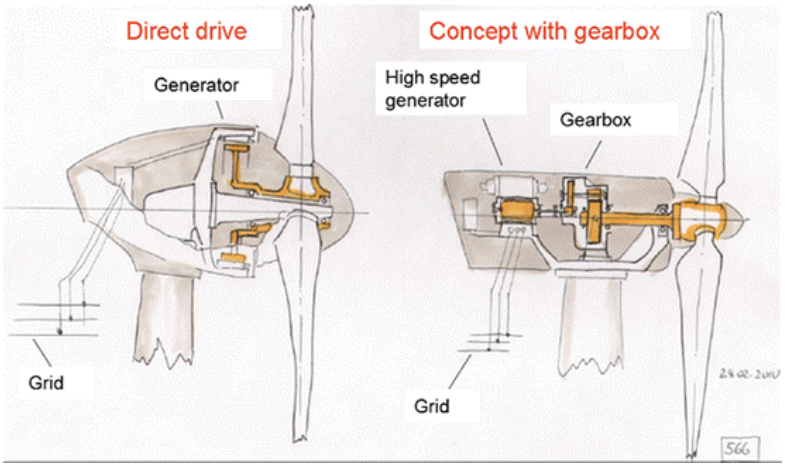

Figure 2.5: Direct drive and conventional drive train nacelles (Friedrich and Lukas, 2017)

The horizontal position of the COG is important since the nacelle should still be stable when the sea-fastening is released. With this remark, the direct drive would not be fit for a lift without a support frame. The nacelle would topple over (forwards) since the COG is not above the flange which is the base where it will be resting on. The conventional drive train nacelle can be used for a direct installation from the feeder since the COG is within the flange diameter. This means that the nacelle would be statically stable on a horizontal ground which allows the nacelle to be sea-fastened without a wide base frame.

Tower

The tower of a 20 MW WTG is expected to be roughly [redacted] meters high. This means that the tip of the tower will move by roughly 2.4-4.9 meters (amplitude) when the barge rolls in the waves only by [redacted] degrees. This makes the connection phase between the crane and the tower almost impossible. Therefore, the tower is split up into multiple segments, as depicted in Figure 2.6 where a full tower is split up into two segments. The tower suppliers normally supply the towers in multiple smaller segments to a storage port. In the port, these can be stacked on top of each other to form the desired number of stacked tower segments for feedering (e.g. two, three or four). Smorenberg (2021) found that the fewer tower segments used, the better the result logistically assuming that each tower has similar workability. Therefore, the tower is split up into two segments in this research. The COG of both segments is within its base since it is along its centre line. This makes it possible to sea-fast each tower segment without a wide base frame.

Figure 2.6: Feeder concept with tower divided into two segments (Huisman Equipment, 2021)

Tower versus Nacelle

The most critical component is the component that would be the most unstable one on the floating vessel. Instability is defined when the component starts toppling due to external forces. First, static toppling will be investigated. Static toppling initiates when the COG is no longer vertically above the base. For now, the assumption is made that the COG is on the centerline on the base and at half the height of the component. The tower segments of a 20 MW WTG have a height of [redacted] meters, a base of [redacted] meters in diameter and a weight of roughly [redacted] metric tonnes. The nacelle is [redacted] meters high and wide and [redacted] meters long, has a base of [redacted] meters in diameter and weighs roughly [redacted] metric tonnes. These components are depicted in scale in Figure 2.7. The angle at which the component will just not topple can be calculated by Equation 2.1. This angle would be created by the feeder which is not fully horizontal.

$$\alpha = tan^{-1}\left(\frac{R_{base}}{H_{COG}}\right) \tag{2.1}$$

Where:

α	is the allowed static angle until toppling	[°]
H_{COG}	is the height of the COG from the base	[m]
R_{base}	is the radius of the base	[m]

The maximum angle before toppling is roughly 31° for the nacelle and roughly 7° for the tower segment. This means that the tower segment will (statically) start toppling at a significantly smaller angle than the nacelle. This is also visually confirmed by Figure 2.7.

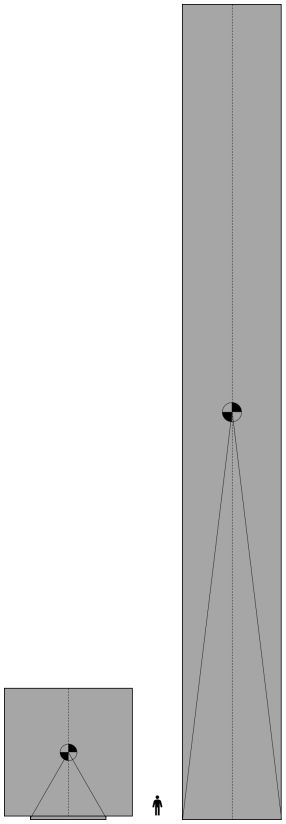

Figure 2.7: Scaled representation of the nacelle (left) and tower size (right)

Besides static toppling, the component can also topple due to the dynamics of the accelerating feeder. The component will either rotate with the vessel or remain at its current angle (delayed response) or keep rotating while the feeder rolls underneath the component as shown in Figure 2.8. This figure shows a feeder with a tower at a heeling angle. The feeder rotates to its upright position but the component remains at an angle. This effect is dependent on how prone a component is to rotational motions and can be determined by the rotational inertia. A higher rotational inertia indicates that a component requires a large moment load in order to rotate (difficult to rotate), while a low inertia requires less moment load (easier to rotate). This is stated by Newton's second law for rotation.

The moment of inertia for the nacelle in pitch and roll direction can be calculated with respectively Equations 2.2 and 2.3. The nacelle is assumed to be a rigid homogeneous block. The tower is simplified to a thin-walled tube due to its large diameter compared to the wall thickness. The thickness is therefore left out of the equation. The moment of inertia for a thin-walled tube is provided in Equation 2.4.

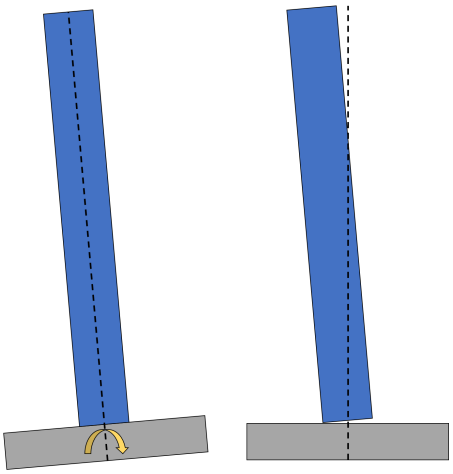

Figure 2.8: Component that does not rotate with the barge due to high inertia

$$I_{nacelle-pitch} = M \cdot \frac{L^2 + H^2}{12} \tag{2.2}$$

$$I_{nacelle-roll} = M \cdot \frac{H^2 + W^2}{12} \tag{2.3}$$

$$I_{tower} = M \cdot \left(\frac{1}{2}R^2 + \frac{1}{12}H^2\right) \tag{2.4}$$

Where:

I	is the moment of inertia	[kg·m^2]
M	is the mass of the component	[kg]
L	is the length of the nacelle	[m]
W	is the width of the nacelle	[m]
H	is the height of the component	[m]
R	is the radius of the tower	[m]

The moment of inertia of the nacelle for pitching and rolling are roughly respectively [redacted] and [redacted] tonnes·m^2 using the input values provided above by Van Oord. These inertia values are relatively small compared to the moment of inertia of the tower which is roughly [redacted] tonnes·m^2. Despite being an estimation due to the assumption of the shape, size and weight of the components, it provides a clear difference in which component is more prone to toppling due to accelerations of the feeder, which is the tower.

The last element to understand which component is most critical during the sea-fastening release is the excitation of the connection point with the crane. A horizontal force will be implemented in the force scheme when the crane is building tension. This horizontal force creates a moment that could be critical for toppling. The more the component moves, the larger the horizontal force. The crane will be connected to the top of both components. The excitation of the tower tip is much larger than the excitation of the nacelle top due to the significant height difference. On top of this, the vertical distance between the crane tip and the component top is much larger for the nacelle than for the tower segment. The crane angle and therefore the horizontal force will be much smaller for the nacelle than for the tower based on this knowledge.

The tower is more prone to toppling than the nacelle on all three elements, static toppling, dynamic toppling and horizontal loads due to the crane tension. For these reasons, the tower is further used in this research as the component that will be investigated for the release to a direct installation method.

Lifting order

After internal discussions with Van Oord, the most logical order to lift the components is to start with the tower segments since these are the highest components and could limit the reach of the crane when other components are to be lifted first. Therefore, removing the tower segments first is a must. The load case in the problem is for a fully loaded feeder where the tower segment is lifted first.

2.3.2 Feeder type

The next element of the problem is the feeder vessel itself. It should be able to carry a full set of WTG components on deck (including sea-fastening). In the first thesis in this double degree program, Smorenberg (2021) found that a Platform Supply Vessel (PSV) would outperform a barge logistically due to its sailing speed as well as its independent positioning capability. However, this research did not perform a market study as well as a stability study to understand if it even would be possible to carry one full WTG set on a PSV. Therefore, the first step in this element is to do a market investigation of the vessel availability in the U.S. Van Oord provided a list of available PSVs to allow for a stability calculation. The largest most common PSV available is 95 meters long and 20 meters in width, while the cargo deck is only 65 meters long. This small deck makes it difficult to position all components on one PSV as one can see in Figure 2.9. The blades have to be located on the side of the feeder close to the living quarters which is a risk during the lift-off. The deck size is large enough to store the nacelle and the tower segments as shown in the figure.

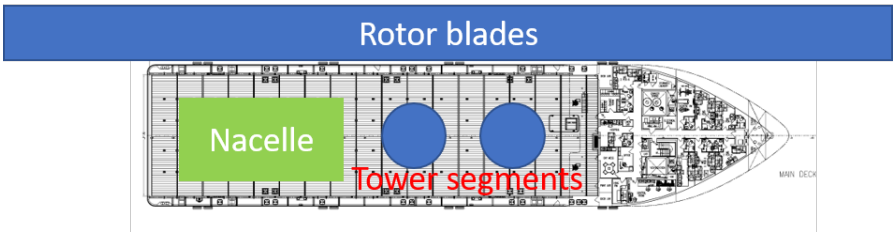

Figure 2.9: PSV deck layout of a 20 MW WTG

In addition, the vessel has to be stable in the water. A vessel would be in equilibrium when the COG (G) is positioned in a vertical line with the Centre of Buoyancy (COB) (B). As soon as an external force rolls the vessel, the COB shifts (B1) and creates a righting moment as shown in Figure 2.10. The metacentre (M) is the point where the vertical buoyant forces of the upright (zero inclination) position intersect with the buoyant forces when the vessel is heeling. The distance between the Centre of Gravity (COG) and the metacentre has to be positive in order to create a righting arm (G-Z) and be stable (stability condition). This distance is called the metacentric height ($\overline{GM}$). The keel is indicated by the 'K'. The upright water line is L-W and the inclined (vessel) water line is L1-W1 where θ is the roll angle. The weight and buoyancy forces are represented by respectively the 'w' and 'b' arrows.

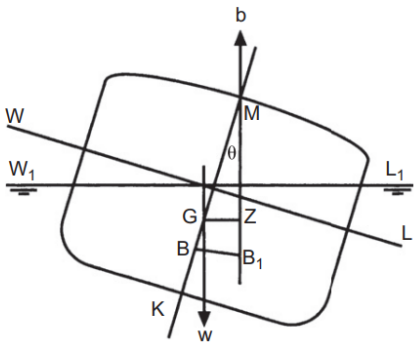

Figure 2.10: Forces scheme for an included vessel (Barrass and Derrett, 2012)

If the $\overline{GM}$ value is negative, the vessel is unstable and the vessel continues rolling in the same direction until the stable condition is reached. According to Barrass and Derrett (2012), a vessel can be stiff, tender or in between. A stiff vessel has a large restoring arm (G-Z), which can be calculated by the $\overline{GM} \cdot \sin(\theta)$. This indicates that the larger the $\overline{GM}$ values, the stiffer the vessel. However, this results in a relatively small rolling period which could be undesired if the roll period is within the wave periods. A tender vessel has a lower $\overline{GM}$ value. The righting moment for these values is small which leads to long rolling periods. This could be more desired if the roll period is above the incoming wave periods. The downside is that the $\overline{GM}$ is low and the vessel could become unstable due to unforeseen circumstances, a negative $\overline{GM}$ leads to instability. For heel angles up to 10 degrees, the $\overline{GM}$ can be calculated by Equation 2.5 since the barge will not roll more than 10 degrees. This 10-degree limit is set because When the angle becomes larger, the buoyancy point starts shifting vertically which must be taken into account (Barrass and Derrett, 2012). The $\overline{BM}$ can be calculated by Equation 2.6.

$$\overline{GM} = \overline{KB} + \overline{BM} - \overline{KG} \tag{2.5}$$

$$\overline{BM} = \frac{I}{\nabla} \tag{2.6}$$

Where:

$\overline{GM}$	is the metacentric height (G-M)	[m]
$\overline{KB}$	is the vertical distance between the keel (K) and COB (B)	[m]
$\overline{BM}$	is the vertical distance between the COB (B) and metacentre (M)	[m]
$\overline{KG}$	is the vertical distance between the keel (K) and COG (G)	[m]
I	is the moment of inertia of the water plane area	[m^4]
∇	is the displaced water volume of the vessel	[m^3]

The $\overline{GM}$ for the largest available PSV that carries all components resulted in a negative value, -7.7 meters, which means that it is not stable. Due to the fact that a PSV has a limited deck space as well as instability, a single PSV cannot be used as a feeder in the U.S to transport WTG components. Other configurations where the components are spread over multiple PSVs still resulted in negative or just above zero $\overline{GM}$ values. Another issue is that the blades are extremely long and are difficult to place on deck or safely overboard. Therefore, in this research, barges need to be investigated despite not being the best option logistically. The available barges according to Van Oord data are roughly 32 meters in width and 120 meters in length. A similar study as for PSVs resulted that a barge has a large enough deck space to locate all WTG components as well as a high $\overline{GM}$ of 19 meters to overcome instability issues. An example of a loaded barge is shown in Figure 2.11. Here the nacelle and tower segments are located around the longitudinal centre line of the barge and the blades are more to the side. This loading pattern can be counter ballasted to prevent the barge from heeling. Due to the aforementioned reasons, the barge will be used as a feeder vessel for the rest of this research.

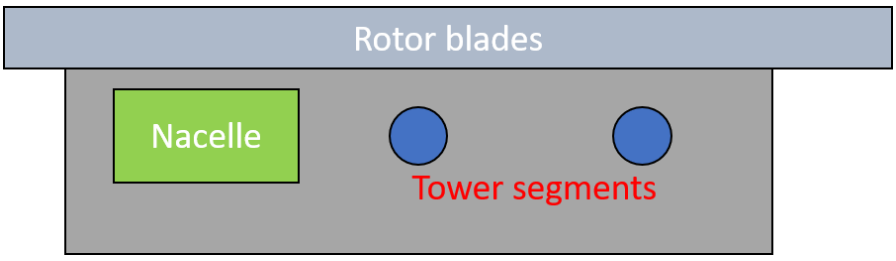

Figure 2.11: Barge deck layout of a 20 MW WTG

2.3.3 Environment

The environment plays a key role in the problem since it causes the motions of the feeder. The environmental elements are the waves, current and wind. The role of each element is explained next including potential assumptions to simplify the problem.

Waves

The waves interact with the feeder vessel. The interaction depends on the shape of the hull and the height, periods and directionality of the incoming waves. For regular waves, there is only one period, height and direction (sinusoidal shape). However, a singular regular wave is not a realistic representation of the real world. A closer more accurate representation of the real world has multiple regular waves at the same time where each has its own height, period (at different phases) and directionality. This is shown (without directionality) in Figure 2.12. These waves are called irregular waves.

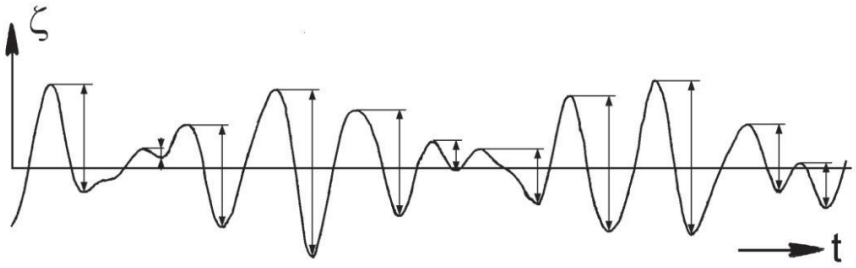

Figure 2.12: A simple time history of an irregular wave (Journee et al., 2015)

Irregular waves can be expressed in a wave energy spectrum as shown in Figure 2.13. Here, each frequency has an accompanying energy in m^2s. Two characteristics are used to determine the wave energy spectrum, which are the significant wave height (H_{m0}) and peak wave period (T_p). The significant wave height is the 'mean value of the highest one-third of the wave heights' recorded (Holthuijsen, 2010). The significant wave height value is a very close representation of visually estimated wave heights in experiments. The peak period is the 'mean period of the highest one-third of the waves' (Holthuijsen, 2010). The wave energy spectrum can then be used to determine the motions of a vessel in irregular waves. This will later be explained in more detail.

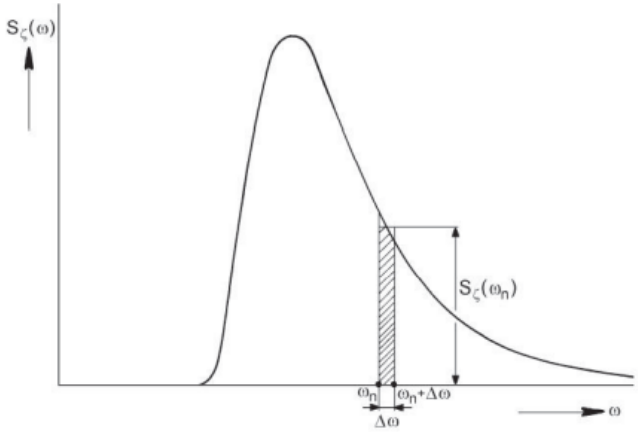

Figure 2.13: Wave energy spectrum example (Journee et al., 2015)

Waves are created by the energy of the wind that passes. The energy is provided by the friction between the surface and the wind (for still water) and the air pressure (Holthuijsen, 2010). Two types of wind-generated waves are defined; wind waves and swell waves. Wind waves are waves that are generated in a wind field and located in that same wind field where they are created. Swell waves are waves that have moved out of the wind field where they were created. These have shorter frequencies than wind waves. A simplified visualisation is provided in Figure 2.14.

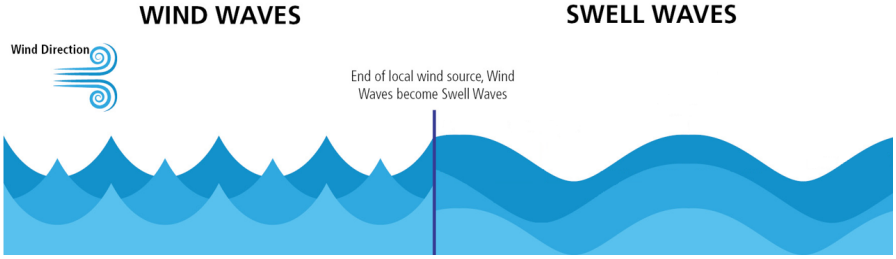

Figure 2.14: wind waves versus swell waves, based on Mazarakis (2019)

The Offshore Wind Farm (OWF) locations in the U.S. encounter both types of waves. According to Van Oord, the peak periods (T_p) of the incoming wind waves range between 4 and 6 seconds while the swell waves range between 4 and 11 seconds. This means that two wave spectra must be merged into one, a so-called, double-peaked spectrum. An example of such a spectrum is shown in Figure 2.15. Here, 'Ss' represents the swell wave spectrum and the 'Sw' the wind wave spectrum. Additionally, directionality plays an important factor in the U.S. since wind and swell waves often come from one direction while the wind wave have a larger spreading.

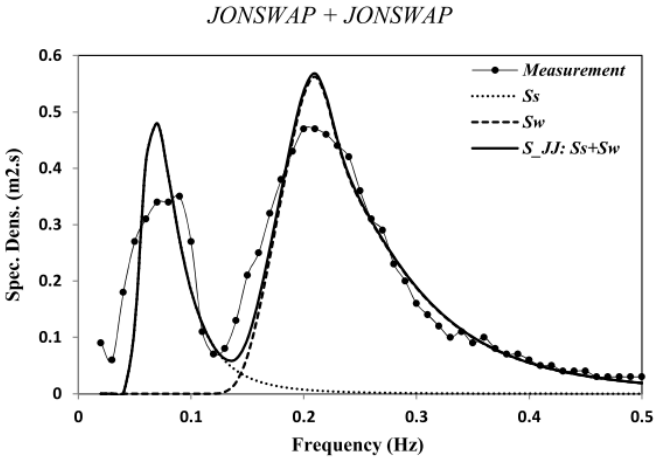

Figure 2.15: Double peak wave spectrum example of two Jonswap spectra (Akbari et al., 2020)

Within a wave, different types of load responses can be defined. First, there are first-order wave reactions in which the vessel response is linearly related to the amplitude of the waves. These responses of the vessel per wave frequency are described by Response Amplitude Operators (RAOs) as shown in Figure 2.16 (Journee et al., 2015). For example, heave contains the heave amplitude motion per meter wave amplitude for a specific frequency. Each incoming wave directing has a specific RAO.

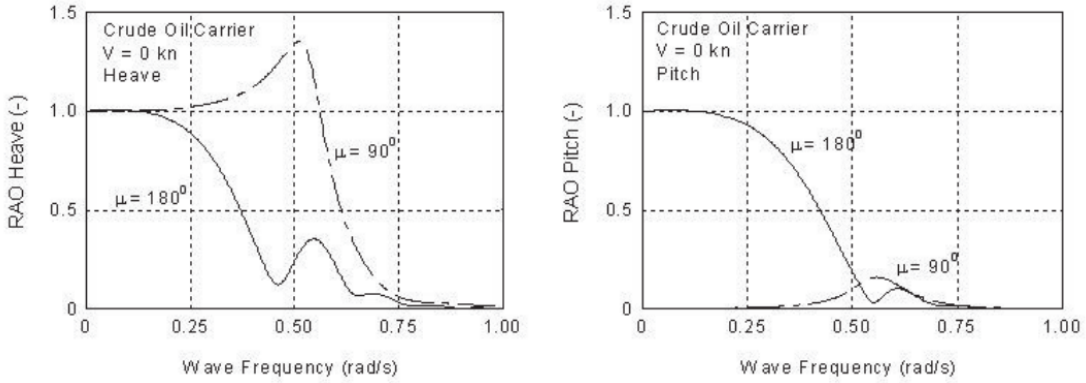

Figure 2.16: Heave and pitch RAOs as an example (Journee et al., 2015)

For irregular waves, the wave energy spectrum and the RAOs are used to determine the response spectrum of the vessel. The response spectrum is determined using Equation 2.7 (Holthuijsen, 2010). This can then be used to determine the significant response amplitude of the vessel (R_{m0}) by Equations 2.8 and 2.9 (Journee et al., 2015).

$$Resp(\omega) = RAO(\omega)^2 \cdot S_\zeta(\omega) \tag{2.7}$$

$$m_{0R} = \int_0^\infty Resp(\omega) \cdot d\omega \tag{2.8}$$

$$R_{m0} = 2 \cdot \sqrt{m_{0R}} \tag{2.9}$$

$$\tag{2.10}$$

Where:

$Resp(\omega)$	is the response spectrum	[m^2s]
RAO	is the response amplitude operator of the respective response	[-]
$S_\zeta(\omega)$	is the wave energy spectrum	[m^2s]
ω	is the wave frequency	[rad/s]
m_{0R}	is the variance squared of the response spectrum	[m^2]
R_{m0}	is the significant response amplitude	[m]

A limiting response (e.g. max allowable roll amplitude) is required to determine the workability of the activity (lift-off). This can be done by an iterative scheme. Here, the significant response amplitude of the vessel for each T_p and steps-wise increasing H_{m0}s are calculated. The limiting H_{m0}s for each T_p are found when the combination reaches the limiting response amplitude. This iterative scheme is shown in Figure 2.17. To truly determine the H_{m0} per T_p. In U.S. waters, a double peak spectrum as described before must be used. This significantly increases the number of calculations, simulations and iterations to be done since each combination of incoming directions should be considered.

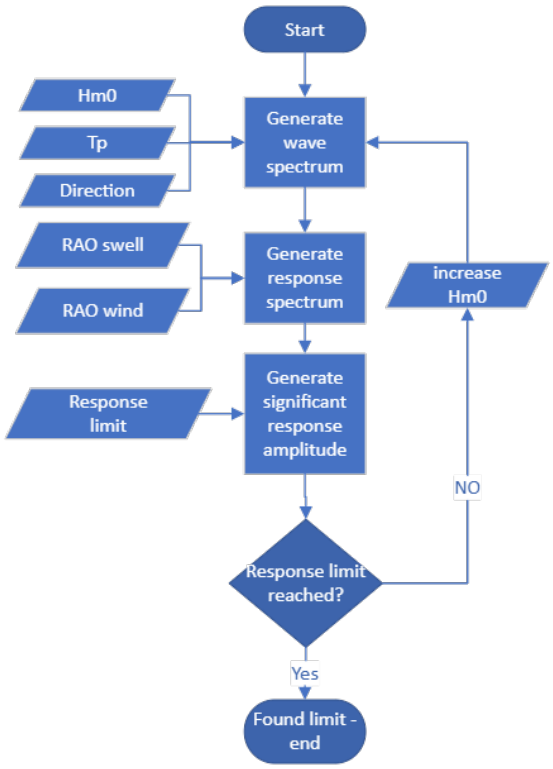

Figure 2.17: Iterative scheme to determine the allowable significant wave height per peak period

However, due to time constraints of the project, it is difficult to include the double-peaked spectrum and the irregular waves as described before. Regular waves are used for now, since this research focuses on the phenomena and physics during the release stage and not the workability. Nevertheless, the effect and the implementation of irregular and double peak spectrum will be discussed in the following chapters.

Next, there are second-order wave reactions. These are quadratically related to the wave height. High-frequency second-order wave forces are generally small compared to the low-frequency second-order wave forces that are large. These low-frequency forces cause the feeder to drift away from its position and are called wave drift forces. A positioning system would reduce the drift and keep the feeder more or less in place. The importance of these waves, as well as the positioning system, will be discussed later.

Current

The current is causing a similar effect to the feeder as the wave drift forces since it is a more or less constant force. The current could enlarge the total drift force or reduce it, depending on the direction relative to the low-frequency second-order waves. Again, the positioning system would reduce the drift motions.

Wind

The wind interacts with the component on two levels, namely, the steady-state drag force and the vortex-induced vibrations. Both interactions could enhance the toppling motion. First, the drag force for steady-state wind is looked into. This is calculated using Equation 2.11.

$$F_{drag} = \frac{1}{2} \cdot C_D \cdot \rho \cdot A \cdot V^2 \tag{2.11}$$

Where:

F_{drag}	is the drag force	[N]
C_D	is the drag coefficient	[-]
ρ	is the density of air	[kg/m^3]
A	is the reference area	[m^2]
V	is the wind speed	[m/s]

The crane of the installation vessel (Van Oord's Aeolus) can operate up to 14 m/s wind speeds, which is therefore taken as the wind speed. The area is the diameter of the tower multiplied by the height. These are provided for a tower segment in Subsection 2.3.1. The drag coefficient is taken for a cylinder is roughly 1.15 according to Cao et al. (2014). This resulted in a steady-state drag force of roughly 84 kN. This is very small compared to the weight of the tower segments, which is roughly 5884 kN. The drag force is just over one percent of the weight for the largest possible wind speed during a lift-off. Therefore, drag forces due to wind are neglected.

The second element are the vibrations caused by the wind due to vortex shedding. The component (tower segment) could start oscillating perpendicular to the wind direction as shown in Figure 2.18 (red arrows) if the vortex shedding period is close to the natural frequency of the component. These motions are called vortex-induced vibrations. The frequency when this occurs can be calculated by Equation 2.12 (MIT, 2014).

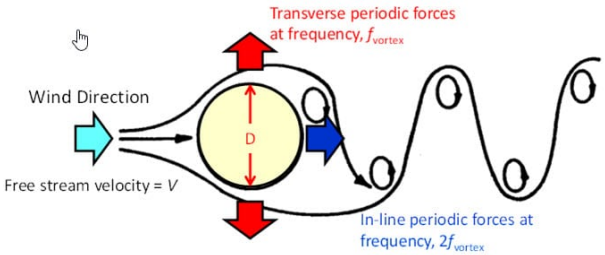

Figure 2.18: Forces due to vortex shedding (MACE, 2019)

$$f_{shedding} = \frac{S(Re) \cdot V}{D} \tag{2.12}$$

Where:

$f_{shedding}$	is the vortex shedding frequency	[Hz]
$S(Re)$	is the Strouhal number	[-]
V	is the wind speed	[m/s]
D	is the diameter of the body	[m]

The Strouhal number is dependent on the Reynolds number which indicates if the flow is laminar or turbulent. The flow around the turbine is turbulent for all wind speeds that could be encountered. with Reynolds number of roughly 5.8x10^5 at the lowest wind speed (1 m/s). Therefore, the Strouhal number is 0.3 (MIT, 2014). The tower is not allowed to topple. It can therefore be seen as a cantilever beam. The first three natural frequency modes of a cantilever beam can be calculated by the equations shown in Figure 2.19 and Equation 2.13.

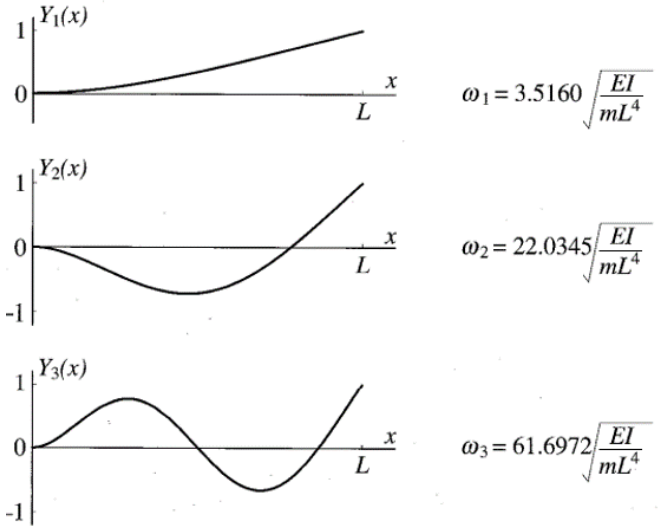

Figure 2.19: First 3 mode shapes of a cantilever beam (Meirovitch, 2001)

$$I_{tube} = \frac{\pi(D_{out}^4 - D_{in}^4)}{64} \tag{2.13}$$

Where:

ω_i	is the natural frequency per mode	[rad/s]
I	is the area moment of inertia	[m^4]
m	is the mass of the tower	[kg]
E	is the Young's modulus of steel	[GPa]
L	is the length of the tower	[m]
D_{out}	is the outer diameter of the tower	[m]
D_{in}	is the inner diameter of the tower	[m]

The results of the frequencies per wind speed are shown in Figure 2.20. It shows that the natural frequency of the second mode of the tower is higher than the vortex shedding frequency. The first mode intersects the vortex shedding frequency at roughly 6 m/s wind speed. This means vortex shedding may occur. However, the drag load is very small and it will therefore take some time before the tower starts oscillating. To prevent this phenomenon, vortex breakers can be placed on the tower. Both wind-tower interactions are not or barely occurring as described. Therefore, wind will not be taken into account in the problem.

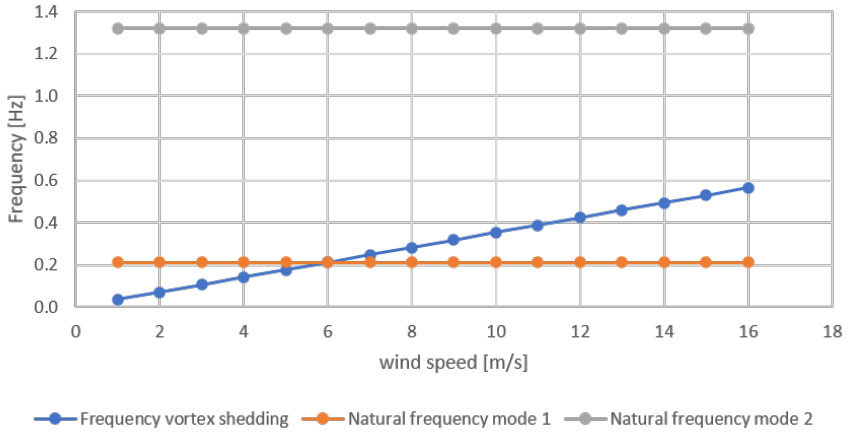

Figure 2.20: Results of vortex shedding frequencies to the natural frequency of the tower

2.3.4 Positioning system

The barge needs to be positioned next to the installation vessel. This position needs to be maintained during the lift-off of all components. Two types of positioning systems are available. The first is a Dynamic Positioning (DP) system, which uses thrusters. It also requires equipment to power these thrusters as well as computing power to steer them. This is not desired on a barge. The second option is mooring, which is more common for barges. The barges can be moored against the jacked-up installation vessel. Mooring lines across the seabed would not always be possible due to the legs of the installation vessel and electrical cables on the seabed. The mooring system should be sufficiently stiff or tender to have its natural frequency far away from the frequency of the incoming waves to avoid large responses. If the designed frequency is within the incoming wave periods, a damping system is required.

The wave drift forces are of low frequencies (long periods). This means that the excitation due to these waves is also slow. Van Oord explained that a crane operator can move the crane with the slow excitations to keep the crane tip above the component as much as possible. Therefore, the effect on toppling due to the drift motions will not be investigated and second-order effects, as well as the current, are not taken into account. This also leaves the positioning system out of the scope, but with a remark that it should be designed properly.

2.3.5 Crane, cables and compensation

The crane is already connected to the component in the problem. When the component is connected, it is normal that the lines below the crane hook become slack after connecting so the motions of the component (nacelle and/or tower segment) do not pull on the crane. However, when the lift is initiated, the tension starts to increase, and the crane and cables will encounter forces. This will activate a new part of the complete system which are the crane and cable stiffness/damping. The crane cables will stretch as more force is applied. Simultaneously, the crane tip bends downwards. This stiffness could be beneficial to the problem since it allows some flexibility in the system for the component to excite without toppling over. However, it could also be disadvantageous since they act like springs and could therefore pull too hard on the component, potentially causing toppling for example.

The stiffness of the system creates difficulties during the lift-off as well. While out of the scope, the lift-off should be considered. The components should be lifted as quickly as possible to avoid re-hits between the lifted component and the feeder. This means a fast lifting speed, leading to high acceleration as well as higher DAFs as explained before and shown in Figure 2.1 right after the lift. The higher the DAF, the more the crane tip will bend downward (due to its stiffness). The crane tip will go to its static position when the acceleration reduces. However, due to the spring element in the crane, the crane will overshoot its static position and act like a catapult (upwards).

Pre-tension is key to reducing the overshoot and therefore the catapult effect. Pre-tension is a certain percentage of the load (component weight) that is already taken by the crane before the lift, thus within the scope of this research. The higher the pre-tension, the closer the crane tip is bent to its equilibrium position when fully loaded. Accelerating the rest of the load (for the lift) leads to a smaller DAF downward motion of the tip and therefore a smaller catapult effect. This is also shown in Figure 2.21, where different pre-tensions are used on a simple mass-spring-damper (crane tip) system as an example. The mass is the crane tip that encounters the oscillations and catapult effects. Three different pre-tensions first will have a build-up stage to reach the desired pre-tension. When the lift starts, the component will be quick-lifted within 1 second and then slowly lifted by the crane. The y-axis shows the displacement of the crane tip due to these loads. The graph shows that smaller oscillating peaks occur (lower DAF) for higher pre-tensions, which would be beneficial for the lift-off itself. However, not only the crane tip is affected by the DAF. The equipment within components is also sensitive to accelerations. Therefore, a lower DAF is also recommended based on equipment sensitivity. The action of the lift-off is not in the scope of the problem but does in fact play a key role in the total problem for feedering.

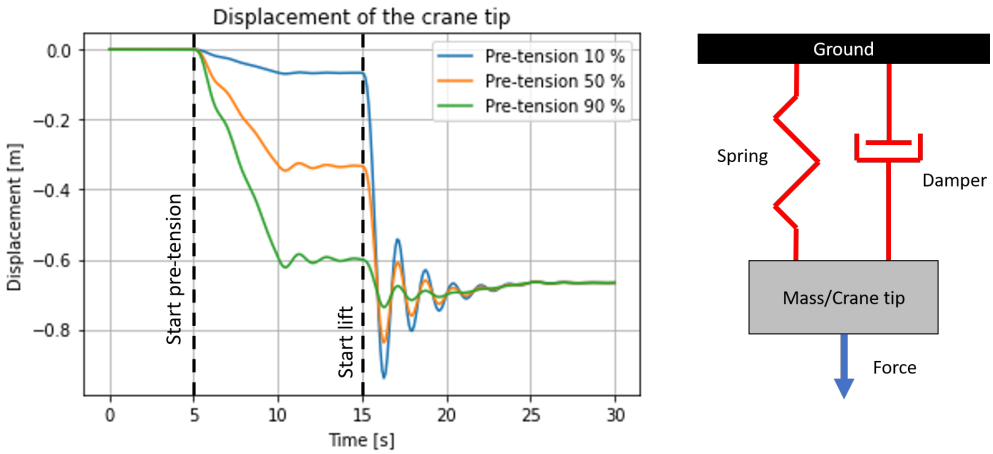

Figure 2.21: Mass spring-damper system that represents the crane tip motions during the lift-off to indicate the effect of pre-tension

A crane attached to the component directly does not allow sufficient time to build up pre-tension due to the snap loads and accidental lift-off that might occur. Therefore, the crane needs to be decoupled from the motions of the component. This can be done by a heave motion compensator between the crane hook and the component. There are two types of heave compensators. First is a Passive Heave Compensator (PHC) that reacts to external forces without any additional energy (Crane Master, 2022). It contains a spring and damper system that should be carefully designed (correct spring and damper parameters) to avoid resonance frequencies for example. It is complicated for such a system to reach high percentages of pre-tension due to the nature of the fluctuating spring forces (damped snap loads).

The other heave compensator is the Active Heave Compensator (AHC) which uses external energy to compensate. The AHC has the ability to maintain an almost constant tension in the crane cables during the lift-off despite the excitation of the component (Seaqualize, 2022). Both compensator types have a quick lift system, which allows for a lift by the tool to quickly increase the distance between the component and the feeder (reduced re-hit probability). This research investigates the release where pre-tension is one of the key elements. The PHC does not allow for all pre-tension levels to be investigated and needs to be designed properly to work accordingly. The AHC does also have these issues but to a much smaller extent, and will therefore be used in this research. The AHC of Seaqualize is recently tested as shown in Figure 2.22.

Besides the AHC tool, a crane block is also present in the crane. Both elements should be considered in the problem since these have a mass that could counteract or even worsen the toppling motions of the component due to swinging motions. The natural frequency should be avoided since this would lead to large excitations of the AHC and crane block and therefore large horizontal forces on the component.

The installation vessel is jacked-up. However, it will still interact with the environment as well as the barge that is moored to the vessel. Internal studies by Marin and Van Oord show that the oscillating motions of the jacked-up Aeolus with a moored barge are around 10 centimetres. This means, that the crane tip will also oscillate but potentially not with the same amplitude and/or period depending on the natural frequency. This means that the crane tip would not exactly be above the component, leading to a horizontal force when tension is applied. However, the amplitude of the crane tip is very small compared to the motion of the tower tip when the feeder is rolling. Therefore, the motions of the installation vessel are not taken into account in this research.

Figure 2.22: Sea trials (lifting tests) of the AHC tool of Seaqualize (Seaqualize, 2022)

2.3.6 Sea-fastening and feeder interface

The tower segments will be sea-fastened to the deck of the barge. Ideally, the position is above the COG of which the vessel rotates around. Here, the top of the tower will be displaced due to the heave, sway, surge, roll, pitch and yaw motions of the feeder. However, since two segments are used, the other segments must be located more to the aft/fore of the feeder as shown in Figure 2.11. This location is less ideal since pitching starts playing a role even more. The same holds for rolling if the segments are located more to the side (away from the centreline). Investigating the two locations as shown in Figure 2.11 would be best to gain an understanding of the tower's motions. However, this means that all simulations have to be done twice, due to time constraints, only one location has been chosen to be simulated.

An object has six Degrees of Freedom (DOF) (three translations and three rotations) when it is free. The tower has all six DOF fixed when it is sea-fastened. However, this changes when it is released. The horizontal DOF depend on the sliding motion of the tower on deck. However, sliding is relatively easy to control when released. Therefore, sliding is not considered and the horizontal DOF remain fixed after the release. Accidental lift-offs and toppling are important, so these DOF (all others) must be released to gain understanding. The release timing is important since this determines the initial motions of the 'free' tower segments. Multiple companies are currently investigating the possibility of using a motion compensation system between the sea-fastening and the barge. This will not be investigated in this study since it is unknown whether it is even required. In this study, it is not important to design a sea-fastening release system since it is key to gain understanding to provide input for such a design investigation.

2.3.7 Key elements

As an overview, all key elements that are included in the problem are listed below and schematically shown in Figure 2.23.

- Focus on the component responses after the release and before the lift
- 20 MW WTG components
- Tower segments allocated components
- Barges used as feeder vessels
- Regular waves
- First-order waves including height, period and directionality (not other environmental loads)
- Crane and cable stiffness
- Pre-tension
- Snap loads
- Accidental lift-offs
- Toppling
- Crane block
- Active heave compensator
- Release timing
- Heave, roll and pitch DOF released (toppling and accidental lift-offs)
- Fully loaded barge, tower lifted first

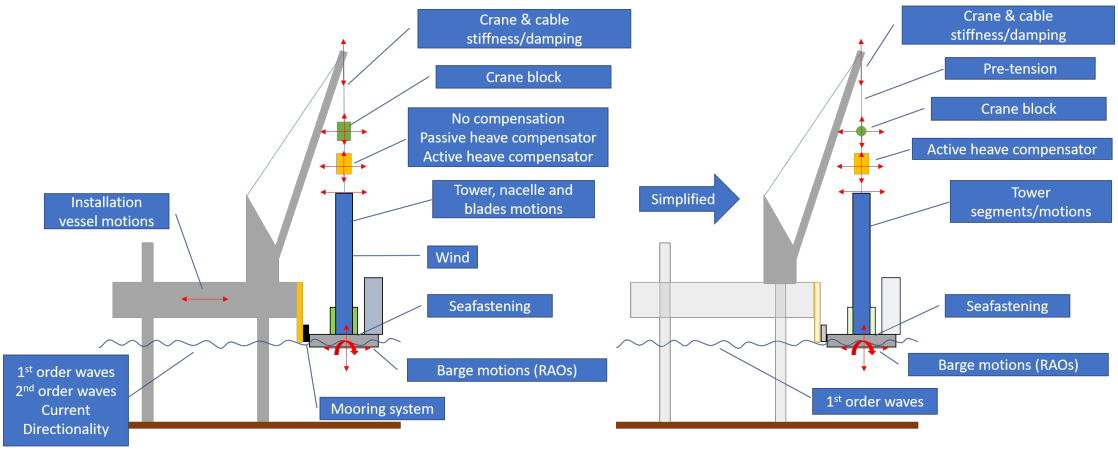

Figure 2.23: Schematic overview of all elements (left) and the key elements (simplified problem) in this research (right)

Chapter 3: Methodology

This Chapter firstly explains the general approach that is taken to answer the main research question. The approach is then explained in more detail including the verification, validation and how the results are reached.

3.1 Approach

The problem as described in Chapter 2 starts with a sea-fastened tower segment to a barge and ends with release sea-fastening. This means that the problem changes dynamically over time (from fixed to loose tower segment). It is a highly complex problem where many elements can have an impact on the result as explained. According to Sekaran and Bougie (2016), simulations are the best way to find the dynamic effect of changes over time without conducting high costs and high-risk (scaled) experiments. Therefore, simulations are the best choice to gain an understanding of the release phase of a tower lift-off from a floating barge.

Within the simulation category, there are two types that are well used in the industry, namely, **frequency** and **time-domain** simulations. For hydrodynamic-related studies, the frequency domain analysis is used to determine the response of the system based on the frequency and amplitude of the incoming waves. To do so, the equations of motions based on Newton's second law that are frequency-dependent need to be created. The result is a motion amplitude (translation/rotation) per meter wave amplitude (RAOs), per wave frequency and direction. This analysis does not include non-linear effects but is significantly faster than time-domain simulations (Journee et al., 2015).

A time-domain analysis is used in cases where the problem is transient and non-linear behaviour, such as non-linear damping (of the heave compensator), needs to be considered (Journee et al., 2015). Again, the equations of motions are required but here as a function of time. Each time step needs to be solved by an integration scheme in order to find the next position, velocity and acceleration which is then used for the following time step. This makes the simulation more time-intensive.

Since the problem is transient, a time-domain analysis is the best approach to gain an understanding of what causes the tower to topple and what could be done to prevent toppling. The simulations are done in a software program called OrcaFlex which is a well-known and used time-domain simulation program in the offshore industry. The simulation model as well as the theory behind the program is explained in Section 3.2. This model still requires to be verified and validated before simulations are run. Here, the frequency-domain analysis created by hand is used (mainly for the validity). This will be further explained in Section 3.3.

As a next step, the simulations must be run. The downside of time-domain simulations, as described before, is the long simulation time per case and the enormous amount of cases that need to be run in order to find the critical toppling wave amplitude for a specific wave period, directionality, pre-tension and release timing (e.g. 10 wave amplitudes/heights, 10 wave periods, 7 directions, 5 pre-tension and 3 release points $\rightarrow$ 10,500 cases). These simulations have to be run as well as analyzed in order to determine whether the simulation went correct and to understand the results. Here, the quick frequency domain calculations come in handy since specific limits can be set and the maximum allowable wave height (in regular waves) can be found in a matter of seconds per frequency, direction, pre-tension and release point. These so-called 'critical' wave heights are plotted to show the limiting wave height per frequency (for each case). These critical points can then be used to gain understanding and to find patterns that lead to a reduced number of time-domain simulations that actually need to be run. This is explained in Section 3.4

3.2 Time-domain simulation modelling

A simulation model has to be built so it comes close to the real world. Chapter 2 explained how to reduce the scope of the problem as well as some of the assumptions to simplify the simulation model. Here, the elements in the model are explained in more detail first. This is then followed by an explanation of the theory behind the program. All input parameters can be found in Appendix F. The Python code to run the OrcaFlex model is explained in Section 3.4.

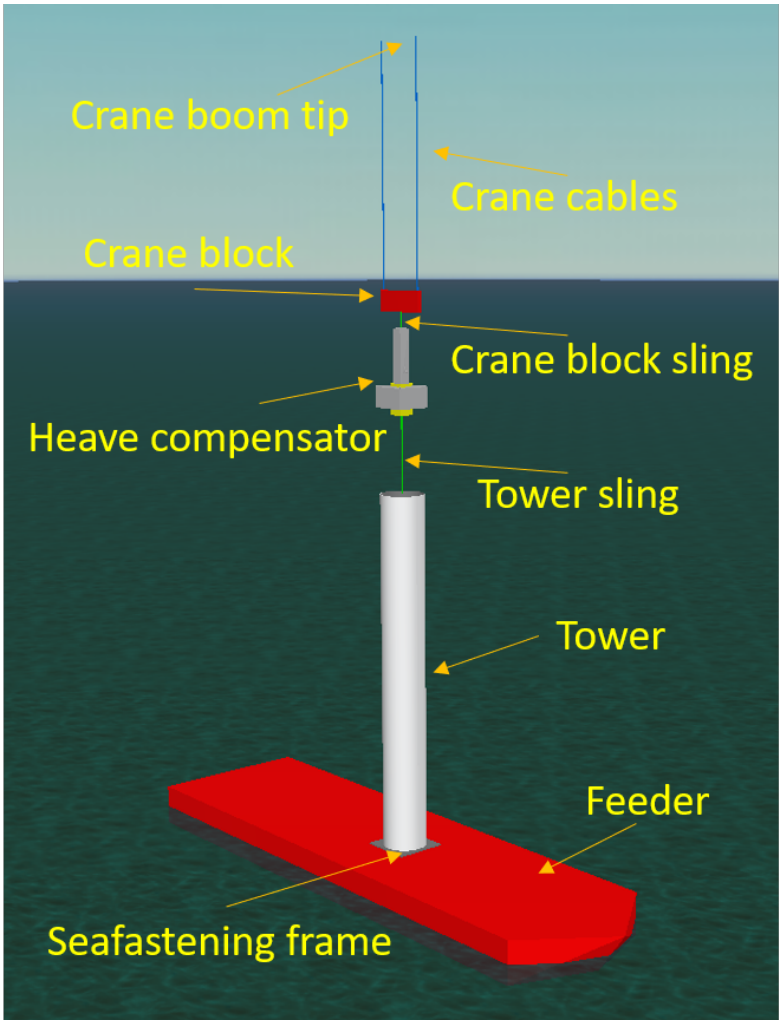

Figure 3.1: OrcaFlex model overview

3.2.1 Model building

The components of the problem are placed in OrcaFlex. The program allows the user to recreate the problem set-up from the ground up by placing the components one by one and connecting them accordingly. Figure 3.1 provides a visual overview of what the fully assembled system looks like. Now, the system is discussed to provide an understanding of how it is built.

Environment

Airy Waves are chosen for regular waves in the model. These represent sinusoidal waves under the condition where the wave height is small compared to the wavelength and the water depth.

Feeder

The data of the feeder, being the (load and displacement) RAOs, (added) mass and damping, hydrostatic stiffness, shape, etc. is provided by Van Oord. These are calculated by them using Ansys Aqwa for the load case where all components of a 20 MW Wind Turbine Generator (WTG) are located on deck as described in the previous chapter. The RAOs have been examined in order to check if the RAOs make sense and are error-free (no obvious discrepancies). This is also on in collaboration with hydrodynamic engineers of Van Oord. The displacement RAOs of the barge for 90-degree incoming waves, direct from the side to the ship (beam waves), are shown in Figure 3.2. The figure shows all six motions of the vessel. It makes sense that the surge, pitch and yaw RAOs are (very close to) zero since the waves are directly coming from the side. The other RAOs (sway, heave, and roll) are affected by these waves. RAOs for directions 0 until 90° are provided in Appendix C.

When moving the 90 to 0°, the sway RAO reduces while the surge RAO increases. The same happens for pitch and roll since the vessel will only pitch in head waves. Noticeable is the difference in natural frequency response peak which is much higher for rolling than pitching. This is due to the shape of the barge (a rectangle) which is more prone to rolling than pitching and clearly visible when comparing head and beam waves.

Besides a visual check of for example heave which should and does start at 1 m/m at low frequencies (moving directly with the waves), a natural frequency check is also performed. The peaks of the heave and roll in the figure indicate the natural frequencies, which are 1.3 and 0.9 Hz respectively. The natural frequencies for heave and roll are calculated using Equations 3.1 to 3.3 and the vessel parameters provided by Ansys Aqwa. The last equation shows the natural frequency of the damped system. Both calculated damped natural frequencies are (roughly) the same as the frequencies which are read from the graphs. The damping ratio for rolling is roughly 0.01 which indicates that these damped and undamped natural frequencies are the same. The damping ratio for heave is roughly 0.21. The natural frequency of the damped system will therefore only slightly shift to a low frequency since it is underdamped.

$$\omega_n = \sqrt{\frac{k}{m+a}} \tag{3.1}$$

$$\zeta = \frac{c}{2\sqrt{k \cdot (m+a)}} \tag{3.2}$$

$$\omega_d = \omega_n \sqrt{1-\zeta^2} \tag{3.3}$$

Where:

ω_n	is the undamped natural frequency	[rad/s]
ω_d	is the damped natural frequency	[rad/s]
ζ	is the damping ratio	[-]
k	is the stiffness	[N/m]
m	is the mass or inertia	[kg or kg·m^2]
a	is the added mass or inertia	[kg or kg·m^2]
c	is the damping	[M/m·s]

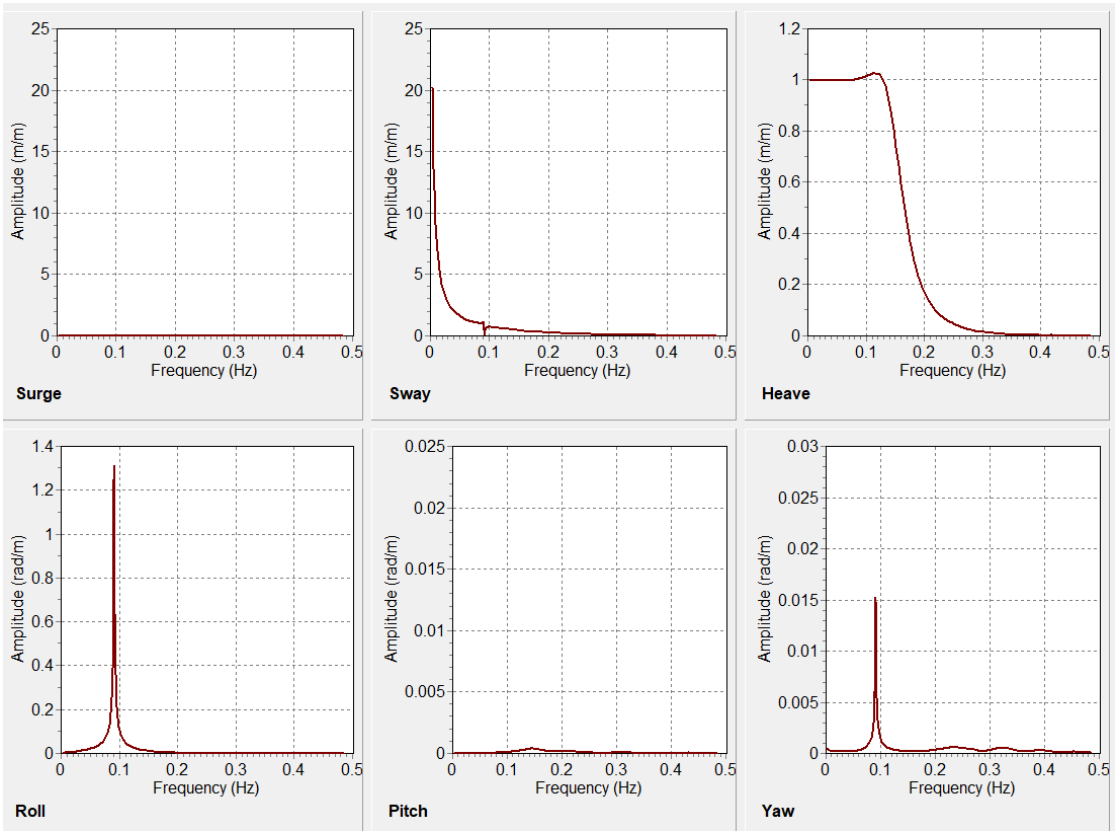

Figure 3.2: Displacement RAOs of the feeder barge in beam waves provided by Van Oord

When the 'to be lifted' tower is added on top of the deck, as shown in Figure 3.1, the mass/inertia of the tower is also considered (as an addition). OrcaFlex has the option to subtract a mass/inertia with a certain Centre of Gravity (COG) from the feeder specifications so the combined feeder and tower (as an added object) will not deviate from the original mass and inertia and draft.

The tower is located on a sea-fastening frame (grey square in the figure). This frame has a stiffness to recreate the stiffness of the deck. Between the tower and the frame is a constraint (not visible in the figure) that acts as the release mechanism. The constraint can either be fixed or set loose so the tower is able to topple. As stated in the problem, sliding is not considered. Therefore, the horizontal transnational Degrees of Freedom (DOF) will still be fixed. How the release is programmed will be explained later in Section 3.4. The chosen location of the tower will be discussed later in the next section.

Heave compensator

The heave compensator tool in the problem is an active heave compensator. However, after investigating, the active heave compensator behaves like a a passive heave compensator with a low and constant stiffness during the pre-tension phase. This decouples the vertical motions of the tower and heave compensator. The heave compensator is also underdamped for that same reason.

Cables and slings

All cables and slings are included with a stiffness which was provided by Van Oord. The initial length of the slings are assumed at 6 and 15 meters for respectively the crane block sling and the tower sling. The crane cables do not have a set initial length since the pre-tension is one of the variables in the problem. OrcaFlex allows for a pre-tension as an input.

Crane

The problem analysis explained that the crane stiffness should be considered. The horizontal displacement is expected to be smaller than the vertical displacement, both being expected to be in the order of centimetres due to the high stiffness. As stated in 2.3, small horizontal displacements of the crane tip are neglected. Therefore, the assumption is made that the crane tip can only move in the vertical direction.

3.2.2 OrcaFlex theory

The first thing OrcaFlex does is create the time-dependent equations of motions based on Newton's second law. This is done by Equation 3.8 according to the OrcaFlex manual and Chung and Hulbert (1993). An integration scheme is required in order to find the position, velocity and acceleration of each element for the next time step. OrcaFlex uses an implicit integration scheme as described in the OrcaFlex manual. An implicit integration scheme uses the current time step (t) output as well as the next time step (t+1) output in order to determine the (in this case) position on t+1. Often, multiple iterations are required in order to find the stable value for the next time step. Another method called the explicit integration method can also be chosen but is not advised since this method requires very small time steps compared to the implicit method. This is because the explicit method only looks at the outcome of the current or previous time step(s). Large time steps will increase the error. Therefore, small time steps are required to increase accuracy but increase the simulation time. OrcaFlex uses the Euler method as shown in Equations 3.4 and 3.5 for the explicit scheme as explained in the OrcaFlex manual. Based on these above-mentioned reasons, OrcaFlex recommends the use of the implicit integration scheme, which is also chosen for this study.

$$v_{t+dt} = v_t + dta_t \tag{3.4}$$

$$p_{t+dt} = p_t + dtv_{t+dt} \tag{3.5}$$

OrcaFlex uses the implicit integration scheme called the Generalized-α Method by Chung and Hulbert (1993) and is shown in Equations 3.6-3.12. All equations are dependent on α, which can be calculated by ρ_∞, 'a user-specified value of the spectral radius in the high-frequency limit' (Chung and Hulbert, 1993). This paper as well as the OrcaFlex manual do not explain how to obtain this value. Therefore, this research will not go into detail about the integration scheme any further.

$$d_{n+1} = d_n + \Delta t v_n + \Delta t^2 \left(\left(\frac{1}{2} - \beta \right) a_n + \beta a_{n+1} \right) \tag{3.6}$$

$$v_{n+1} = v_n + \Delta t \left((1-\gamma) a_n + \gamma a_{n+1} \right) \tag{3.7}$$

$$M a_{n+1-\alpha_m} + C v_{n+1-\alpha_f} + K d_{n+1-\alpha_f} = F\left(t_{n+1-\alpha_f}\right) \tag{3.8}$$

Where:

$$\gamma = \frac{1}{2} - \alpha_m + \alpha_f \tag{3.9}$$

$$\beta = \frac{1}{4} \left(1 - \alpha_m + \alpha_f\right)^2 \tag{3.10}$$

$$\alpha_m = \frac{2\rho_\infty - 1}{\rho_\infty + 1} \tag{3.11}$$

$$\alpha_f = \frac{\rho_\infty}{\rho_\infty + 1} \tag{3.12}$$

3.3 Hand calculations

As explained before, hand calculations serve a double purpose. The first is the validation of the OrcaFlex model and the second is to quickly find the limiting wave height in order to reduce the number of time-domain simulations. First, the theory behind the hand calculations will be discussed.

3.3.1 Hand calculation theory

Fully recreating the OrcaFlex model in 3D would be too time-consuming. Therefore, the decision was made to only look at the problem in 2D (y-z plane). A schematic overview of the problem is provided on the left side of Figure 3.3. Additionally, assumptions were made to simplify the model. The first assumption is to fix the tip, so no crane stiffness. The second assumption is to take the crane block as a point mass instead of a block with inertia and height. Since these calculations are done in the frequency domain, the tower is fixed to the barge and the combined COG is the reference point (origin) of the system (lowest black dot - at the tower). The heave compensator contains a mainframe and a slider block which are connected by the spring-damper system.

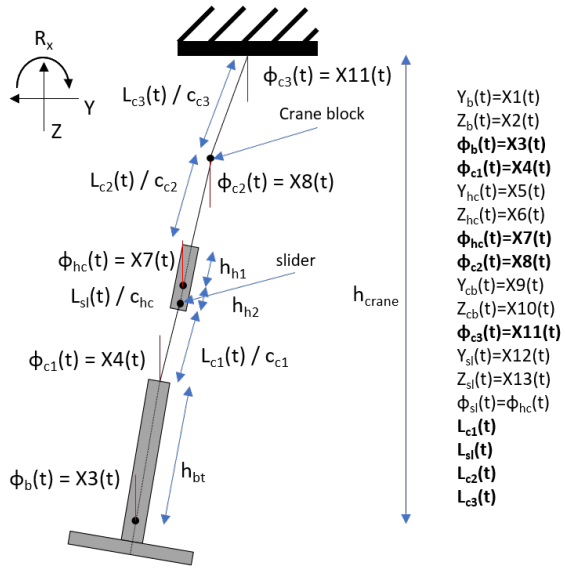

Figure 3.3: Schematic overview of the system of the hand calculations

Surge, pitch and yaw are not included in the problem since the hand calculations are only done in 2D. The limiting wave heights are therefore also for the 2D problem. In 2D, only beam waves will give a good representation of the model since other wave directions would include coupled motions, such as pitch that could influence the outcome. The time-domain simulation can thus only be done for beam waves. The location of the tower being at the COG or more to the aft of the barge will not influence the outcome. Therefore, for simplicity, the 'to be lifted' tower is located at the COG of the loaded barge.

Before formulating the equations of motion, the required time-dependent DOFs on which the system is dependent must be determined. The list on the right side of Figure 3.3 shows all motions of the objects in the problem, such as Y_b (sway motion of the barge), z_b (heave motion of the barge) and ϕ_b (roll motion of the barge). The 'Xn(t)' names behind the motions are simplifications of the names that are used in Maple as shown in Appendix D. Some motions are dependent on other motions. DOFs are independent by definition. The transnational motions (Y and Z motions) are dependent on the angles and the length since the slings/cables are assumed not to bend. Therefore, only the lengths (extensions of the springs) and angles need to be considered (shown in bold). This results in nine DOFs which set the requirement of nine equations of motion which are explained next. These kinematic constraints are also found in the Maple script in Appendix D.

Deriving the equations of motion by means of the energy in the system is deemed to be much more error and time friendly than by balance of forces. The total energy in the system is the kinetic energy (T) plus the potential energy (V) → E(t) = V(t) + T(t). The total energy of the system (including the initial energy, E_0) must be equal to the work that is created by external forces (W), in this problem, the wave loads → W(t) = E_0 + V(t) + T(t). The flux of energy is then used to remove the initial energy since this is a constant → $\frac{d}{dt}(E_0) = 0$. This leads to the following energy equations in equations 3.13-3.18. Rotational energy is also taken into account in these equations and Equations 3.15 and 3.17 need to be changed. The mass changes to inertia, the stiffness to rotational stiffness and displacement/velocity to rotational displacement/velocity.

$$\frac{d}{dt}(V(t) + T(t) - W(t)) = 0 \tag{3.13}$$

$$V_{gravity}(t) = \sum m_{object} \cdot g \cdot h_{object}(t) \tag{3.14}$$

$$V_{spring}(t) = \sum \frac{1}{2} \cdot c \cdot \Delta L_{cable/spring}(t)^2 \tag{3.15}$$

$$V(t) = V_{gravity}(t) + V_{spring}(t) \tag{3.16}$$

$$T(t) = \sum \frac{1}{2} \cdot m_{object} \cdot v_{object}(t)^2 \tag{3.17}$$

$$W(t) = F_{external} \cdot d(t) \tag{3.18}$$

Where:

$V_{gravity}$	is the potential energy due to height	[J]
V_{spring}	is the potential energy due to spring stiffness	[J]
m_{object}	is the mass of an element	[kg]
g	is the gravitational acceleration	[m/s^2]
h_{object}	is the height of an element	[m]
c	is the stiffness	[N/m]
$\Delta L_{cable/spring}$	is the extension of a cable or sling	[m]
v_{object}	is the velocity of an element	[m/s]
$F_{external}$	is the external load	[N]
d	is the displacement due to the external load	[m]

The next step is to determine the nine equations of motion by taking the partial derivatives of the energy balance with respect to the velocities in the DOFs as shown in Equation 3.19. Next, the external forces are divided into wave loads in y, z and rotational directions which include the added mass and damping of the feeder. The damping of the heave compensator is also added to the external loads. All these steps for the system can be found in Appendix D.

$$EoM_i : \frac{\partial}{\partial_{\dot{x}_i}} \left(\frac{d}{dt}(V(t) + T(t) - W(t)) \right) = 0 \tag{3.19}$$

Where:

EoM_i	is the ith equation of motion
$\dot{x}_i$	is the time derivative of the ith DOF

The equations of motion still contain non-linear elements such as sine and cosine functions. However, the equations of motion must be linear in order to solve the system in the frequency domain. Therefore, the first linearization is the small-angle approximation. For small angles, the $\sin(\phi) = \phi$ and $\cos(\phi) = 1$. After this linearization, higher-order terms and multiplications of DOFs are still present in the equations (e.g. ϕ^2 and $\ddot{\phi} \cdot \phi$). To linearize these terms, small motion amplitudes are assumed. This states that a small value multiplied by another small value is equal to an extremely small value which is close to zero and can therefore be neglected.

Now the equations of motions are linearized so they can be used in the frequency domain analysis. The equations are firstly placed in a matrix format so they are easier to be solved as shown in Equation 3.20 and Figure 3.4. The external force from the waves comes from the RAO which is provided by Van Oord.

$$\begin{bmatrix} m_{11} & \cdots & m_{1j} \\ \vdots & \ddots & \vdots \\ m_{i1} & \cdots & m_{ij} \end{bmatrix} * \begin{bmatrix} \ddot{X}_1 \\ \vdots \\ \ddot{X}_i \end{bmatrix} + \begin{bmatrix} b_{11} & \cdots & b_{1j} \\ \vdots & \ddots & \vdots \\ b_{i1} & \cdots & b_{ij} \end{bmatrix} * \begin{bmatrix} \dot{X}_1 \\ \vdots \\ \dot{X}_i \end{bmatrix} + \begin{bmatrix} c_{11} & \cdots & c_{1j} \\ \vdots & \ddots & \vdots \\ c_1 & \cdots & c_{ij} \end{bmatrix} * \begin{bmatrix} X_1 \\ \vdots \\ X_i \end{bmatrix} = \begin{bmatrix} F_{ext1} \\ \vdots \\ F_{exti} \end{bmatrix}$$

Figure 3.4: Matrix notation of the equation of motions

$$[A] \cdot \ddot{X} + [B] \cdot \dot{X} + [C] \cdot X = F \tag{3.20}$$

Where:

$[A]$	is the (added) mass matrix
$[B]$	is the damping matrix
$[C]$	is the stiffness matrix
F	is the external force vector RAO
$\ddot{X}$	is the acceleration of the DOFs as a vector
$\dot{X}$	is the velocity of the DOFs as a vector
X	is the displacement of the DOFs as a vector

This notation of the DOF is still as a function of time which cannot be used in the frequency-domain analysis. Each DOF and external force can be rewritten to the frequency domain with Equations 3.21-3.24. These equations can be filled in in Equation 3.20.

$$X = \zeta_a \cdot e^{j(\omega \cdot t + \epsilon_x)} \tag{3.21}$$

$$\dot{X} = j \cdot \omega \cdot \zeta_a \cdot e^{j(\omega \cdot t + \epsilon_x)} \tag{3.22}$$

$$\ddot{X} = -\omega^2 \cdot \zeta_a \cdot e^{j(\omega \cdot t + \epsilon_x)} \tag{3.23}$$

$$F = F \cdot e^{j(\omega \cdot t)} \tag{3.24}$$

Where:

X	is the DOF	[-]
X_a	is the DOF for a wave amplitude	[-]
ω	is the wave frequency	[rad/s]
ϵ_x	is the phase difference	[rad]

There is one common multiplier which can be divided away, namely, $e^{j(\omega \cdot t)}$. This leaves $\zeta_a \cdot e^{j \cdot \epsilon_x}$ which includes the phase difference between the waves and the response. This can be rewritten as $\hat{X}_a$ and filled in, in Equation 3.20 which results in Equation 3.25 which is only frequency-dependent. It must be noted that the phase differences should still be considered in the rest of the steps. Equation 3.26 is then used to determine the RAOs of all DOFs. This result has a real and a complex part. Taking the absolute value will give the motion amplitude. However, if any other calculations must be done with the outcome, the value must remain in its complex state to maintain the phase difference. The absolute values may only be taken at the end of the calculations.

$$(-\omega^2 \cdot [A] + j \cdot \omega \cdot [B] + [C]) \cdot \hat{X}_a = [H_{sys}] \cdot \hat{X}_a = F \tag{3.25}$$

$$\hat{X}_a = [H_{sys}]^{-1} \cdot F \tag{3.26}$$

All steps to reach the RAOs for the system are provided in Appendix D. Here a maple script is used to quickly derive the Equations of motions (matrix form). This can now be used for the validation of the OrcaFlex model. This is done by Python of which the script is shown in Appendix F.

3.3.2 Verification

This step focuses on making sure that the equations are providing the expected answers and that the 'hand calculations' can be used for the validation. Determining the natural frequency by hand is a good way to verify the calculations when including all elements as described in the previous subsection. Rolling is chosen to be the investigated for the verification since can directly be derived from the equation of motions. In order to find the natural frequency, Equation 3.27 is used. The trivial solution to this equation is $\hat{X} = 0$. The other solution (natural frequencies, can be found by solving the determinant (which needs to be zero) of the matrix $[C - \omega_n^2 \cdot A]$.

$$[C - \omega_n^2 \cdot A] \cdot \hat{X} = 0 \tag{3.27}$$

Where:

A	is the mass matrix	
C	is the stiffness matrix	
ω_n	is the natural frequency	[rad/s]

An iterative process is required to find the natural frequency for rolling. First a pre-tension and initial frequency, due to frequency-dependent added masses, is chosen for the first iteration. This results in a new frequency which is then filled back in the matrix to determine a new frequency. The resulting frequency did not change anymore (barley any change) after a couple of iterations. This is then deemed to be the natural frequency for rolling. For a 90% pre-tension case, the natural frequency is determined at 0.681 rad/s (9.23 seconds). This value is almost exactly the same as where the peak lies in the RAO plot for rolling in Figure 3.5. This figure is explained in more detail in the next subsection. This proves that the calculations are done accordingly and that the calculations can be validated.

3.3.3 Validation

Firstly, all input parameters are provided by Van Oord. They have knowledge of the offshore industry being a marine contractor. After the model was built, all parameters and elements were checked (face validity) by hydrodynamic engineers of Van Oord to make sure they are correct and if the model is close to reality within the scope of the project.

Next, the 'hand calculations' are validated on if they solve the right equations This is done by comparing the RAO results of the frequency-domain hand calculations and the frequency-domain analysis of the OrcaFlex model. The validation is only done for the 90° wave direction (beam waves) since the hand calculations are in 2D. The other variable is the pre-tension, these are 0, 10, 30, 50, 70 and 90%. The 90% pre-tension is chosen to be discussed in this subsection. The plots of the other pre-tensions are found in Appendix E. The roll, heave and sway RAOs of the feeder are analyzed below.

Roll RAO

Figure 3.5 shows the roll RAO for the feeder. The x-axis shows the incoming wave period and the y-axis the accompanying roll motion in degree amplitude per incoming meter wave amplitude. As one can see, the lines of OrcaFlex and the hand calculations are almost fully on top of each other. This means that the OrcaFlex model is in accordance with the hand calculations for this motion.

There are two distinct peaks visible which represent two different natural periods. The peak of just above 9 seconds is the natural rolling period of the feeder itself. This can be seen from the figure as well as the calculation for the verification in the previous subsection. The peak of around 3 seconds is the natural rolling period of the feeder created by the swinging motion of the heave compensator and crane block. Here, a clear difference between the peaks is visible. This difference is created by the assumption that the crane block is a point mass in the hand calculations instead of an actual crane block as in OrcaFlex. However, the difference in the natural periods is sufficiently small. Therefore, it is stated that OrcaFlex correctly models the roll motion of the feeder. The same holds for the other pre-tensions. However, the peaks for lower pre-tensions are at relatively higher periods due to the decrease in tension.

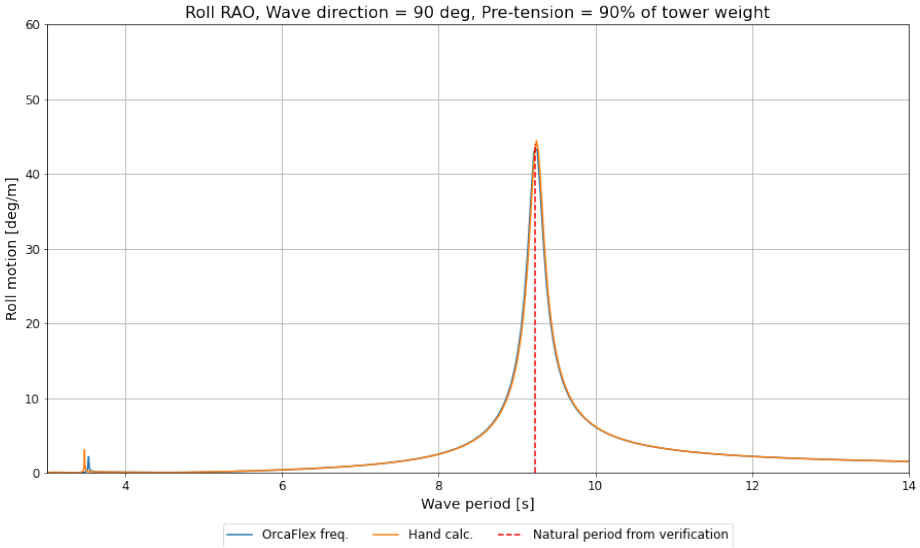

Figure 3.5: Roll RAO validation at 90% pre-tension

Heave RAO

Figure 3.6 shows the heave RAO for the feeder. The x-axis shows the incoming wave period and the y-axis the accompanying heave motion in meter amplitude per incoming meter wave height. The shape of the plot is in line with a normal heave RAO. At small periods, like 4 seconds, the waves have very little impact on the heave motion of the vessel. The longer the period, the more the impact on heave will be. For a free-floating vessel, the RAO will move to 1 m/m (move with the wave amplitude) since the vessel will only interact with that one wave instead of multiple for short periods, as shown in Figure 3.2. In this case, the lines go to roughly 0.9 m/m. This is because the vessel is not free-floating but coupled to the crane.

The lines of OrcaFlex and the hand calculations are the same until roughly 7 seconds of the wave period. For longer waves, the hand calculations show a deficit of roughly 5 centimetres per wave amplitude. This deficit can be explained by the assumption that the crane tip is fixed in the hand calculations while the OrcaFlex model includes the crane stiffness. The stiffness of the crane allows for a more flexible motion of the feeder when the vessel starts moving more with the wave amplitude. However, the deficit is extremely small compared to the draft of the vessel (roughly 1%). Therefore, this is barely noticeable when looking at the complete system and it can be stated that the OrcaFlex model simulates the heave motion accordingly. The same holds for the other pre-tensions. This effect could be included by adding an additional spring term (of the crane tip) to Equation 3.15. This would give an additional DOF since the vertical displacement of the crane tip is independent.

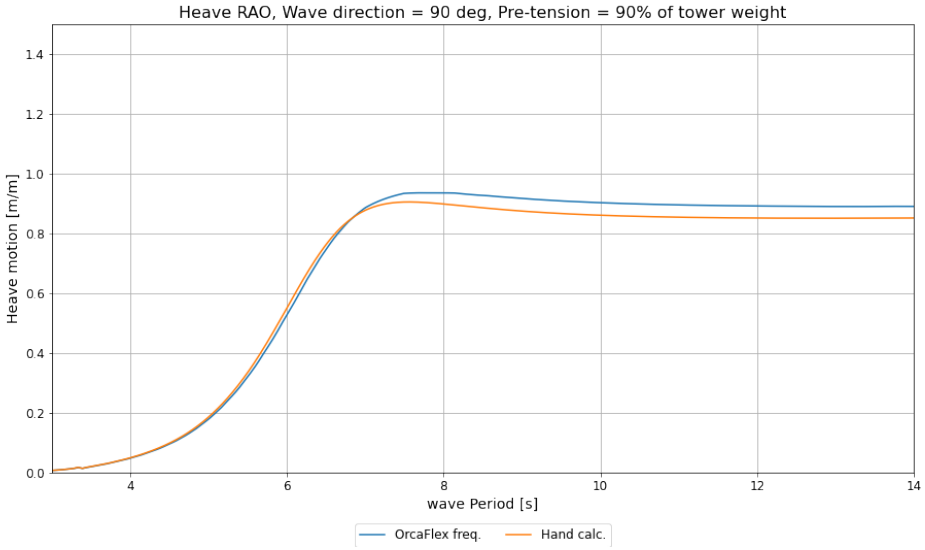

Figure 3.6: Heave RAO validation at 90% pre-tension

Sway RAO

Figure 3.7 shows the swat RAO for the feeder. The x-axis shows the incoming wave period and the y-axis the accompanying sway motion in meter amplitude per incoming meter wave amplitude. The plot shows an increasing line with two peaks at the same periods as the natural periods for roll RAO. It is reasonable that the line is increasing with the period since the system is actually a (quadruple) pendulum. This means that the longer the wave, the longer the horizontal 'sway' force is applied to the feeder and therefore the sway motion becomes larger with increasing periods. This holds for the problem in the study where no mooring is applied (no external counter-acting force). If a mooring system (and second-order waves) would be applied, the sway motion would be restricted since there is a counter-acting force. It is expected that the line would move up much less. On top of this, the mooring system will also have a natural frequency which needs to be considered as well. This natural frequency would be preferred to be out of the range of the incoming wave periods.

Again the lines of the hand calculations show the same behaviour as for the OrcaFlex model. Therefore, it is stated that the sway motion is correctly modelled in OrcaFlex. The same holds for the other pre-tensions.

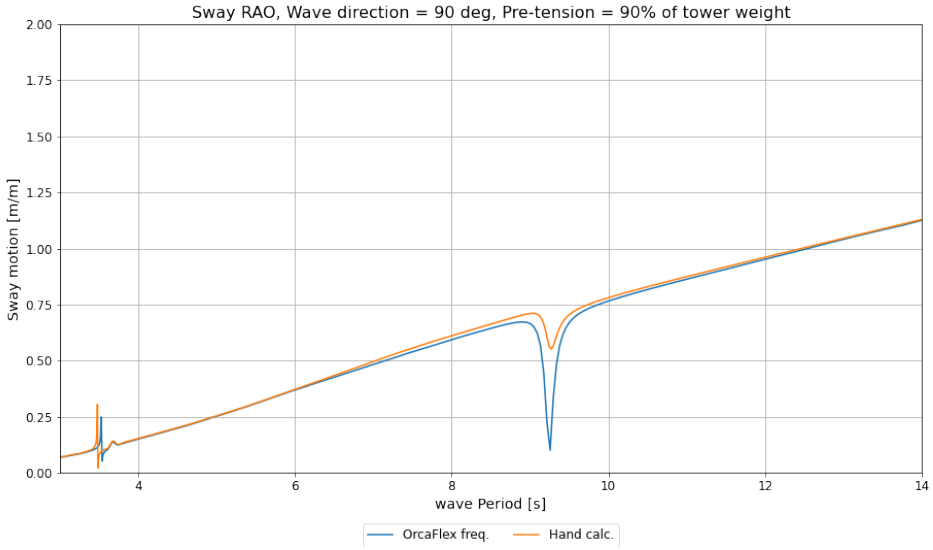

Figure 3.7: Sway RAO validation at 90% pre-tension

3.4 Model run

The previous two sections verify 'hand calculations' and validate these to the OrcaFlex model in order to check where the system correctly calculated/simulated and the assumptions are valid. Next, the frequency-domain analysis (by 'hand calculations') will be used again in order to find the critical wave height in order to reduce the number of simulation cases. Following, the code on how to run the time-domain simulations is explained and the scenarios are run.

3.4.1 Critical wave height

The toppling of the tower is deemed to be the limiting mechanism. This will only occur when the moment at the bottom of the tower is greater than the maximum allowable moment. The first step is to determine the moment at the bottom of the tower. All applied loads are shown in Figure 3.8. As long as toppling does not occur, the tower will move with the feeder. Therefore, the rotation of the tower is the same as for the feeder. The translational accelerations of the tower (at its COG) are dependent on the translational accelerations of the feeder (at the combined COG).

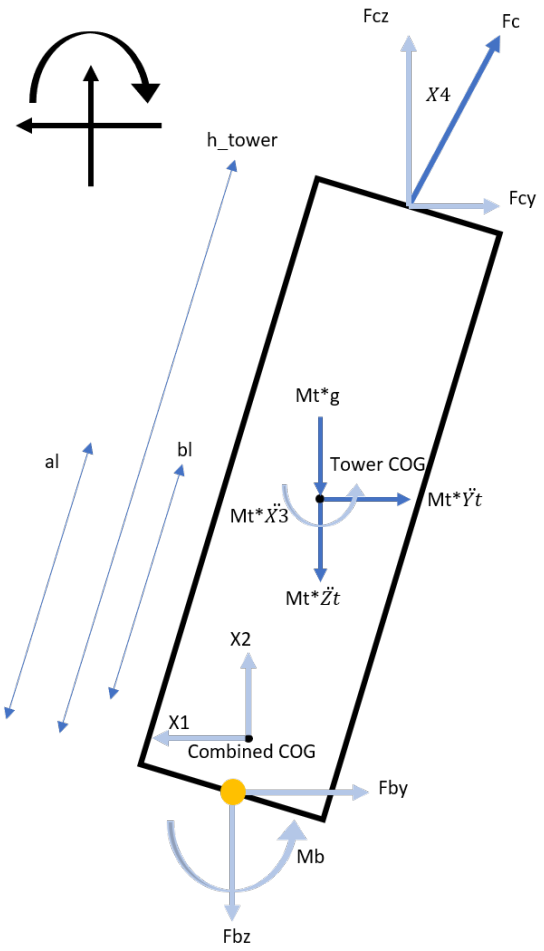

Figure 3.8: Schematic overview of all forces and moments on the tower

The moment is taken around the yellow dot in the figure which is the centre of the bottom of the tower segment. This means that the cable, the accelerations, gravity of the tower and the moment of the sea-fastening (since it is assumed to be fixed) play a role in the moment balance. This sea-fastening moment (Mb) in Equation 3.28 is used to determine the critical wave amplitude. Again, the small amplitude and angle approximation are applied to solve the equation. The parameters that are not fixed are RAOs. Therefore the result will also be a moment RAO (as complex numbers).

$$M_b = -F_{cz} \cdot h_{tower} \cdot sin(X3) + F_{cy} \cdot h_{tower} \cdot cos(X3) - J_{xx} \cdot \ddot{X}3 + m_t \cdot (g + \ddot{Z}_t) \cdot a_l \cdot sin(X3) + m_t \cdot \ddot{Y}_t \cdot a_l \cdot cos(X3) \tag{3.28}$$

Where:

M_b	is the moment that is taken by the sea-fastening	[Nm/m]
F_{cz}	is the vertical cable force	[N/m]
F_{cy}	is the horizontal cable force	[N/m]
h_{tower}	is the height of the tower	[m]
m_t	is the weight of the tower	[kg]
J_{xx}	is the rotational inertia of the tower around the x-axis	[kg· m^2]
a_l	is the distance between the tower COG and the tower bottom	[m]
$X3$	is the rotation of the feeder	[rad/m]
$\ddot{Y}_t$	is the acceleration of the horizontal motion of the tower	[m/s^2/m]
$\ddot{Z}_t$	is the acceleration of the horizontal motion of the tower	[m/s^2/m]

The moment RAO is plotted in Figure 3.9 for both the hand calculation as well as the frequency-domain analysis of OrcaFlex. This is used as an additional check for the validation as well the to gain an understanding of the effect of the moment between the tower and the barge. The figure has incoming waves from 90° and has a pre-tension of 90%. The other pre-tensions are shown in appendix E. Again, the same conclusion about the validation is drawn as in the previous section.

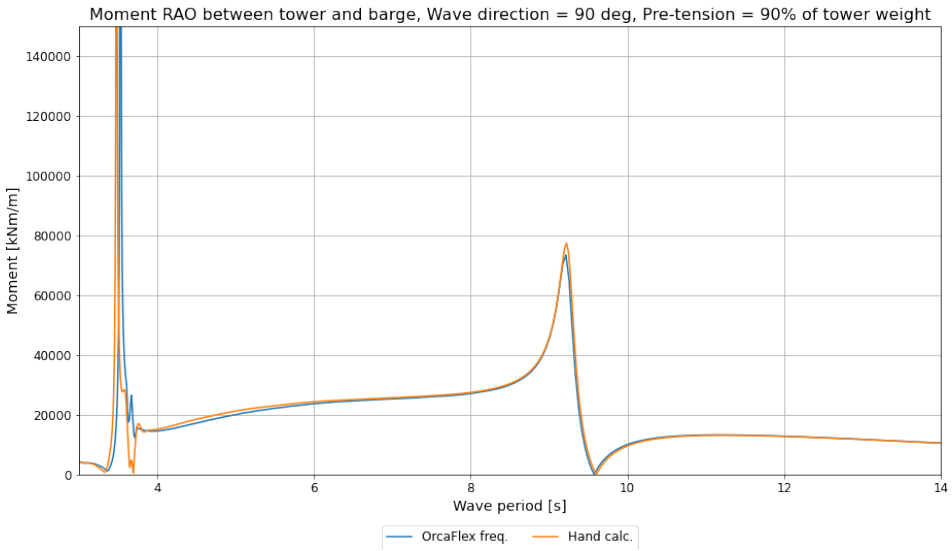

Figure 3.9: Moment RAO validation at 90% pre-tension

A pattern occurs when all pre-tensions are compared to each other, see Appendix E. Both peaks are created due to the rolling natural periods of the feeder and the swinging of the heave compensator. Both peaks move to higher periods when the pre-tension is reduced. This phenomenon is similar to the frequency of a guitar string, the more tension, the higher the frequency (lower period).

When comparing the different pre-tensions, a very interesting phenomenon is found. The moment between the natural frequency peaks is more or less a straight line. The moment per meter wave amplitude (indicated by the lines) is the lowest for the highest pre-tension. This would indicate that the higher the pre-tension is, the better the toppling moment is countered. Therefore, it is expected that toppling occurs when the barge rolls back from a rolling motion while the tower keeps rotating (due to its inertia) instead of moving back with the barge.

The next step is to determine the critical toppling moment. The critical moment occurs when the normal force between the tower and the barge is on the edge (flange) of the tower. The arm for the moment is then a full tower radius and the critical moment is therefore the radius multiplied with the normal force. However, this normal force is under an angle as shown in Figure 3.10. The horizontal and vertical force balances have to be calculated to determine the angled normal force. This is done by Equations 3.29 and 3.30. These forces can then be rotated to determine the normal force as shown in Equation 3.31. The full calculations of these equations are shown in Appendix D.

$$F_{by} = F_{cy} + m_t \cdot \ddot{Y}_t \tag{3.29}$$

$$F_{bz} = F_{cz} - m_t \cdot g - m_t \cdot \ddot{Z}_t \tag{3.30}$$

$$F'_{bz} = F_n = F_{bz} \cdot cos(X3(t)) - F_{by} \cdot sin(X3(t)) \tag{3.31}$$

Where:

F_{by}	is the horizontal force between the barge and the tower	[N]
F_{bz}	is the vertical force between the barge and the tower	[N]
F_n	is the normal force between the barge and the tower	[N]

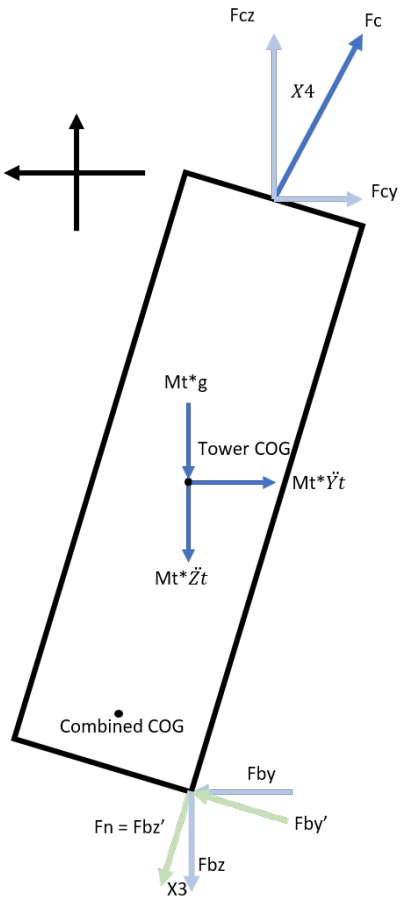

Figure 3.10: Schematic overview of the balance of vertical and horizontal forces

The critical moment is shown in Equation 3.32. This is the simplified equation where a small angle and displacement approximation are used. The normal force contains terms that are constant (the gravity and the pre-tension terms) as well as wave amplitude varying terms such as the (heave compensator-tower) sling stretch as these are in the form of a RAO. In order to determine the max allowable wave amplitude (for regular waves), the critical moment must be equal to the moment between the tower and the barge. This is shown in Equation 3.33. Now the critical wave amplitude per frequency and pre-tension can be determined by Equation 3.34. The critical wave height (h_{lim}) that will be used in the rest of the results is the critical wave amplitude multiplied by 2. For irregular waves, limiting significant wave height must be determined using the iterative loop as described in Section 2.3.

$$M_{crit} = \underbrace{R_t \cdot (1-\alpha) \cdot m_t \cdot g}_{M_{crit-constant}} + \underbrace{R_t \cdot (m_t \cdot (\ddot{L_{c1}} + \ddot{L_{c2}} + \ddot{L_{c3}} + \ddot{L_{sl}}) + c_{c1} \cdot L_{c1}(t))}_{M_{crit-varying}} \tag{3.32}$$

$$|M_b| \cdot \zeta_{lim} = M_{crit-constant} + |M_{crit-varying}| \cdot h_{lim} \tag{3.33}$$

$$\zeta_{lim} = \frac{M_{crit-constant}}{|M_b - M_{crit-varying}|} \tag{3.34}$$

Where:

$\ddot{L_{cn}}$	is the acceleration of the cable/sling extension	[m/s^2]
M_{crit}	is the critical toppling moment	[Nm]
c_{c1}	is the heave compensator-tower sling stiffness	[N/m]
α	is the pre-tension percentage of the load	[%]
R_t	is the radius of the tower	[m]
ζ_{lim}	is the limiting wave amplitude	[m]

Figure 3.11 shows the maximum allowable wave height (in regular waves) per frequency and pre-tension for beam waves. The x-axis shows the wave period and the y-axis the limiting wave height. Each colour represents a different pre-tension. The natural periods of each system (different pre-tension) are clearly visible since the limiting wave height almost reaches zero meters. Transparent and clear lines of each colour are shown. They represent respectively the h_{lim} lines with and the h_{lim} lines without $M_{crit-varying}$ terms. The transparent lines are not precisely following the clear ones due to these terms. Especially the sling stiffness causes these effects since the extension accelerations are relatively small. The sling gets slightly less or more extended to increase or decrease the normal force. The higher the pre-tension, the smaller the humps since the varying extension force becomes relatively smaller than the pre-tension force.

Before was stated that the lowest toppling moment between the natural frequency peaks is for the highest pre-tension. However, also between the peaks, the lowest allowable wave height is found for the highest pre-tension. This is caused by the smaller vertical force (F_{bz}) due to the higher pre-tension. The lower the pre-tension, the more favourable the wave height will become. This plot can now be used as a critical line in order to reduce the number of time-domain simulations.

As explained in Section 3.2, the response for rolling reduces when the wave direction changes more to head waves while the response for pitching increases. This also changes the outcome of the limiting wave height when looking into 3D instead of 2D since both rolling and pitching should be considered. It is hard to provide proof of what will happen to the results without doing the calculations in 3D for regular waves since these are dependent on directional/period-specific moment RAO values. What can be stated is that the lower the moment RAO, the higher the limiting wave height will be. Natural frequency values should be avoided as the limiting wave height plots show values close to zero at these frequencies.

Irregular waves are a better representation of the real world. However, as explained before, due to time constraints of the project, these can only be investigated and discussed on a qualitative level. The response spectrum is calculated by multiplying the RAO squared with the wave spectrum. The significant response is the area below the response spectrum. The smaller the response spectrum, the lower the significant response, and the higher the limiting significant wave height. The natural frequency for the RAOs can be significantly high. The significant response could therefore be high if the natural frequencies encounter some energy from the wave or are near at or close to the peak frequencies of the wave spectrum. Ideally, the peak frequencies (most energetic waves) of the wave spectrum are (far) away from the natural frequencies of the system (lots of wave energy outside the natural frequency range) while the natural frequency does not encounter any wave energy (natural frequency out of wave spectrum). This is hard to reach since the system should undergo iterative design steps to change the system's natural frequencies to create a more ideal solution.

The moment RAO that is used for toppling for the 90% pre-tension case in beam waves, shown in Figure 3.9, indicates that the natural frequencies are around 3 and 9 seconds (visually based). With some margin, it is desired to have wave energy peaks of the double peak spectrum between 4 and 8 seconds or after 10 seconds to avoid the natural frequencies. Section 2.3 describes the peak periods of the wind waves in the U.S. between 4 and 6 seconds, which is good for the response spectrum looking at the above-mentioned statement. However, the swell waves range between 4 and 11 seconds. Within these periods, the natural roll frequency can be found (around 9 seconds). When the peak period for swell is around this value, the response of the vessel could be significant and the limiting significant wave height very low. When lowering the pre-tension, the left natural period, caused by the swinging motion of the elements in the crane as well as the right one that is caused by rolling, shifts to higher periods (so lower frequencies). This could worsen the results (limiting significant wave height) since this dives the left natural frequency into wind wave peak periods while the right natural frequency remains within the swell wave range.

The effect of directional spreading of wind and swell waves as well as the system in 3D is not considered in these statements. Pitching will start playing a role when the waves are not coming from the 90° direction. The closer the direction goes to head waves, the wider the vessel pitch RAO becomes and the narrower the vessel roll RAO as shown in Appendix C. However, the peak of the natural frequency for rolling remains much higher than for pitching. This means that the response for pitching could also be lower depending on the natural frequency and peak periods. It is expected that the natural frequency for pitching is higher than the rolling natural frequency since the barge is more prone to rolling than pitching (stiffer for pitching).

The natural frequencies (visually based on the plots) for pitching with zero pre-tension range from roughly 0.13 (60° incoming direction) to 0.1 Hz (0° incoming direction) while the rolling natural frequency is around 0.9 Hz for all directions. Both rolling and pitching are expected to be within the swell wave peak frequency range. The pitching natural frequencies are closer to the wind wave peak frequency range and could even be within this range when pre-tension is increased. So wind waves that cause pitching should be avoided. However, the natural frequency peak itself is relatively low (compares to the rolling peak) which could be beneficial to the results of the limiting significant wave height.

The barge can be positioned (if the installation vessel allows it) in such a way that the swell waves, with a narrow spreading, are coming from a favourable direction, increasing the workable limits. For high pre-tensions, pitching would be at the lower side of the swell waves while rolling is near the mid of the potential swell waves. The lifts after the first one should be considered as well since the load will change for the other components. The $\overline{GM}$ is expected to increase when a tower segment is removed, meaning a 'stiffer' vessel which leads to lower higher natural frequencies for roll and pitching. This potentially moves the pitching natural frequency below the swell waves while the rolling natural frequency is still in it. Therefore, the vessel should be positioned in line (with its bow or stern) with the swell waves. The wind wave spreading is much larger, making it more difficult to position the vessel based on wind waves. Extending this research with irregular waves, including directionality and the double peak spectrum is highly recommended to quantitatively prove these statements.

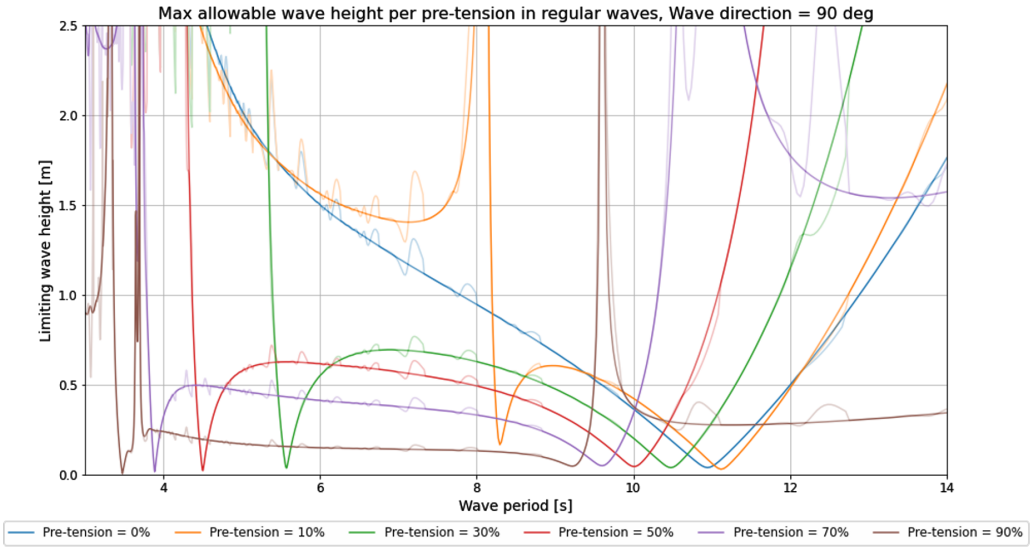

Figure 3.11: Maximum allowable wave height

3.4.2 Simulation cases

Since the hand calculations are done in 2D and the time is limited, only 90° incoming waves are considered in the simulations as explained before. The critical wave height is determined in regular waves. Therefore, regular waves will also be used in the time-domain simulations. The effect of irregular waves on the results is explained above but will further be explained in the results. The wave period must be within the range of periods that are described in Section 2.3, between 4-11 seconds. Due to time constraints, only one incoming wave period can be simulated in time-domain. The chosen period must be below roughly 8 and above 6 seconds to avoid the behaviour of the natural periods (small results) of the system for all pre-tensions according to figure 3.11. The middle is chosen to be simulated in time-domain, which is at a wave period of 7 seconds.

This leaves wave height, pre-tension and release timing as variables. The limiting wave height for the different pre-tensions at 7 seconds is shown in Table 3.1. The values, especially for the higher pre-tensions are extremely low (e.g. 10 cm for 90%). For irregular beam waves, the results (H_{m0}) are expected to be higher at a T_p of 7 seconds since this is out of the incoming peak periods for wind waves is lower and the natural periods of the (barge/tower/crane) system. However, depending on the swell wave peak periods, the outcome could worsen since this has a wider range. The effect of directionality has been explained above.

The h_{lim} values are calculated using Equations 3.32 to 3.34. The equations show that h_{lim} is dependent on three elements, pre-tension (α), RAOs and base radius (R_t) (tower segment radius). For the direct installation method as described in Section 2.1, the base radius is roughly equal to the tower segment radius. These Equations can also be used to determine the limiting wave height for the indirect method where a base frame is used by using three assumptions. The first two are that the mass (m_t) and the RAOs do not differ from the direct method. The third one is that the $M_{crit-varying}$ part in the equations is neglected since this barely plays a role in the outcome. This leaves one variable in the equation that can change, which is the base radius. The limiting wave height for the indirect method thus scales linearly with the limiting wave height as shown in Equation 3.35.

$$h_{lim-indirect} = h_{lim-direct} \cdot \frac{R_{base-frame}}{R_t} \tag{3.35}$$

Table 3.1: Limiting wave height per pre-tension at 7 seconds wave period

Pre-tension [%]	**Wave height [m]**
0	1.15
10	1.35
30	0.65
50	0.55
70	0.35
90	0.10

Pre-tension is an important variable in this research. Therefore, all pre-tensions, as described before, will be considered. Two wave heights are chosen to be simulated. This first one is at the critical wave height determined by the hand calculations in the frequency domain. It is expected that the tower (will not topple or) barely topples at this height due to non-linear effects which the time-domain simulations take into account. On top of this, another wave height, which is 20 cm higher than the critical wave height, will be simulated in case the tower does not topple or in order to find out if the toppling mechanism changes.

The release timing knows three different options. The first release timing is at the top of the heave motion of the feeder. Here the accelerations are the largest and toppling is expected to occur moments after release. The second timing is when the heave motion is at the mean line and moving upward. The third release timing is the moment when the heave motion is at its lowest. These timings are visualised in an example of a sine wave which is representative of a regular wave. The heave motion is chosen as a release indicator since this, based on practice of Van Oord is also used to determine the ideal lift-off timing. The release and lift-off timing can then easily be linked.

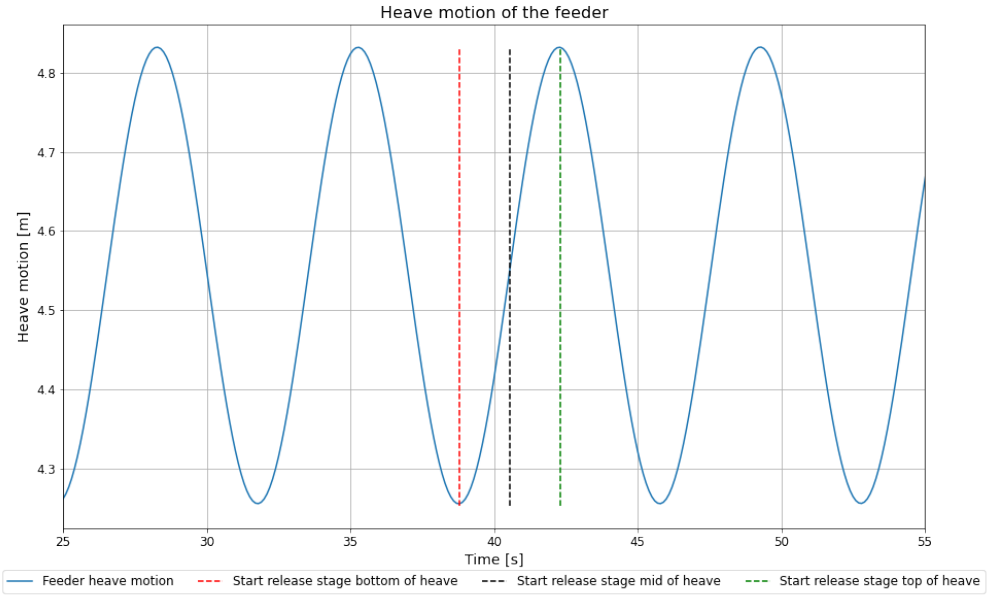

Figure 3.12: Example of different release moments according to the cases

In total, 36 time-domain simulations need to be run, checked and analyzed. To sum it up, 6 different pre-tensions, 2 different wave heights and 3 different release timings for the wave period of 7 seconds and a wave direction of 90 degrees.

Table 3.2: Time-domain simulation cases

Case #	**Pre-tension [%]**	**Wave height [m]**	**Release timing**	**Case #**	**Pre-tension [%]**	**Wave height [m]**	**Release timing**
1	0	h_{lim}	Top of heave	**19**	50	h_{lim}	Top of heave
2	0	h_{lim}+0.2	Top of heave	**20**	50	h_{lim}+0.2	Top of heave
3	0	h_{lim}	Mid of heave	**21**	50	h_{lim}	Mid of heave
4	0	h_{lim}+0.2	Mid of heave	**22**	50	h_{lim}+0.2	Mid of heave
5	0	h_{lim}	Bottom of heave	**23**	50	h_{lim}	Bottom of heave
6	0	h_{lim}+0.2	Bottom of heave	**24**	50	h_{lim}+0.2	Bottom of heave
7	10	h_{lim}	Top of heave	**25**	70	h_{lim}	Top of heave
8	10	h_{lim}+0.2	Top of heave	**26**	70	h_{lim}+0.2	Top of heave
9	10	h_{lim}	Mid of heave	**27**	70	h_{lim}	Mid of heave
10	10	h_{lim}+0.2	Mid of heave	**28**	70	h_{lim}+0.2	Mid of heave
11	10	h_{lim}	Bottom of heave	**29**	70	h_{lim}	Bottom of heave
12	10	h_{lim}+0.2	Bottom of heave	**30**	70	h_{lim}+0.2	Bottom of heave
13	30	h_{lim}	Top of heave	**31**	90	h_{lim}	Top of heave
14	30	h_{lim}+0.2	Top of heave	**32**	90	h_{lim}+0.2	Top of heave
15	30	h_{lim}	Mid of heave	**33**	90	h_{lim}	Mid of heave
16	30	h_{lim}+0.2	Mid of heave	**34**	90	h_{lim}+0.2	Mid of heave
17	30	h_{lim}	Bottom of heave	**35**	90	h_{lim}	Bottom of heave
18	30	h_{lim}+0.2	Bottom of heave	**36**	90	h_{lim}+0.2	Bottom of heave

Coding python

Python is used to execute the equations, create the graphs and to run the simulations. Python is open source and can therefore be used by everyone. Two scripts are created for the frequency and time-domain simulations. These scripts can easily be looped to run all cases back to back.

The Python code for the frequency-domain analysis is provided in Appendix F. The result of these runs are the RAOs and the limiting wave heights as shown above. The OrcaFlex model is used to determine the length of the crane cables for the frequency-domain analysis. The OrcaFlex API in python is used to run the statics of the model and to retrieve the initial crane cable length. The API creates an interface between Python and OrcaFlex, This is useful in case multiple simulations of the same system (with multiple changing variables) have to be run like in this research. The critical wave height is determined for every investigated pre-tension and all frequencies. The run time for this, where the start is creating the RAOs and the end the limiting wave height is roughly 1 hour. The steps of the frequency-domain analysis are shown in a simplified scheme in Figure 3.13.

The output of the frequency-domain model (limiting wave heights) is then used as input for the time-domain model in OrcaFlex. The python code to run the simulation (via the API) can be found in the same appendix. Load RAOs are used to implement the effect of the pre-tension in the simulation. This is not included when using displacement RAOs. A parent-child configuration is used since there is a transient element, namely, the release. This type of configuration is used when for example a constraint is first fixed and partly released (not all DOF) at a specific stage. The release timing must firstly be found. Since regular waves are used, the heave motions have the shape of a sine. The first part of the code is a normal simulation where the tower is fixed. This simulation is used to find the designated release moment, In this case, the 6^{th} heave peak (minus a period depending on the case) after the wave build-up period. The wave build-up period is required since the motions of the vessel are not fully developed due to the inertia when the first wave is encountered).

Figure 3.13: Simplified schematic overview of the frequency-domain analysis steps

The second simulation is the parent simulation where again the wave build-up period is used and the period until the release. The simulation will stop and all data is stored. Then the child simulation will start with the initial input being the last data points of the parent simulation. This provides a smooth transition from fixed to partly loose (the tower is not able to slide, only topple). Since the regular wave has a period of 7 seconds, the mid and bottom heave release is respectively at 1.75 and 3.5 seconds before the top is reached.

Twelve different measurement points called support points, are used to determine whether the tower starts to topple. The location of these points are displayed in Figure 3.14. These points are connected to the tower and the distance between the tower and the contact points of the barge can be retrieved via OrcaFlex. A support point is not directly loose from the barge as the distance (for a specific point) becomes larger than zero. After discussions with the hydrodynamic engineers of Van Oord, a threshold is set at 2mm due to potential numerical errors in OrcaFlex and the fact that the tower stands on the deck of the barge which is modelled with a stiffness.

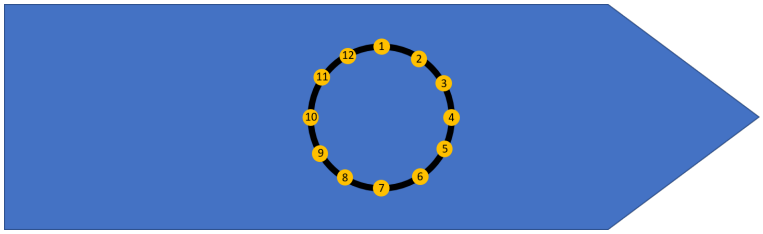

Figure 3.14: Support point locations on the tower (out of scale)

Now the simulation model is verified and validated and the time-domain simulation code is set, the cases can be run and the results analyzed in the next chapter. Proof that the tower does topple when going over the critical wave height is provided in Section 4.2/ Only running these 36 cases took roughly 3-4 hours which is significantly more than the 1 hour for all frequency-domain simulations, showing the time-efficiency of frequency-domain simulations. The steps of the time-domain analysis are shown in a simplified scheme in Figure 3.15.

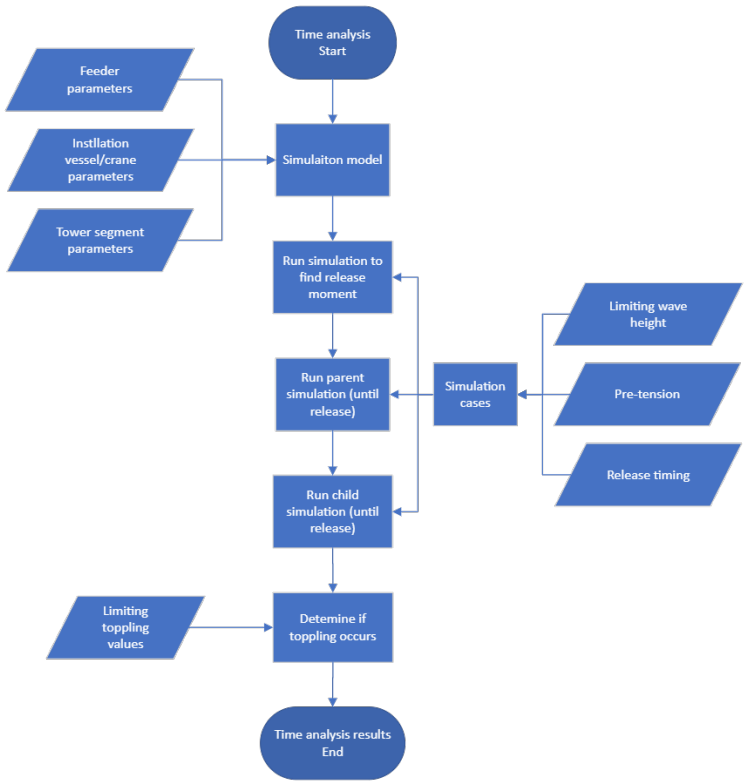

Figure 3.15: Simplified schematic overview of the time-domain analysis steps

Chapter 4: Results

This chapter covers the results of the simulation cases which are explained in the previous chapter. First, an analysis of the snap loads and accidental lift-offs is performed being two of the three failure mechanisms. Next, the toppling failure mechanism is investigated for the cases where snap loads and accidental lift-offs not occur.

4.1 Snap loads

As explained before, snap loads occur when the sling or cable (with zero tension) suddenly experiences a significant tension which could lead to a failure in the sling or cable. This can already be investigated before the actual release of the tower. OrcaFlex provides the results of the tension for the simulated time. The sling between the heave compensator and the tower is used to determine the potential snap loads.

Figures 4.1 to 4.3 show the tension on the y-axis and the time on the x-axis. The pre-tension is increased from 0 - 30%. Each plot has three lines where the horizontal one is the static pre-tension level for that case. The other two lines are the tension results for the cases with the limiting wave height and the wave height+0.2m.

The tension in the sling drops to zero for the cases where 0 and 10% pre-tension is used. They also show a very sharp inclination in tension which indicates that snap loads occur. The lines go from slack to tight. At 30% pre-tension, the graph shows fluent (sinusoidal) behaviour around the static pre-tension. Additionally, the tension does not reach zero which indicates that the sling does not go slack. The sinusoidal motion of the tension can be explained by the heave and the roll motion of the vessel. This leads to a fluctuating tension around the static pre-tension. Higher pre-tensions show the same behaviour as the 30% pre-tension as shown in Appendix G.1.

The reason for snap loads to occur is the amount of pre-tension used. The plots show that, for these cases used, a minimum of 30% pre-tension is required to allow the tension fluctuation. This removes the 0 and 10% cases for the rest of the results because snap loads is the failure mechanism. It is expected that the snap load results will not change when using other periods in regular waves. The same is expected for irregular waves and directionality since the cause of snap loads is the low pre-tension, slings can easily go slag.

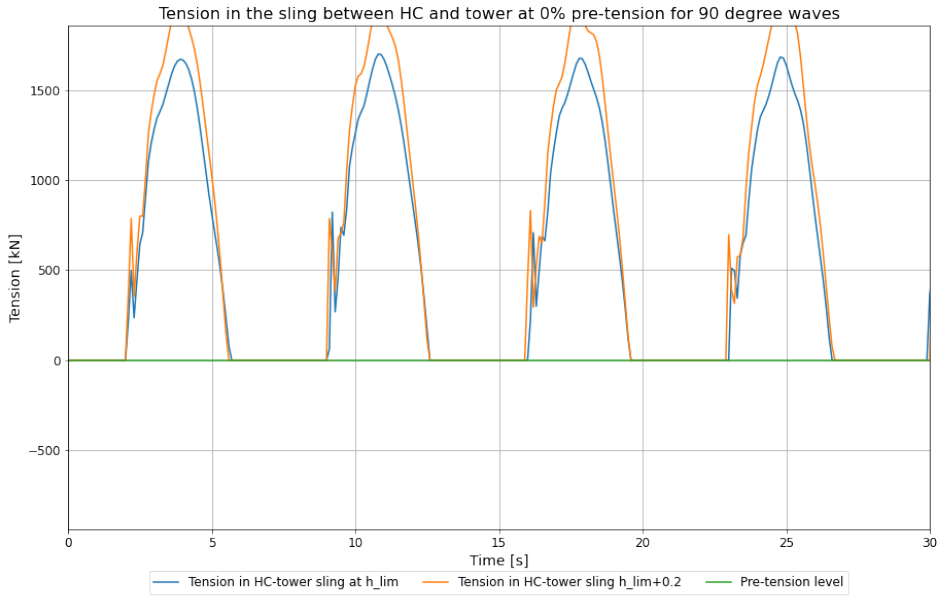

Figure 4.1: Tension in the lowest sling at 0% pre-tension

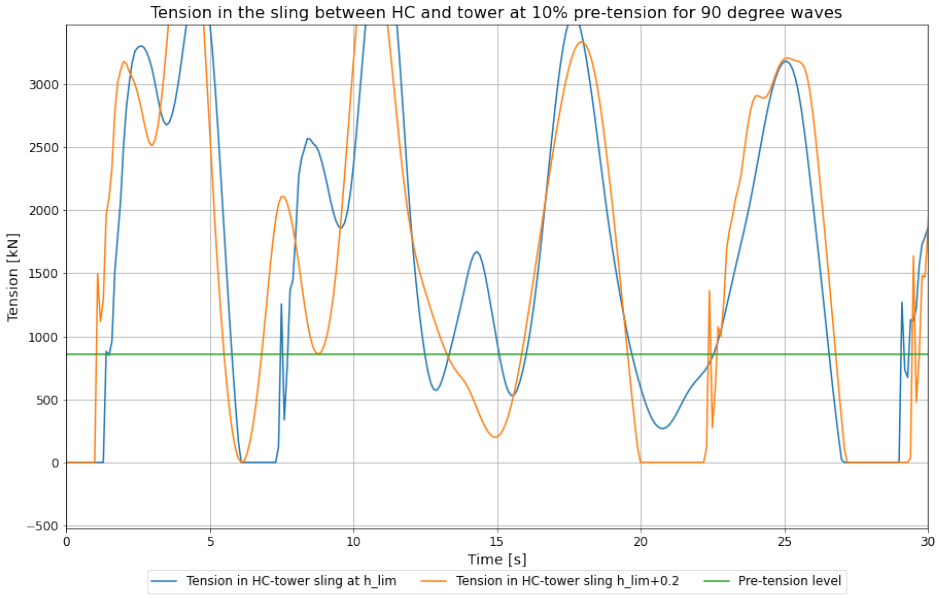

Figure 4.2: Tension in the lowest sling at 10% pre-tension

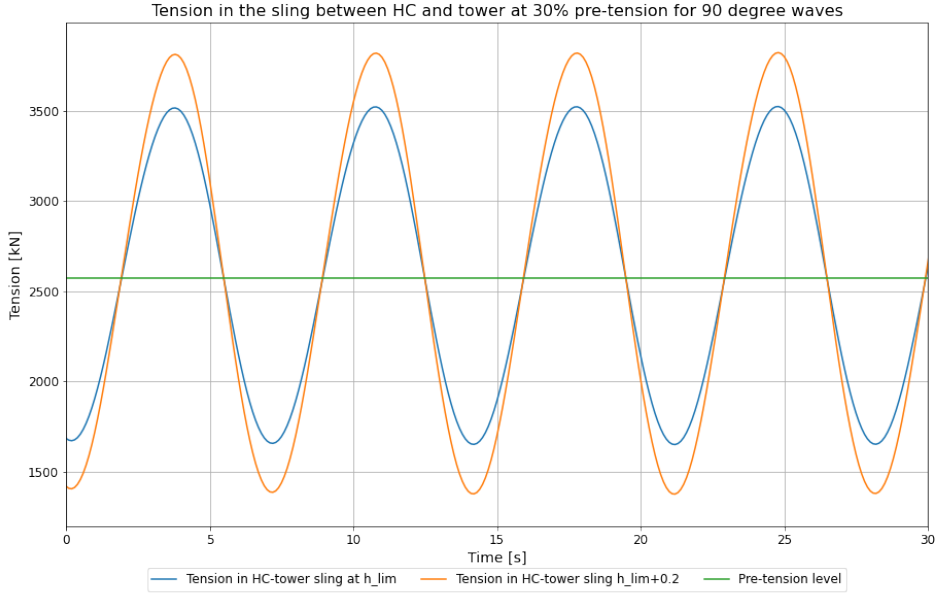

Figure 4.3: Tension in the lowest sling at 30% pre-tension

4.2 Accidental lift-offs

An accidental lift-off occurs when the tower fully loses contact with the barge before the actual lift takes place. Based on the results of OrcaFlex, the time it takes for a support point to come loose (as defined before) from the barge is determined. First, the results of the cases from 30% and higher pre-tension at h_{lim} are discussed. this will then be followed by a discussion about the same cases but for h_{lim}+0.2m.

Tables 4.1 to 4.3 show the results for the cases at h_{lim}. Each value in a cell is the number of seconds it takes (after the release) for a support point to lose contact. The support point does not come loose from the barge if the call is empty. For an accidental lift-off to be found, all support points must be loose at roughly the same time. Most cells are empty, indicating that accidental lift-offs will not occur in these cases.

The tables do show some values that hint that the tower could topple. However, this is only for points (often) 1, 2 and 12, which are located next to each other. This means that these points just exceed the threshold. The same holds for point 7 in Table 4.2 since this is at a much later stage than the others. These results can also be explained by the fact that h_{lim} is right at the edge for when toppling starts to occur according to the hand calculations.

Table 4.1: Time [s] for a support point to loose contact with barge at h_{lim}, bottom of heave

Support point #	**1**	**2**	**3**	**4**	**5**	**6**	**7**	**8**	**9**	**10**	**11**	**12**
30% pre-tension	0.7	0.8					12					0.8
50% pre-tension	0.8	0.9										0.9
70% pre-tension												
90% pre-tension												

Table 4.2: Time [s] for a support point to loose contact with barge at h_{lim}, mid of heave

Support point #	**1**	**2**	**3**	**4**	**5**	**6**	**7**	**8**	**9**	**10**	**11**	**12**
30% pre-tension	6.6	19.9										19.9
50% pre-tension	6.5											
70% pre-tension												
90% pre-tension												

Table 4.3: Time [s] for a support point to loose contact with barge at h_{lim}, top of heave

Support point #	**1**	**2**	**3**	**4**	**5**	**6**	**7**	**8**	**9**	**10**	**11**	**12**
30% pre-tension	4.3	4.5										4.5
50% pre-tension	4.5											
70% pre-tension												
90% pre-tension												

Now, the results of the h_{lim}+0.2m are analysed based on Tables 4.4 to 4.6. Here, (almost) all cells have a value, meaning, an accidental lift-off or toppling occurs. None of the pre-tensions have similar values for all support points. This indicates that accidental lift-offs for all cases do not occur. This is confirmed by analysing the tension in the lowest sling (in Appendix G.1) because none of the values (lines) for all cases reach the total load of the tower. The same result is expected for the other periods as well as when irregular waves are considered. This expectation can be explained by the tension in the lowest. Again, This is a pre-tension-related failing mechanism. Increasing the pre-tension even higher than 90% could create accidental lift-offs.

However, there is an interesting pattern visible which does indicate toppling. Since beam waves are used, rolling is the dominant rotational motion. Therefore, it stands to reason that either support point 1 or 7 comes loose first (depending on the timing) which is confirmed by the tables for all cases. It is also logical that the points around the other centre line (points 4 and 10) have larger values since these are the 'pivot' points for the expected toppling motion. This is further analysed in the next section.

Table 4.4: Time [s] for a support point to loose contact with barge at h_{lim}+0.2m, bottom of heave

Support point #	**1**	**2**	**3**	**4**	**5**	**6**	**7**	**8**	**9**	**10**	**11**	**12**
30% pre-tension	0.6	0.6	0.7	8.3	3.9	3.7	3.6	3.7	5.4	8.3	0.7	0.6
50% pre-tension	0.6	0.6	0.7	1.3	3.9	3.8	3.8	3.9	4	1.3	0.7	0.6
70% pre-tension	0.6	0.7	0.8	1.2	4.2	2.8	2.8	2.8	4.2	1.2	0.8	0.7
90% pre-tension	0.6	0.6	0.7	1	3.3	3.2	3.2	3.2	3.3	0.9	0.7	0.6

Table 4.5: Time [s] for a support point to loose contact with barge at h_{lim}+0.2m, mid of heave

Support point #	**1**	**2**	**3**	**4**	**5**	**6**	**7**	**8**	**9**	**10**	**11**	**12**
30% pre-tension	5.3	5.3	5.6	13.2	10.4	2.8	2.8	2.8	16.2	13	5.5	5.3
50% pre-tension	5.4	5.4	5.8	20.3	9.1	2.8	2.8	2.8	9.1	20.3	5.6	5.4
70% pre-tension	5.6	5.6	5.8	6.1	8	2.8	2.8	2.8	8.1	6	5.8	5.6
90% pre-tension	5.4	5.4	5.4	3.6	3.2	3	3	3	3.2	3.5	5.4	5.4

Table 4.6: Time [s] for a support point to loose contact with barge at h_{lim}+0.2m, top of heave

Support point #	**1**	**2**	**3**	**4**	**5**	**6**	**7**	**8**	**9**	**10**	**11**	**12**
30% pre-tension	4.5	4.6	11.3	11.7	14.4	0.8	0.7	0.8	14.4	11.7	11.3	4.6
50% pre-tension	4	4.4	11.2		14.4	0.8	0.7	0.8	14.5		11.2	4.3
70% pre-tension	3.7	3.8	4	4.7	7.7	0.9	0.8	0.9	7.7	4.6	4	3.8
90% pre-tension	3.7	3.7	3.7	1.9	1.5	1.3	1.2	1.3	1.5	1.9	3.7	3.7

4.3 Toppling

As shown and explained in the previous section, toppling does occur. In this section, plots of the load cases where 90% pre-tension is used are shown. Discrepancies with the other pre-tension cases (30, 50 and 70%) will be discussed and shown if necessary. All plots can be found in Appendix G.

4.3.1 Heave motion results

Figures 4.4 to 4.5 show the heave motion of the feeder and the tower for the cases at h_{lim} and h_{lim}+0.2m. The horizontal axis shows the time and the vertical axis the heave motion at the bottom centre of the tower with respect to the water level (Therefore, fluctuation around 4.68m). It is directly visible that the heave amplitude is greater for the larger wave height. These three plots indicate the release timing as explained before, at the bottom, mid and top of the heave motion. These are indicated by the vertical red dashed line (as it is in all result plots). The black vertical dashed line indicated the moment the tower starts toppling as defined by the threshold. This line only applies to the h_{lim}+0.2m cases since the other cases do not indicate a clearance.

The difference in disconnection times after the release for the shown cases are also clearly visible (also provided in the timetables). This effect will be explained in the next subsection. From these plots, it is not clearly visible if the tower actually topples at the disconnection line and how it will (direction-wise). This will also be explained in the next subsections. However, it is clearly visible that after more than one heave period, the tower topples back and forth and even slams against the barge which is indicated just before the 50-second mark by the hump at the peak of the red line.

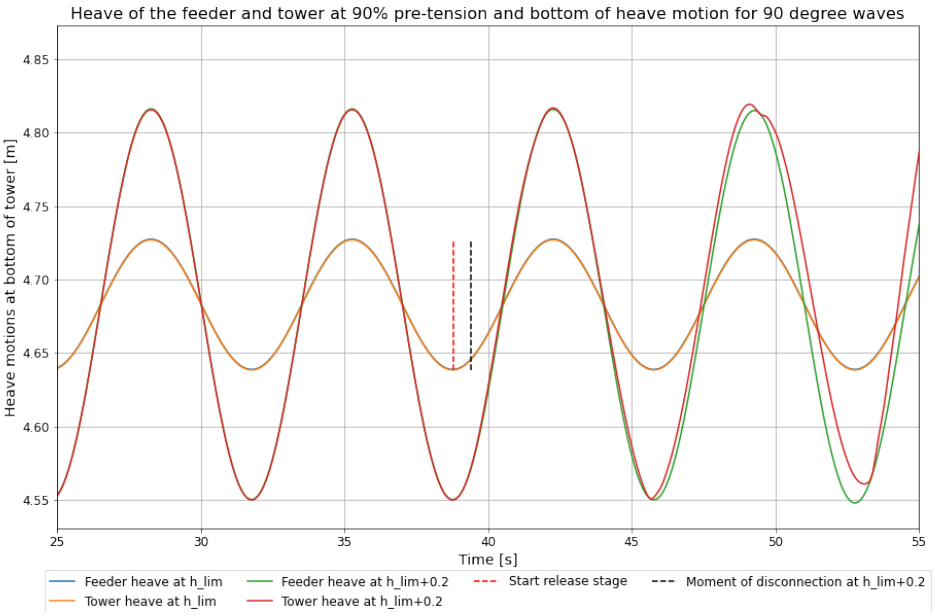

Figure 4.4: Heave motion at 90% pre-tension, beam waves and release bottom of heave

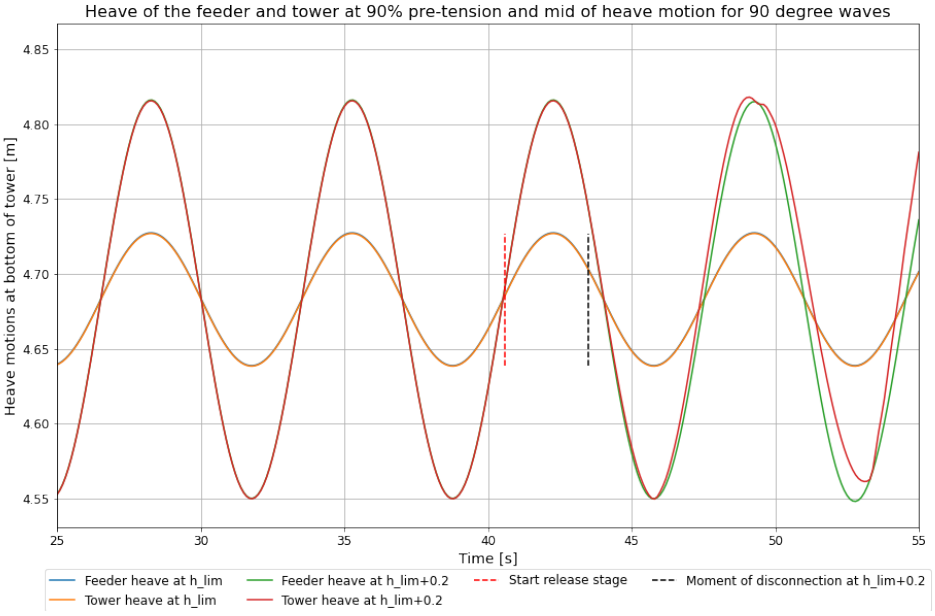

Figure 4.5: Heave motion at 90% pre-tension, beam waves and release at mid of heave

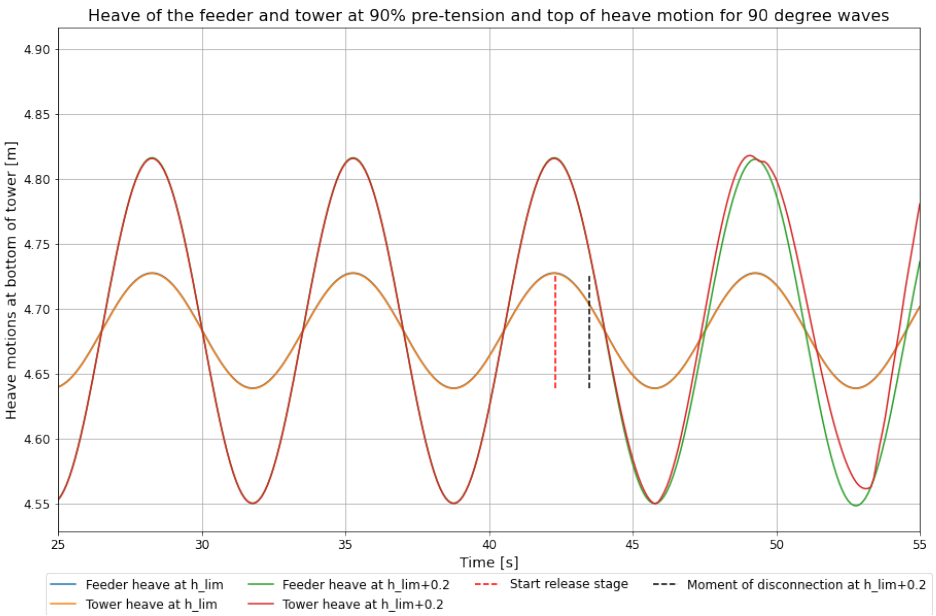

Figure 4.6: Heave motion at 90% pre-tension, beam waves and release at top of heave

4.3.2 Rotation results

Next, the roll motion of the tower and feeder (at 90% pre-tension) are analysed by means of Figures 4.7 to 4.9. Here the y-axis shows the rotations in degrees. The lines are the same as explained in the previous subsection. Before the release, the plots show clear sinusoidal behaviour. After the release, this changes.

All three plots show that the tower will disconnect around (or just after) the peak of the rotation. For both the bottom and top release cases, the release is just before reaching the maximum roll displacement. At this point, the feeder already started decelerating the rotational motion. The max deceleration is reached at the top of the rotation motion. The tower, as shown in the plots, keeps rotating while the feeder starts or already is rotating back. It cannot keep up with the accelerations. This indicates that the tower segment initially topples due to its inertia. The toppling time after release as shown in the previous tables is extremely short (less than one second) due to these reasons. The accelerations for the h_{lim} cases are lower which is the reason the tower will not topple here.

When the tower is released (mid-heave) after it already started accelerating back, the tower remains on the barge until the next rotational deceleration peak is reached. Here, the tower will topple again due to its inertia. This explains why the disconnection time for the mid-heave release is much larger than for the others. These findings hold for all analysed pre-tensions. This means that the pre-tension does not/barely affects the duration between release and disconnection (toppling). These same findings are expected to hold for other periods than 7 seconds in regular waves (with their corresponding wave heights) as well as irregular waves since the toppling mechanics is inertia driven. The limiting significant wave height per peak period is expected to differ from the regular waves as explained in Section 3.4.

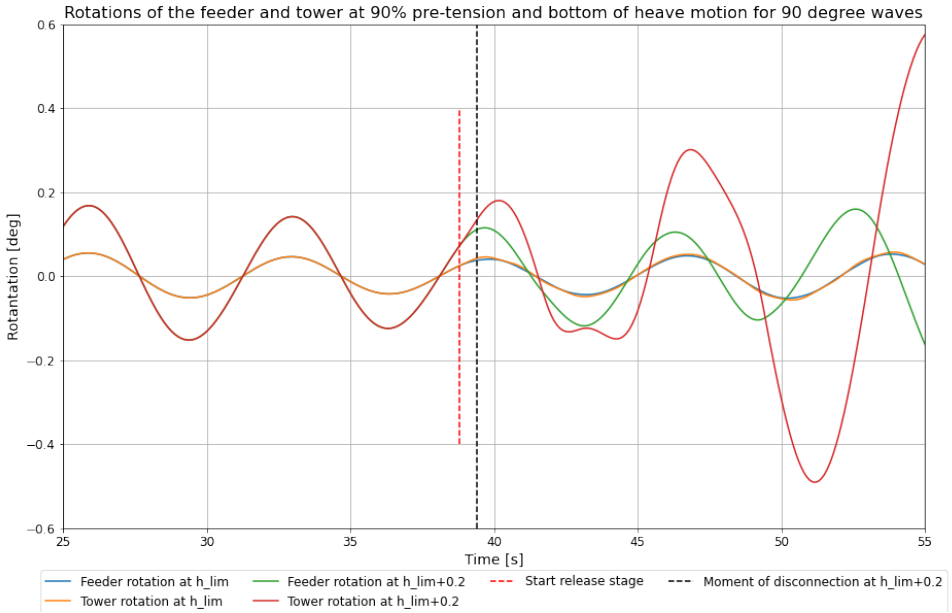

Figure 4.7: Tower and feeder x-axis rotations at 90% pre-tension, beam waves and release at bottom of heave

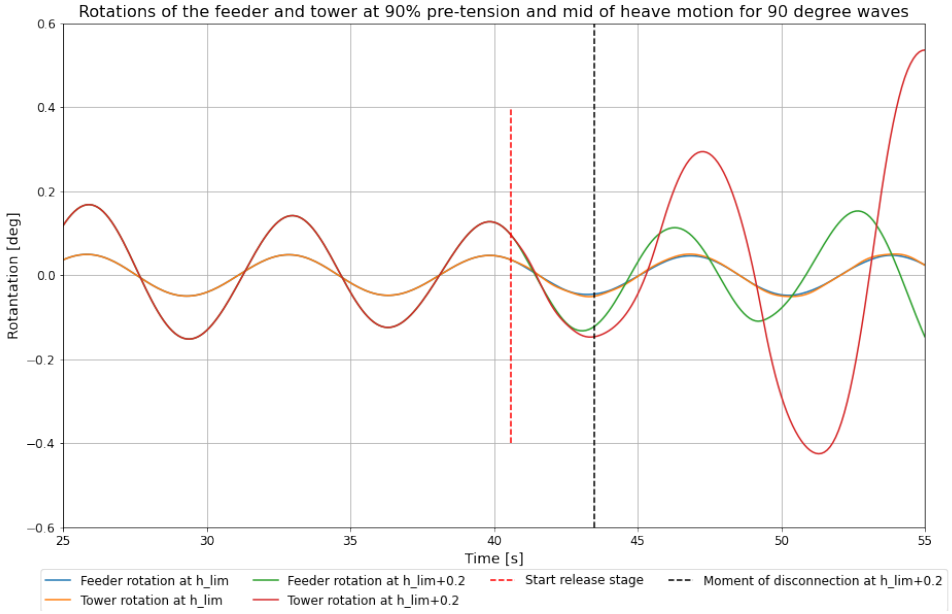

Figure 4.8: Tower and feeder x-axis rotations at 90% pre-tension, beam waves and release at mid of heave

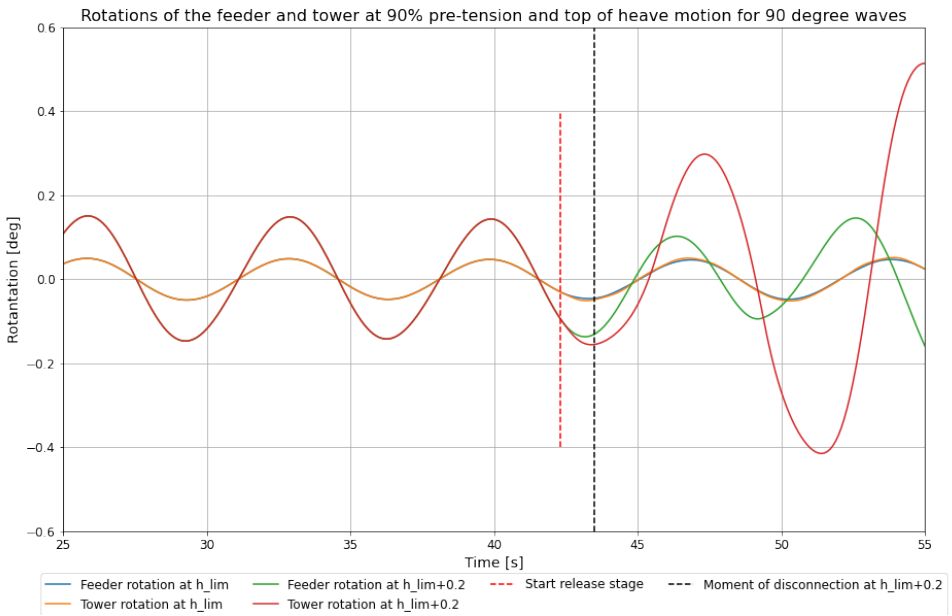

Figure 4.9: Tower and feeder x-axis rotations at 90% pre-tension, beam waves and release at top of heave

4.3.3 Disconnection

Next, the actual disconnection as well as the period after is analysed. Only support points 1 and 7 are used in the results since one of these points is the first to come loose. Figures 4.10 to 4.12 are used for this analysis. The y-axis shows the displacement of the support point relative to the deck level (at the support point). Before the release, the displacement is negative. This is due to the fact that the deck/sea-fastening has a stiffness, so the tower will not be perfect on deck level. The combination of the heave motion, as well as the stiffness, explains why the lines before the release fluctuate. The tower starts to come loose when the y-axis gives a positive value and it is deemed loose when the support point exceeds the threshold of 2mm, indicated by the purple dashed line. For lower pre-tension cases, the negative distance before the release is larger since more weight is resting on the deck.

The plots show that the support points do not exceed the threshold for the h_{lim} cases. As explained before, when they do exceed the limit, e.g. at 30% pre-tension, it is just exceeded as shown in Appendix G.4. The h_{lim}+0.2m cases confirm that the disconnection moment is precisely the moment when the threshold is reached. This also means that the other side will take more of the tower weight since (at least) one contact point is loose. This is clearly visible in the figures below as when the red line (support 7 at h_{lim}+0/2) goes up, the green line (support 1 at h_{lim}+0/2) goes down, and vice versa. For the mid-heave release plot, Figure 4.11, the tower stays fully connected to the barge until the deceleration as explained before.

The plots also show heave oscillations after the tower slams back at the deck such as for the red lines (support 7 at h_{lim}+0/2) after roughly 53 seconds. These oscillations can be explained by the slamming force of the tower, the stiffness of the 'deck' and the motions of the barge. The incoming tower point(s) will hit the deck and push it in. The barge and the tower are almost in opposite rotational phases (at 53 seconds), increasing the slam load. At the same time, the stiffness wants to push the connecting point(s) upwards. The deck is extremely stiff and therefore these short oscillating periods.

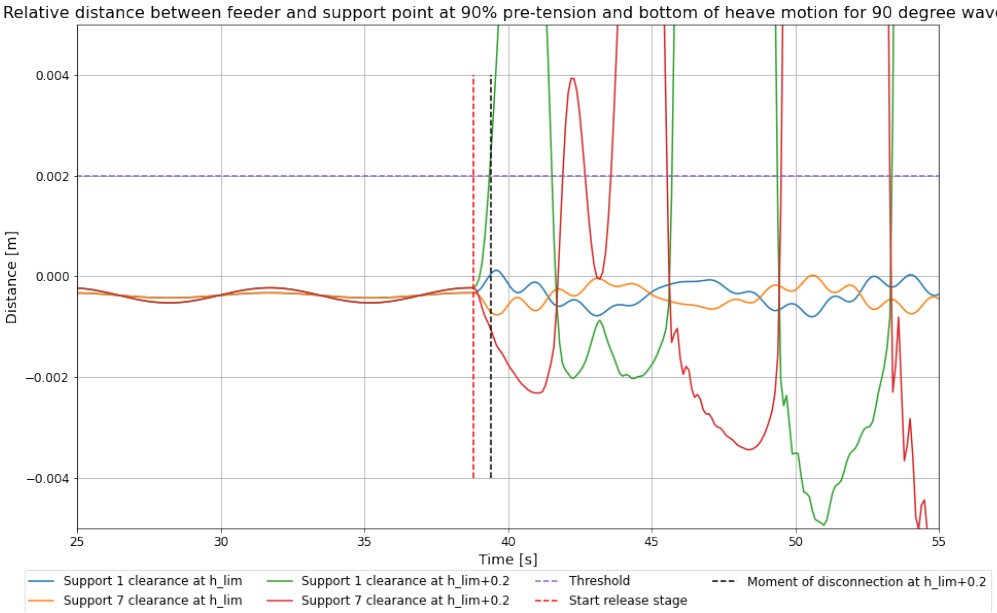

Figure 4.10: Distance between support points and barge at 90% pre-tension, beam waves and release at bottom of heave

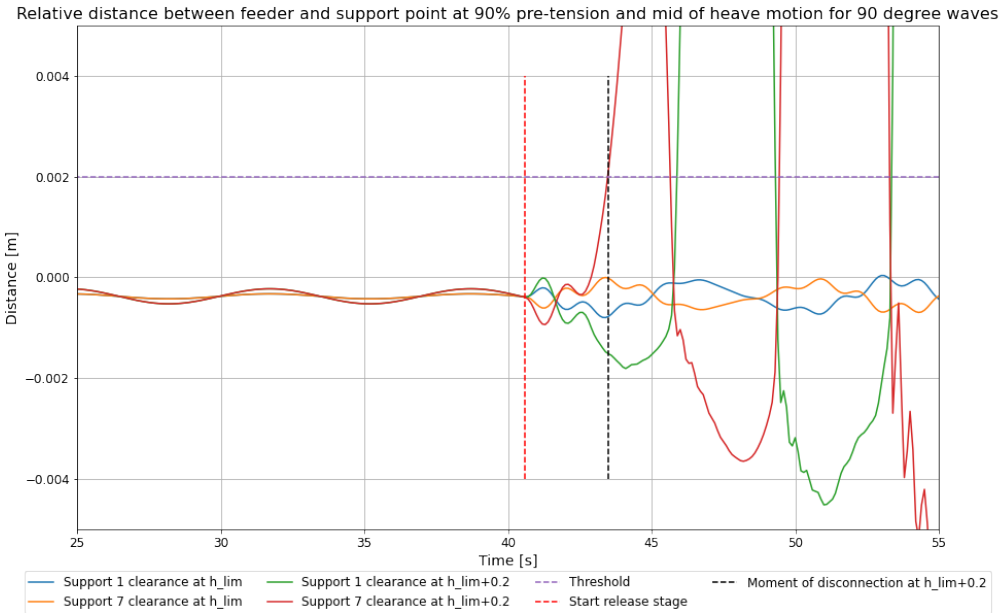

Figure 4.11: Distance between support points and barge at 90% pre-tension, beam waves and release at mid of heave

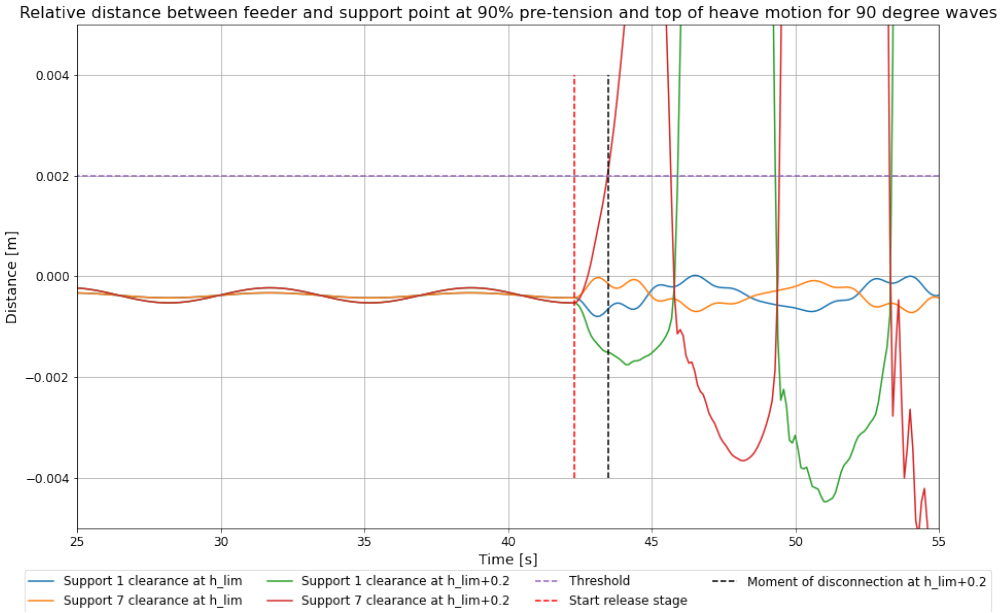

Figure 4.12: Distance between support points and barge at 90% pre-tension, beam waves and release at top of heave

4.3.4 Support point loads

Figures 4.13 to 4.15 show the contact forces of each of the support points on the vertical axis. When a support point is loose, the opposite support point will take more load as shown in the figures below. For these plots, the focus of the analysis lies in the period at and after the disconnection moment. The load curve goes to zero when a point is loose from the barge (disconnection). The point slams at the barge when it rotates back. This can be seen by the extremely steep red line (support 7 h_{lim}+0.2m) just after 45 seconds. The loads are significantly higher than the loads before the release. They increase even further the longer the tower is toppling from left to right on the sea-fastening. These slam loads are not found for the h_{lim} cases since the tower segment does not topple. There are some oscillations in the lines (of h_{lim}+0.2m cases) at for example the red line after roughly 53 seconds. These oscillations are caused by the same reason as explained in the previous subsection.

Slam loads could damage the tower (equipment), sea-fastening and/or deck of the barge and should therefore be avoided. So not allowing toppling to occur. Lowering the pre-tension does increase the limiting wave height (for toppling) as shown in table 3.1. However, a high pre-tension is desired/a must for the lift-off as explained in Section 2.3. Counteracting the moment that causes toppling by a temporary system after the release is a potential solution to increase the limiting wave height. Here, a load at the disconnecting side of the tower should counteract that moment. This 'counteracting' load can be taken from the graphs below since these must (at least) be equal to the contact loads at the moment of disconnection (black dashed line). These loads for each pre-tension and release timing are presented in table 4.7. This table shows the load values as well as the values expressed in percentages of the weight of the tower segment for the h_{lim}+0.2m cases. This means that to prevent disconnection at h_{lim}+0.2m, an increase of at least the provided load is required. The table shows a clear difference in loads for different pre-tensions. Much less load is required for the 90% cases than for the other ones. This is caused by the smaller load (normal force) that is on the deck of the feeder due to the higher pre-tension.

The h_{lim}+0.2m at 90% pre-tension is roughly 0.30 meters and the h_{lim} at 70% pre-tension is roughly 0.35 meters. The difference in pre-tension is 20% while only roughly 3% 'counteracting' load is needed to almost reach the same limiting wave height. This 3% must be added to the to-be-lifted load if the temporary system is for example spring-loaded clamp which the crane needs to be pulled open during the lift-off. It must be stated that at least two of such counteracting systems are required since toppling can go in multiple directions. This means the 3% needs to be doubled at least.

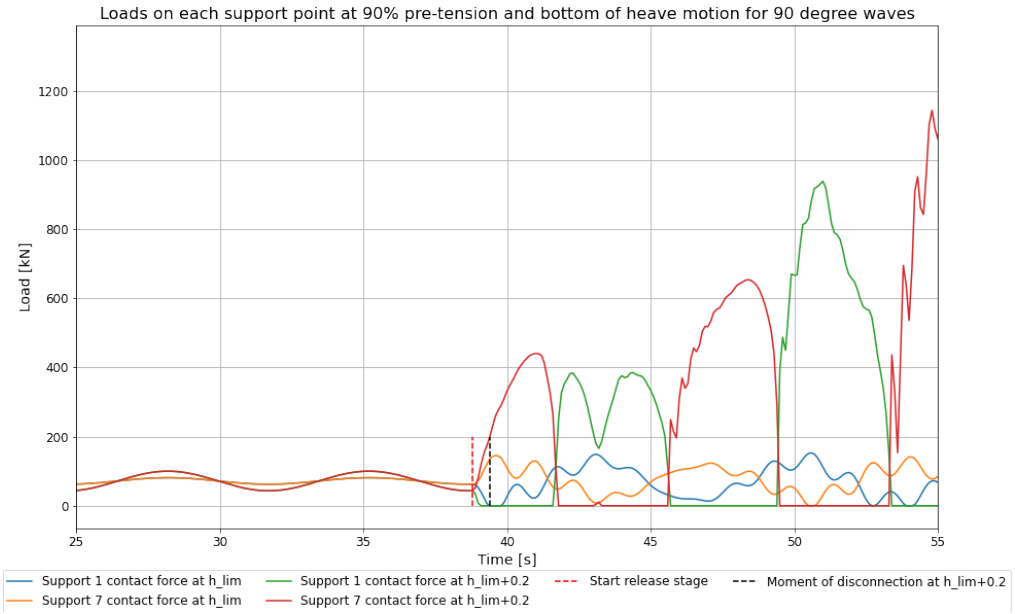

Figure 4.13: Support point loads at 90% pre-tension, beam waves and release at bottom of heave

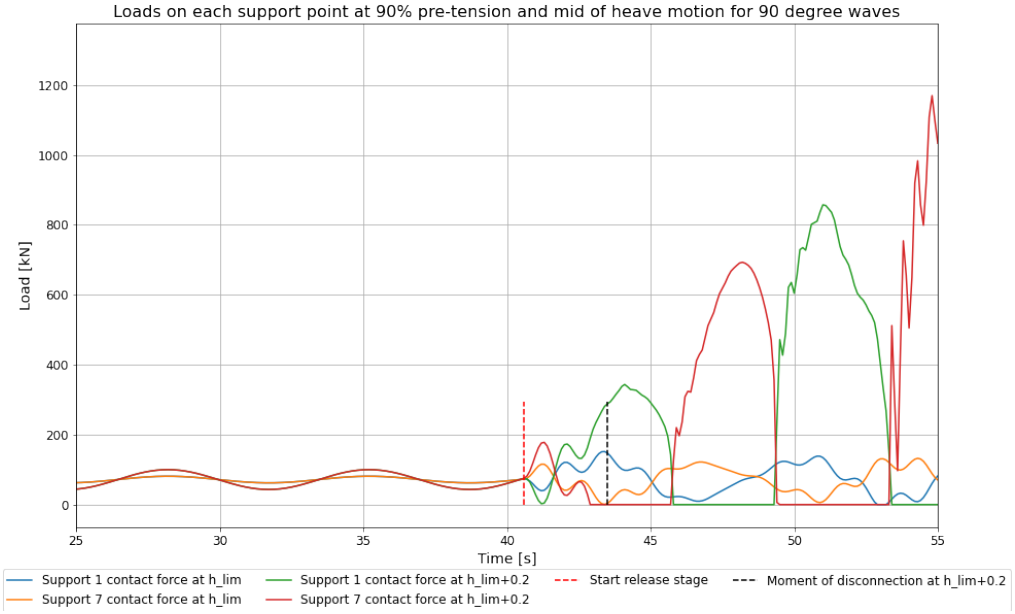

Figure 4.14: Support point loads at 90% pre-tension, beam waves and release at mid of heave

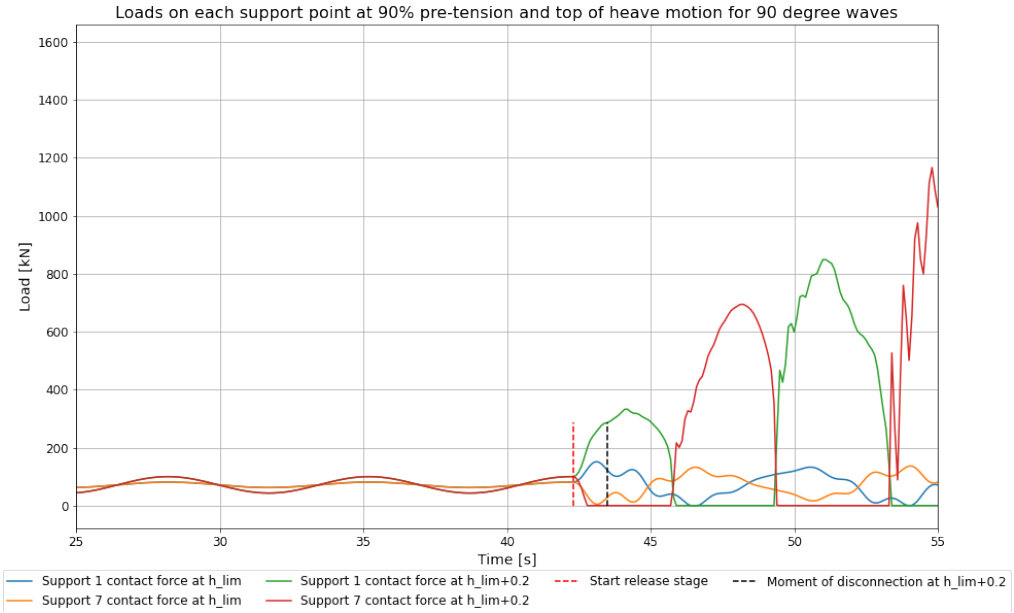

Figure 4.15: Support point loads at 90% pre-tension, beam waves and release at top of heave

Table 4.7: Support point loads during disconnection at h_{lim}+0.2m

Release timing	**Pre-tension**	**30%**	**50%**	**70%**	**90%**
Bottom	**Support load [kN]**	1165	842	513	198
	% of tower segment weight	13.6%	9.8%	6.0%	2.3%
Mid	**Support load [kN]**	1402	1065	674	294
	% of tower segment weight	16.3%	12.4%	7.9%	3.4%
Top	**Support load [kN]**	1363	1036	682	286
	% of tower segment weight	15.9%	12.1%	7.9%	3.3%

Chapter 5: Discussion

In this chapter, the results are discussed with respect to the literature, problem assumptions and approach, potential future studies to extend this research and managerial recommendations.

5.1 Literature

Very limited literature was available when it comes to a technical investigation of the lift-offs from a floating vessel since this is mostly done in-house by for example contractors. This research eventually used a passive heave compensator to decouple the motions of the tower from the crane, by means of the heave compensator. This was one of the suggestions by qualitative research by Haselsteiner et al. (2019) to decouple the motion of the component and the crane. They also recommended using a motion compensation platform in order to decouple the motions of the feeder from the tower. This was not implemented in the problem for this research. However, the results show that, for high pre-tensions, the limiting wave height in regular waves is extremely small. This is mainly caused by the rolling motions of the feeder. Therefore, recommendations by Haselsteiner et al. (2019) to use a motion compensation platform should be considered in future research to understand the effect.

Zhu et al. (2017) investigated a lift-off procedure where a tripod is located on a feeder and is lifted by an installation vessel. They used irregular waves as this is close to reality. They found that, when using zero pre-tension and no heave compensator, snap loads and accidental lift-offs occur. Although for regular waves, the results of this research confirm that snap loads do occur for the same pre-tension simulation case. They did not use higher pre-tensions to investigate the effect of for example the snap loads. This research did and showed that with high pre-tensions, snap loads do not occur anymore. Accidental lift-offs in this research have not been found due to the heave compensator in the crane.

Another difference with the research of Zhu et al. (2017) is the usage of a tripod which has a wide base frame and would therefore not topple. Their focus lies in the tension in the cable while this research focuses on both the tension and the toppling motion of the tower since the base is much smaller and therefore less stable. This holds for the direct installation method from the feeder.

In the first thesis of this double degree, Smorenberg (2021) proposed the direct installation method that is used in this research. Now, the results for the direct method in regular waves are known for the cases used in this research. Despite not being deemed the most limiting factor in Smorenberg (2021), the release/lift-off limiting wave height is much lower than the limiting wave heights used in the discreet event simulation model. As mentioned, the calculated wave height is for regular waves which have been used to increase understanding of the process. To provide insight for a workability study, irregular waves need to be used since these represent reality. To fully implement the technical study in the workability study, the significant limiting wave height (in irregular waves) should be used as input on the model of Smorenberg (2021) to check whether the outcome changes. The effect of irregular waves will be explained in the next section.

5.2 Assumptions, approach and results

Multiple assumptions were made when setting and reducing the scope of the problem. The first assumption made was the type of Wind Turbine Generator (WTG) component that is used in the research. The direct installation method allowed only for the lift of the tower segments as well as the nacelle with the note that it can only be a conventional drive train nacelle. The tower was chosen since this was deemed the most prone to toppling of the two. This led to limiting wave height results that are very low with increased pre-tensions. It is expected that the results for the nacelle, when analysed, are more favourable since the inertia is much lower and Centre of Gravity (COG) is closer to the base. These points indicate that it is more difficult for the nacelle to topple. On the other hand, the nacelle has a smaller base (flange diameter) since the tower has a conical shape at the top. This would counter the previously made statement. Additional calculations and simulations are required in order to determine the outcome.

A 20 MW WTG has been chosen in this research in order to find out if feedering via the direct method would be possible in the future. However, feedering is currently needed to start up the U.S. offshore wind market with the current turbine sizes. These WTGs are smaller in height, weight and inertia. Reducing all three elements relative to the 20 MW size, especially inertia, would improve the results of the simulations when it comes to toppling. Snap loads and accidental lift-off outcomes are not expected to change since these are pre-tension-related failure mechanisms. Further research with these smaller WTGs is required to find the exact change in results.

Barges are the allocated feeder vessels since none of the available Platform Supply Vessels (PSVs) in the U.S. are large enough to carry a full or partial set of 20 MW WTG components. It could be that in the future, larger PSVs would be available that can carry a full set of WTG components. This would be beneficial for the sailing speed compared to a towed barge. However, PSVs are more prone to rolling than barges due to the more rounded shape of the hull. This can be investigated by using the vessel input values of such a larger PSV in the hand calculations of this research. Nevertheless, it could still be that a barge would be more attractive since the results indicated that rotational accelerations are the main cause for the tower to topple. Reducing the accelerations could be a solution to improve the limiting wave height results. This can for example be done by lowering the $\overline{GM}$ values (while remaining positive). This increases the rolling period, and therefore reduces the accelerations.

The location of the tower is chosen at the Centre of Gravity (COG) position of the fully-loaded feeder. As described before, the other tower segment is located more to the aft or the fore of the barge. As long as the beam waves are used, the assumption that the locations along the x-axis centre line do not affect the results holds. However, as soon as the incoming wave direction changes, the pitch motion will start playing a role. Then, the location does matter and the further the tower is located from the COG, the more the pitch motion will play a role in limiting the wave height. This has to be taken into account when the other directions and irregular waves are used in future research.

Irregular waves, as shown in Section 2.3, represent the reality where regular waves do not. This research did not investigate the irregular waves but provided a qualitative explanation of what the expected results, being the limiting significant wave height for specific peak periods could become. Key elements are the natural frequencies of the system and the peak periods that represent the swell and wind waves (in a double peak spectrum). These frequencies should not be close to each other to avoid large responses. The RAOs show that the peak periods of wind waves can be avoided by using a high pre-tension in beam waves. Swell wave peak periods are more difficult to avoid since these have a larger range. Increasing (in this research) the rolling natural period by decreasing the (rolling) $\overline{GM}$ value could bring this natural period outside of the swell wave peak period range.

Pitching will start playing a role when the problem is looked into in 3D and multiple directions. The natural frequency for pitching is higher is the natural frequency for rolling. The brings natural pitch frequency, especially for higher pre-tensions, close to the wind wave peak periods. The natural frequency peak is much smaller than for rolling but could still cause issues. The same potential solution as for rolling can be applied to pitching. Here, the pitch $\overline{GM}$ value can be reduced to avoid the wind and potentially swell peak periods.

The barge's draft, Centre of Gravity (COG) and total inertia change when the first tower is lifted from the feeder (new load case). The $\overline{GM}$ value will increase in this new case making the vessel more 'stiff'. The $\overline{GM}$ potentially needs to be lowered again in order to move the natural frequencies away from the swell and wind frequencies. The calculations should be run again for each component and the new load case.

Another option to avoid the large responses is to position the barge (if possible) in such a manner that the responses are much smaller. In the current RAOs, pitching has a lower natural period and natural period peak than rolling. This means that the longer swell wave can more easily be avoided and it could be beneficial to place the barge in line with swell waves. Sheltering from the incoming wave is also an option to reduce the response. However, this is not always possible.

This research only uses the direct method. However, the results for the indirect method can also be estimated using the formulas to determine the limiting wave height, as explained in Section 3.4. For the indirect method, the edge of the 'radius' of the base frame becomes the point of toppling. According to the formulas, the limiting wave height scales linearly with the base frame and tower 'radius'. This does not hold for irregular waves since the iterative steps as explained in Section 2.3 are still required but the limiting response is different (higher).

The chosen approach uses hand calculations to determine the (critical) limiting wave height per wave period. These are then used to reduce the number of cases and as input for the time-domain simulations. This approach saves a significant amount of simulation time since the time-domain simulations are time-consuming (minutes versus hours). Recreating the model by hand provided a lot of insight into the physics behind the system as well (RAOs of the complete system). Determining the equation of motions was experienced to be time-consuming too. However, redoing this (for another project) will speed up the process. Besides, it allows for extensive verification and validation of the calculations and simulation model. Overall, the approach leads to a more hybrid way of working where hand calculations (frequency-domain) and simulations (time-domain) are used. The more expensive (money and time-wise) simulations are reduced while the insight in the system increases. This approach shows that time-intensive simulations do not always have to be run for every single case and quick 'hand calculations' can be used for case reduction (back to basic).

The OrcaFlex model can easily run in all directions since these feeder RAOs are provided. The tower segment can also be located at different positions on the barge. However, the hand calculations have been done in 2D (y-z plane) and will not represent a correct limiting wave height when other directions are used. Therefore, the hand calculations have to be extended to 3D. This is an important extension since pitch does seem to play a more important role. The validation shows that the simplifications of a fixed crane boom and crane block as a point mass barely affect the outcome of the results for the used cases. The extension to irregular waves should also be done in order to create more realistic results. OrcaFlex can be set to irregular waves where multiple spectra (wind and swell) with different directions can be applied.

The results show that the time it takes after release for the tower to start toppling at h_{lim}+0.2m is very short. The tower topples almost immediately when it is released at the peak of a heave motion. When released after the peak, it takes roughly 3 seconds to initiate the toppling motion. This can be explained by the chosen wave period (7 seconds). 3.5 seconds is the time it takes to roll from one side to the other. Therefore, when released after the peak, it takes less than 3.5 seconds to reach the other roll amplitude peak. These 3 seconds are still very short. Disconnecting and lifting the tower (remotely) will take more than 3 seconds since there are delays/checks in the system. The results show that when the tower starts toppling back and forth the loads in the deck/sea-fastening frame become significantly high. The rotational motion of the tower also drastically increases every time it hits the frame. This will cause damages and make it impossible to lift.

The limiting wave heights for all toppling-related cases at high pre-tensions are fairly low. These high pre-tensions are desired to reduce the Dynamic Amplification Factor (DAF) during the quick-lift. In order to increase limiting wave height, a special release system that keeps the tower temporarily in place can be used, e.g. a spring-loaded lock. This lock would still be in place when the seafastening is released and the crane needs to pull through the spring to lift the tower segment. The load it should take should be large enough to prevent the tower from toppling for a specific limiting wave height. These loads for h_{lim} are shown in Table 4.7. The downside of this system is that the 'counteracting load' is added to the load in the crane which is the weight of the tower as well as the Dynamic Amplification Factor (DAF) during the lift-off. The table shows that the smallest 'counteracting loads' are when the pre-tension is at 90% (2.5-3.5% of the tower segment weight). However, this is also for the lowest limiting wave height in regular waves. On top of this, multiple of these systems are required due to different topple directions due to wave spreading. This increases the total 'load' during the lift even more, potentially making this option not beneficial anymore.

Another potential option to improve the results is to increase the number of tower sections, which reduces the size, weight and inertia terms. However, this is not recommended by Smorenberg (2021), since the time/costs will increase. In practice, directly installing a tower segment without some sort of motion compensation system between the barge and tower segments, locking system or an instant lift after the release is very difficult and risky.

The results like limiting wave height for feedering are highly offshore related. Results to improve the system can be put into a broader perspective. For example, the option to increase the number of tower segments to lead to a better limiting wave height/workability. This can be related to the transport industry in general where a larger object needs to be transported but have difficulties due to its size since only a few e.g. trucks in the world can carry it. It could be more beneficial (time-efficient) to transport the object into smaller parts in one truck. Here, the more parts the object is transported in, the more time it will take to assemble them on site as for the number of tower segments. However, a larger variety of 'smaller' trucks would be available compared to the large and rare trucks. This could lead to shorter waiting times for the trucks to become available. This would be similar to increasing the workability/limiting wave height with smaller tower segments in this research.

5.3 Future research

This research used simplifications to speed up the calculation process. The biggest simplification is the 2D calculation which significantly reduces the scope of the problem. Therefore, the hand calculations should be extended to 3D. This allows for calculations from other directions as well as other WTG component locations of the barge. The next elements that should be added in future research are the nacelle and other WTG sizes to find whether the results would improve and how much. The usage of PSVs should only be considered if a larger PSV is available. Research has to be done to determine the size of the future PSV with a feeder purpose.

The positioning system of the feeder has not been implemented in this research. A barge requires a mooring system to maintain its position. Second-order waves and current will be key elements in this design. An investigation of such a mooring system is required. For a PSV, a Dynamic Positioning (DP) system will be used. The system should be redundant and strong enough to allow for operations close to the installation vessel. The positioning should also be investigated to complete the entire system of the feeder process.

Another element which is left out of the research are the irregular waves including the double peak spectrum with directionality. These should be added to the hand calculations, as explained in Section 2.3, to provide a more realistic view of the problem. Further, the sea-fastening system (with additional lock mechanisms) should be investigated on a deeper level since the tower starts toppling almost directly after the release. The options should be compared to the results of when an indirect method is applied and if the number of tower segments is increased. To create more understanding of how the limiting wave height can be further increased, motion compensation tools which decouple the component from the feeder should be investigated and used in the comparison.

The investigation in this research is focused on the release of the sea-fastening. However, the problem in real life does not stop there. The tower will also need to be lifted. Therefore, the lift-off should also be implemented in future research. This would create more insight into the combination of release and lift-off and what is required to safely lift a WTG component (tower) from a floating feeder.

5.4 Managerial recommendations

Vessel availability, as well as stability studies, show that barges have to be used in the U.S as feeder vessels when feedering 20 MW Wind Turbine Generator (WTG) components. The direct installation method does seem an interesting feeder strategy logistically according to Smorenberg (2021). However, the limiting wave height for safely releasing the tower (in regular waves) at high pre-tensions is very low. It is expected that this would hamper the installation process. Smorenberg (2021) found that using motions compensation tools is a highly expensive solution (third party charter) since multiple compensators per barge are required and the gain in workability is not known yet.

Investigating in a release system as explained before would be more cost-efficient since this can be built in-house and used in multiple projects (spreading the costs). However, the effectiveness of such a system should be investigated more thoroughly. Using more tower segments is always an option to improve the limiting wave height/workability as long as there is space enough on the barge due to the smaller sizes of the segments. However, Smorenberg (2021) indicated that this is not process time/cost-efficient since more segments need to be lifted (instead of two). A combination of these 2 options would provide a better solution limiting wave height/workability-wise, for direct feedering for now, but potentially not the most cost-effective one.

The last resort option is to move away from the direct method for the tower segments and implement the indirect method. The base frame of this method could significantly improve the limiting wave height, depending on its size. This can also be developed in-house and is cost-effective. However, as explained by Smorenberg (2021), this method will have more installation steps. The nacelle could still be directly installed depending on the outcome of that study since this is less prone to toppling.

Chapter 6: Conclusion

In this chapter, the answers to the research questions are given and explained. Conclusions are drawn based on the results and the discussion.

SQ1: What elements are key to understanding the release of the WTG component?
First of all, the lifting procedure needs to be set. A direct installation method is chosen, which means that the component is directly installed after lifting and nothing is allowed to be attached to the bottom. Next is the allocated component which is the tower due to its height, weight, inertia and base size. The feeder vessel in this research is a barge since the available PSVs in the U.S. are not large enough to carry a 20 MW turbine in separate components. The installation vessel is a jack-up vessel which is already jacked above the water. In the crane, below a crane hook is an active heave compensator which is connected to the tower segment. During the pre-tension phase, the heave compensator acts like a passive one with a constant spring characteristic. The environment plays a key role since this causes the feeder to move. Only first-order wave loads are considered due to the time restriction of the project. The investigation is checked on three failing mechanisms, snap loads, accidental lift-offs and toppling of the component after the release.

SQ2: What is the suitable approach to determine the reactions?
The most suitable approach is using a time-domain simulation that takes nonlinear behaviour into account. However, time-domain simulations are time-consuming which makes them not very suitable if many calculations need to be run. A high-performance computer can be used to speed up the process, but still, all cases have to be individually checked for discrepancies. Reducing the number of cases would be ideal since this brings the simulations as well as the post-process time down.

The reduction in this research is best to be done by hand calculations using a frequency domain analysis. Here, critical cases can be found which can then be simulated in the time domain. Therefore, a hybrid approach where frequency and time-domain simulations are used is the best approach.

SQ3: How will the model be verified and validated?
Frequency-domain calculations are verified using natural frequency calculations. The time-domain simulation model that is created in OrcaFlex is validated using hand calculations by linearized frequency-domain analysis.

SQ4: What are the parameters that can be used in a sensitivity analysis?
Of all parameters in the system, the pre-tension, release timing and wave height are the parameters chosen in the sensitivity analysis. Pre-tension is chosen since this can range from 0-90%. The effect of different pre-tension is important to gain an understanding of the limiting mechanisms. The release timing is important since this can determine when the release can partake and how much time there is before the lift-off. The wave height indicates the environmental limit of the cases for toppling. The higher the limiting wave height, the better the case.

SQ5: What parameters is the system most sensitive to?
The combination of pre-tension and wave height are the most important parameters since these determine the limiting cases for the simulation. The release timings in regular waves do not show a large difference in the cases. All cases indicate toppling due to the acceleration of the rotational motion of the barge and the inertia of the tower. Each case shows toppling as soon as the barge rotates back to its upright position.

MRQ: What are the reactions of a next-generation WTG component when released from its sea-fastening on a feeder vessel in the U.S. offshore wind market?
As explained before, very limited knowledge is available on this topic. As a scientific contribution, this research aims to provide more insight/understanding into the release phase for a direct installation method of WTG lift-offs and to open up new/more research in this area.

First of all, Snap loads occur at the low pre-tensions of 0 and 10%. These snap loads are not detected anymore for pre-tensions equal to or higher than 30% (based on the simulation cases). This outcome is pre-tension related. Toppling becomes the limiting factor for higher pre-tensions. Accidental lift-offs do not occur for the investigated pre-tension. This is also a pre-tension-related failure mechanism and would, due to the heave compensator, only occur at extremely high pre-tensions (higher than 90%).

Toppling does not occur at the same wave height for each pre-tension. The lower the pre-tension, the higher the limiting wave height due to the normal force on the barge, h_{lim} = 0.65m at 30% and h_{lim} = 0.10m at 90%. Toppling only occurs when the limiting wave height is exceeded and the barge is around or at its maximum roll displacement and starts rotating (rolling) back. The inertia of the tower segment is the initial cause for the tower to topple. Toppling should be avoided since the tower segment keeps topping back-and-forth and creating large slam loads that could damage the component, feeder deck and/or seafastening.

Irregular waves with a double peak spectrum including directionality are investigated on a qualitative base. The swell waves from a small issue for pitching since the natural frequencies are near the low side of the swell wave range whereas rolling is more significant since the natural frequency is in the middle of the range. On top of this, the natural frequency peak for pitching is much lower than for rolling. Wind waves are more of an issue for pitching since the natural frequencies are close to the wind wave peak periods. Swell waves have a smaller directional spreading than wind waves, and both types do not have to come from the same direction necessarily. Locating the barge with its bow or stern into swell waves is therefore advised.

Multiple options can be considered to increase the limiting wave height. The first is to increase the number of tower segments and therefore decrease the COG, mass and inertia per segment. This increases the limiting wave height for use but also increases the installation time since additional steps need to be taken.

The second option is to implement a motion compensation tool to decouple to motions of the feeder and the tower. This is a highly interesting option but has never been used/proven in practice on this scale. On top of this, the costs for implementing multiple (expensive) tools can be very high as each feeder requires multiple systems.

The third option is to design a sea-fastening system that either release almost simultaneous with the lift or has a spring-loaded clamp that counteracts the moment caused by the motions. This spring load needs to be pulled open during the lift-off. For low pre-tension, the required load to increase the limiting wave height by 0.2m is much higher than for higher pre-tensions. However, the limiting wave height is also much higher (for low pre-tensions) On top of this, multiple 'clamps' are required due to the directionality of the waves. This increases the total load to pull all clamps open. Yet, it is uncertain if these clamps would be a good solution looking at the Dynamic Amplification Factor (DAF) during the lift as well as the limited effect of the increase in limiting wave height since this is not investigated thoroughly.

The first thesis in this double degree did not look into these technical challenges. It can be stated that the release before the lift-off of a 20 MW tower segment on a floating barge for the direct method is extremely challenging. This research revealed new hurdles that require more investigations, either being an extension of this research, like the other wave directions/irregular waves or new research in for example the sea-fastening system. This research also shows that hand calculations can be extremely powerful to reduce the number of cases when simulations must be done.

The indirect method suggested by the MOT thesis can be used as a final resort if the additional research concluded that the direct installation method is not workable. The larger base frame at the bottom of the tower segment allows for a larger allowable moment than for the direct method. This would improve the workability of this action for sure. Findings from the direct installation method to improve the workable limits can also be applied to the indirect method.

All in all can be concluded that when looking at both master thesis in the double degree, feedering, in general, is highly complex. Offshore wind farms should be installed more quickly to cope with the growing demand for offshore wind energy. Shuttling (the conventional method) would still be the desired solution when comparing the installation methods on both logistical/costs and technical levels.

References

Ait Alla, A., Oelker, S., Lewandowski, M., Freitag, M., and Thoben, K.-D. (2017). A study of new installation concepts of offshore wind farms by means of simulation model. *ISOPE*, pages 608–609, 612.

Akbari, H., Panahi, R., and Amani, L. (2020). Improvement of double-peaked spectra: Revisiting the combination of the gaussian and the jonswap models. *Ocean Engineering 198*, page 4.

Barrass, C. and Derrett, D. (2012). *Ship Stability for Masters and Mates*. Butterworth-Heinemann, 7th edition.

Cao, D., Song, L., Li, J., Yuan, J., and Zhou, Y. (2014). Determining the drag coefficient of a cylinder perpendicular to water flow by numerical simulation and field measurement. *Ocean Engineering*, pages 93–99.

Chung, J. and Hulbert, G. M. (1993). A time integration algorithm for structural dynamics with improved numerical dissipation: The generalized-en? method. *Journal of Applied Mechanics*, pages 371–375.

Crane Master (2022). What is the difference between active heave compensation (ahc) and passive heave compensation (phc)? `https://www.cranemaster.com/f-a-q-frequently-asked-questions/what-is-the-difference-between-active-heave-compensation-and-passive-heave-compensation/`. Retrieved on 23-02-2022.

Friedrich, K. and Lukas, M. (2017). *State-of-the-Art and New Technologies of Direct Drive Wind Turbines*. Springer International Publishing.

Haselsteiner, A. F., Ohlendorf, J.-H., Oelker, S., Ströer, L., Thoben, K.-D., Wiedemann, K., De Ridder, E., and Lehmann, S. (2019). Lifting wind turbine components from a floating vessel: A review on current solutions and open problems. *Offshore Mechanics and Arctic Engineering*, 141:2–3.

Holthuijsen, L. H. (2010). *Waves in oceanic and coastal waters*. Cambridge University press.

Huisman Equipment (2021). Offshore wind / motion compensated platform. `https://www.huismanequipment.com/en/products/renewables/offshore_wind/motion-compensated-platform`. Retrieved on 26-05-2021.

IEA (2018). Renewables 2018: Analysis and forecasts to 2023. `https://www.iea.org/reports/renewables-2018`. Retrieved on 13-11-2020.

IRENA (2019). Future of wind: Deployment, investment, technology, grid integration and socio-economic aspects. *IRENA.org*, pages 48, 50, 56.

Journee, J., Massie, W., and Huijsmans, R. (2015). *Offshore Hydrodynamics*. Delft University of Technology, 3rd edition.

MACE (2019). Take vortex shedding seriously. `https://www.mecaenterprises.com/take-vortex-shedding-seriously/`. Retrieved on 24-02-2022.

Mazarakis, N. (2019). Why douglas sea state 3 should be eliminated from good weather clauses. `https://www.stormgeo.com/products/s-suite/s-routing/articles/why-douglas-sea-state-3-should-be-eliminated-from-good-weather-clauses/`. Retrieved on 09-08-2021.

Meirovitch, L. (2001). *Fundamentals of Vibrations*. McGraw-Hill companies, international edition.

MIT (2014). Vortex shedding and vortex induced vibrations - lecture 15. *MIT - Department of Ocean Engineering*, pages 1–5.

Oelker, S., Ait-Alla, A., Lütjen, M., Lewandowski, M., Freitag, M., and Thoben, K.-D. (2018). A simulation study of feeder-based installation concepts for offshore wind farms. *ISOPE*, pages 578–579, 582.

Pasin, P., Van Nguyen, D., and Ki-Du, K. (2019). Tripod-supported offshore wind turbines: Modal and coupled analysis and a parametric study using x-sea and fast. *marine Science and Engineering*, page 2. DOI = 10.3390/jmse7060181.

Rippel, D., Jathe, N., Lütjen, M., Szczerbicka, H., and Freitag, M. (2019). Simulation and optimization of operations for offshore installations planning using a model predictive control scheme. *IEEE*, page 1721. DOI = 10.1109/WSC40007.2019.9004824.

Seaqualize (2022). Compensated feeder operations. `https://www.seaqualize.com/feeder-operations`. Retrieved on 23-02-2022.

Sekaran, U. and Bougie, R. (2016). *Research Methods for Business, A Skill-Building Approach*. John Wiley & Sons, 7th edition.

Smorenberg, M. (2021). An investigation of installation strategies to install next-generation offshore wind turbine generator components. *TU Delft Repository*. DOI = http://resolver.tudelft.nl/uuid:c0c266bb-ac60-46c5-909d-8beb5dedf7d4.

Snieckus, D. (2020). Global offshore wind fleet could explode 20-fold by 2035. `https://www.rechargenews.com/wind/global-offshore-wind-fleet-could-explode-20-fold-by-2035-if-1-5trn-in-finance-found/2-1-900400`. Retrieved on 15-02-2022.

The White House (2021). Fact sheet: Biden administration jumpstarts offshore wind energy projects to create jobs. `https://www.whitehouse.gov/briefing-room/statements-releases/2021/03/29/fact-sheet-biden-administration-jumpstarts-offshore-wind-energy-projects-to-create-jobs/`. Retrieved on 29-09-2021.

Transportation Institute (2020). Jones act: Critical to economic and national security. `https://transportationinstitute.org/jones-act/`. Retrieved on 29-09-2021.

UNCCC (2020). The paris agreement. `https://unfccc.int/process-and-meetings/the-paris-agreement/the-paris-agreement`. Retrieved on 13-11-2020.

U.S. Department of Energy (2021). Offshore wind market report: 2021 edition. *Office of Efficiency & Renewable Energy*, page 9.

Wind Europe (2021). Offshore wind in europe: Key trends and statistics 2020. *Wind Europe*, page 9.

Zhu, H., Li, L., and Ong, M. (2017). Study of lifting operation of a tripod foundation for offshore wind turbine. *First Conference of Computational Methods in Offshore Technology*, pages 15–17.

Appendices

Appendix A: Conventional method

Step 1: Transfer the WTG components from the production port to the base port by **large transport vessels**. (This step needs to be repeated to constantly supply the base port)

Step 2: Store the WTG components temporarily at the base port.

Step 3: Transfer multiple (as much as possible) full sets of WTG components from the storage to the installation vessel.

Step 4: Transfer the full sets to the installation site by the installation vessel.

Step 5: Install all the WTG components

Step 6: Sail back to the base port to pick up new WTG components.

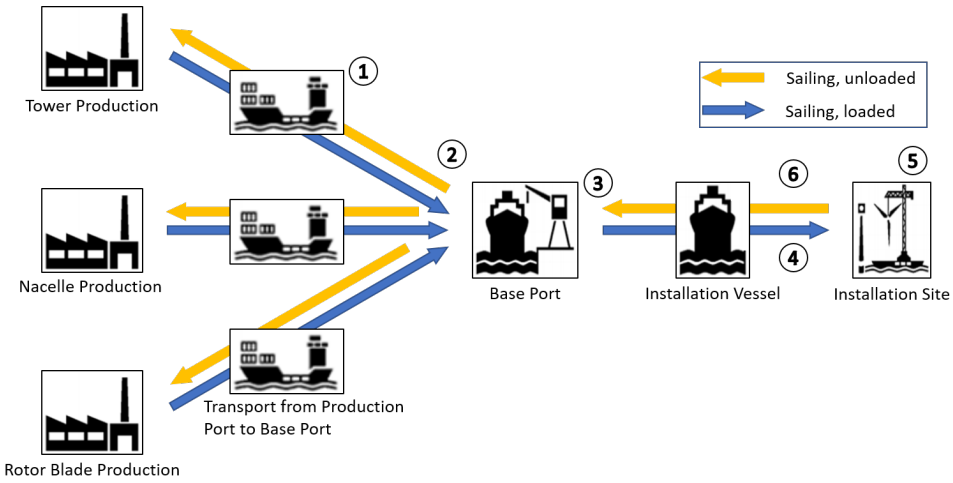

Figure A.1: The conventional method steps based on Ait Alla et al. (2017)

Appendix B: Feeder method

Step 1: Transfer the WTG components from the production port to the base port by **large transport vessels**. (This step needs to be repeated to constantly supply the base port)

Step 2: Store the WTG components temporarily at the base port.

Step 3: Transfer the WTG components from the base port to the installation site by a **feeder vessel**. The number of components that need to be transferred depends on the maximum number of full WTG sets the feeder vessel can carry.

Step 4: Transfer 1 full set of WTG components directly to the installation vessel (at the installation site).

Step 5: The feeder vessel will sail back to the base port to pick up new WTG components only if the feeder is empty. If the feeder has multiple full sets on board. It will stay offshore until all components are supplied to the installation vessel.

Step 6: The installation vessel installs the WTG components.

Step 7: The installation vessel sails to the next installation site where it will receive a new WTG set.

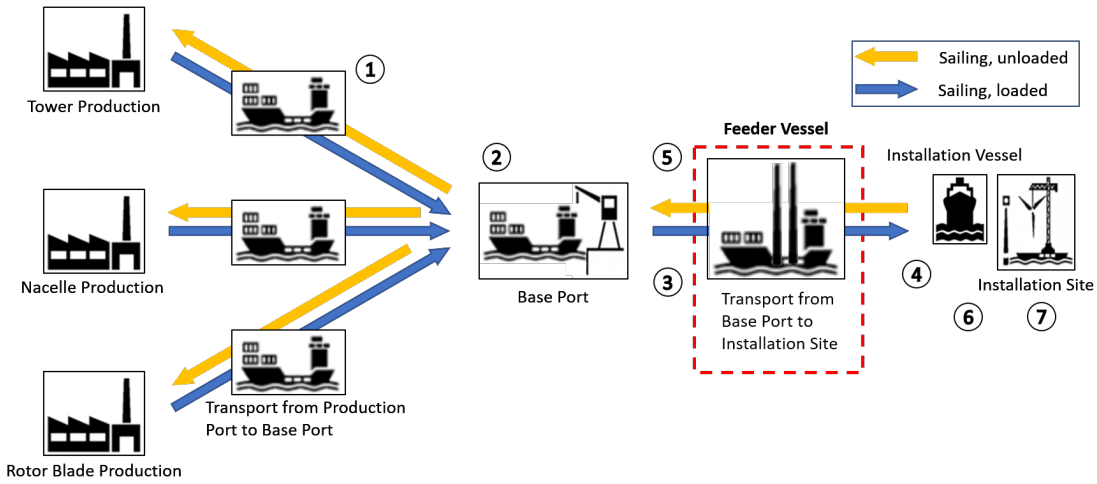

Figure B.1: The feeder-ship method steps

Appendix C: Barge RAOs

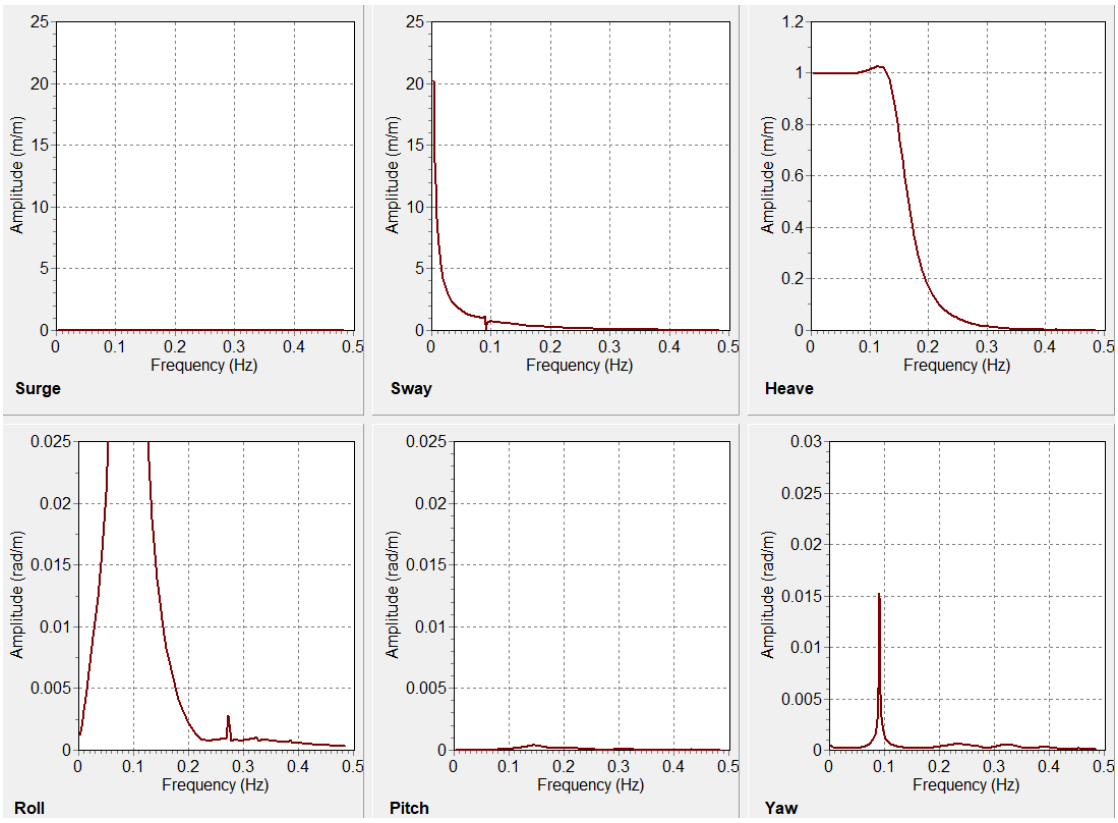

Figure C.1: Displacement RAOs of the feeder barge in 90° incoming waves provided by Van Oord

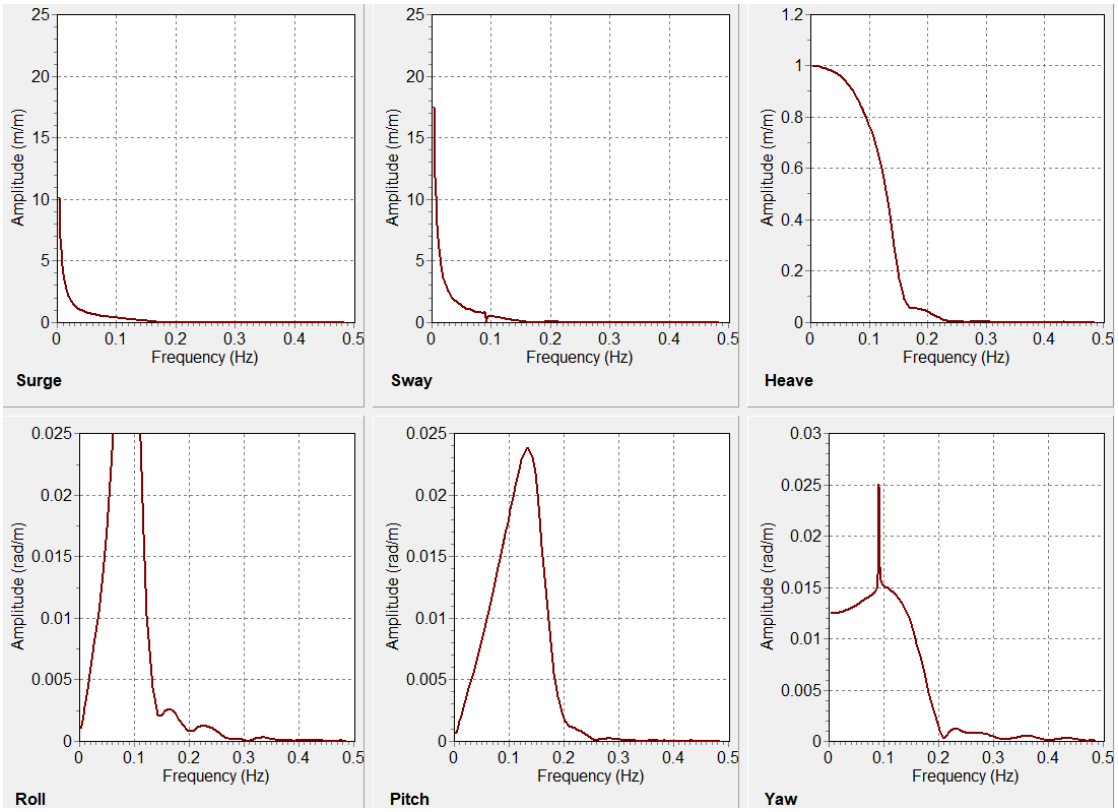

Figure C.2: Displacement RAOs of the feeder barge in 60° incoming waves provided by Van Oord

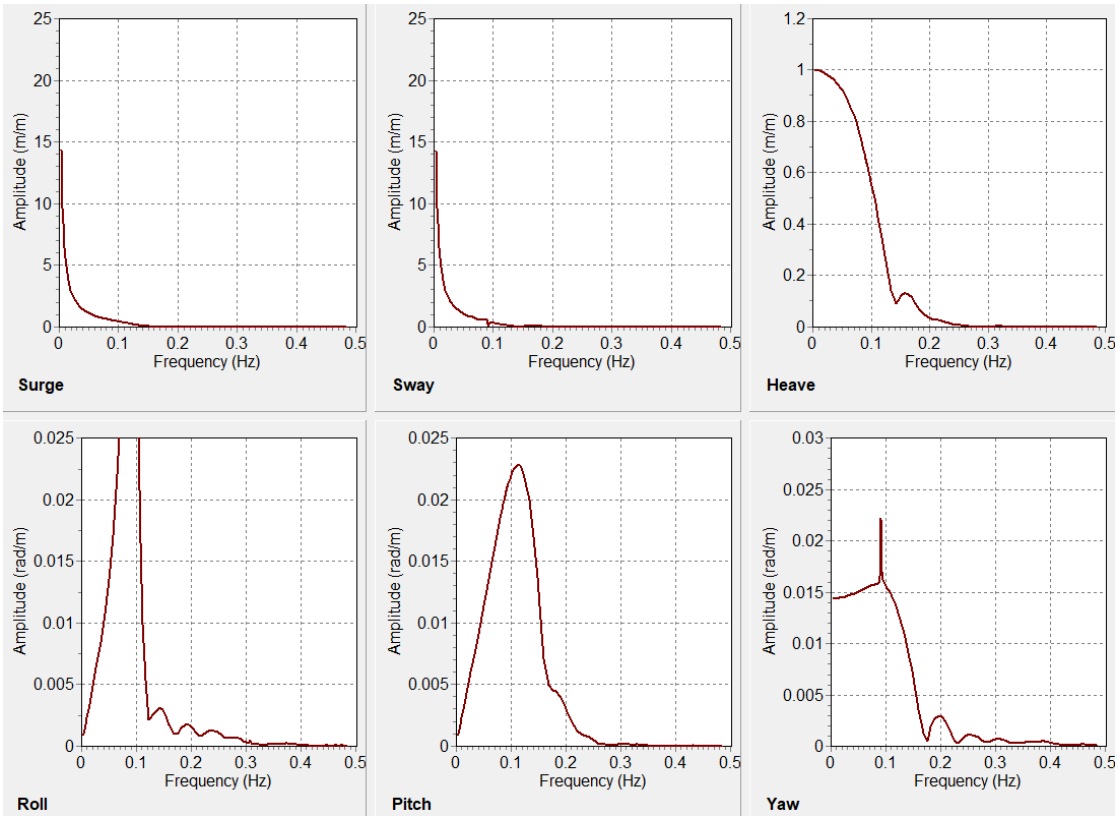

Figure C.3: Displacement RAOs of the feeder barge in 45° incoming waves provided by Van Oord

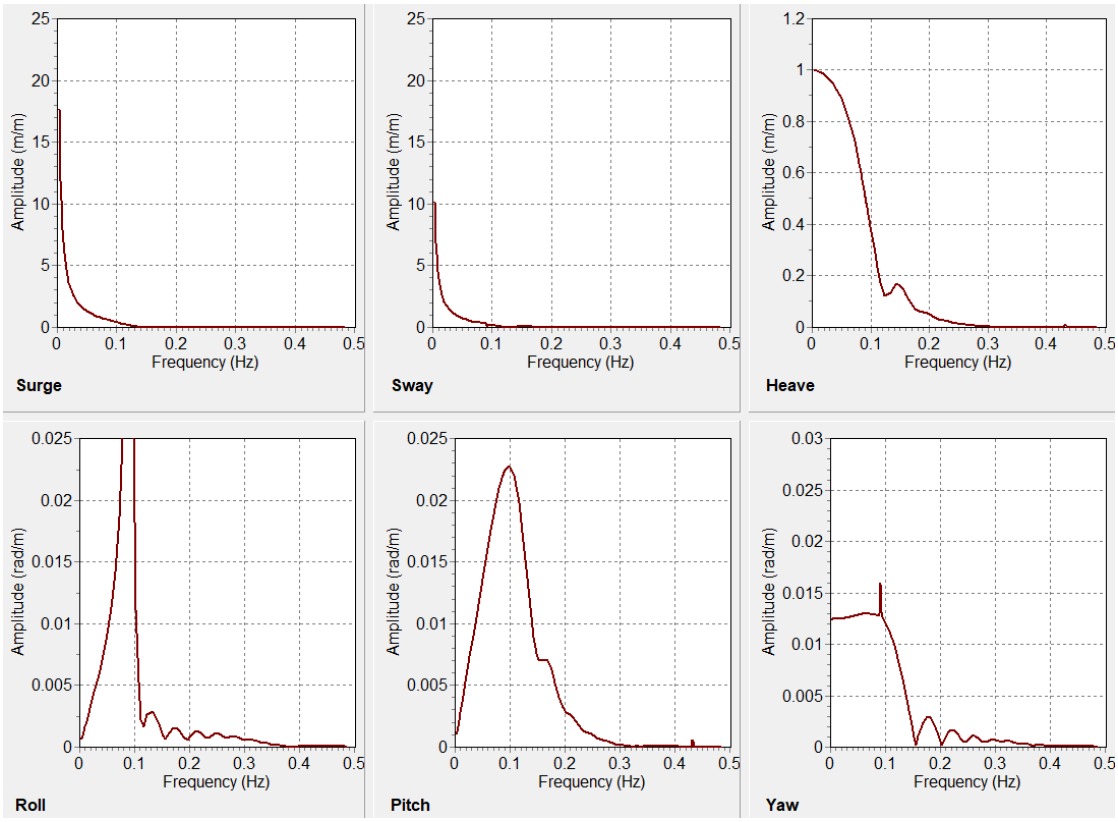

Figure C.4: Displacement RAOs of the feeder barge in 30° incoming waves provided by Van Oord

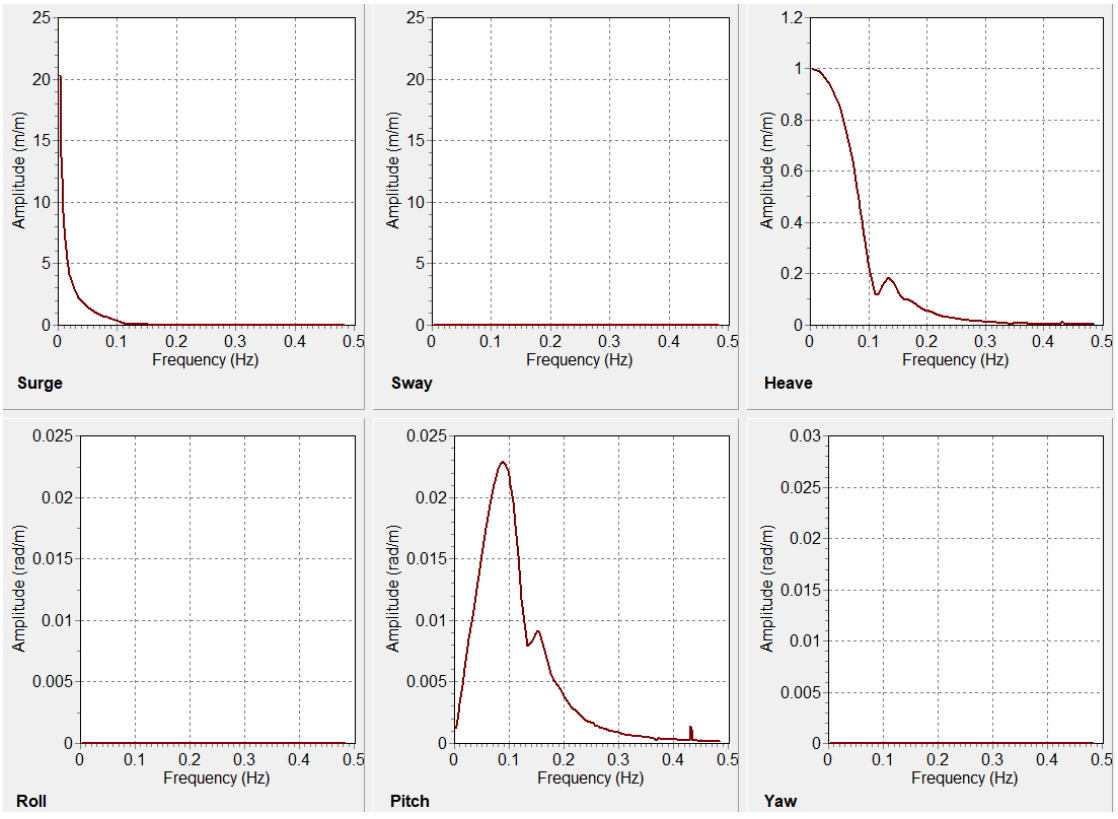

Figure C.5: Displacement RAOs of the feeder barge in 0° incoming waves provided by Van Oord

Appendix D: Maple script

D.1 EoM Maple script

```
> restart
> with(Physics):
```

Potential energy

```
> Vg(t) := m_cb·g·X10(t) + m_hc·g·X6(t) + m_b·g·X2(t) + m_sl·g·X13(t):
> Vs(t) := 1/2·c_c1·(Lc1Pre-Lc1(t))^2 + 1/2·c_c2·(Lc2Pre-Lc2(t))^2 + 1/2·c_c3·(Lc3Pre-Lc3(t))^2
        + 1/2·c_b33·(X2(t))^2 + 1/2·c_b44·(X3(t))^2 + 1/2·c_hc·(LslPre-Lsl(t))^2:
> V(t) := Vg(t) + Vs(t):
>
```

Kinetic energy

```
> Tb(t) := 1/2·m_b·(X1'(t))^2 + 1/2·m_b·(X2'(t))^2 + 1/2·J_bxx·(X3'(t))^2:
> Thc(t) := 1/2·m_hc·(X5'(t))^2 + 1/2·m_hc·(X6'(t))^2 + 1/2·J_hcxx·(X7'(t))^2 + 1/2·m_sl·(X12'(t))^2
        + 1/2·m_sl·(X13'(t))^2 + 1/2·J_slxx·(X7'(t))^2:
> Tcb(t) := 1/2·m_cb·(X9'(t))^2 + 1/2·m_cb·(X10'(t))^2:
> T(t) := Tb(t) + Thc(t) + Tcb(t):
>
```

Total energy

```
> E(t) := T(t) + V(t):
>
```

External forces

```
> Wb' := F_wy·X1'(t) + (F_buoyancy + F_wz)·X2'(t) + M_wx·X3'(t) + F_bhc·Lsl'(t):
> W'(t) := Wb':
>
```

Kinematic constraints

crane **to** *crane hook*

```
>
> X9(t) := (L30 + Lc3Pre-Lc3(t))·sin(X11(t)):
> X10(t) := h_crane - (L30 + Lc3Pre-Lc3(t))·cos(X11(t)):
```

crane hook **to** *hc*

```
> X5(t) := X9(t) + ((L20 + Lc2Pre-Lc2(t))·sin(X8(t))) + h1_hc·sin(X7(t)):
> X6(t) := X10(t) - ((L20 + Lc2Pre-Lc2(t))·cos(X8(t))) - h1_hc·cos(X7(t)):
```

hc **to** *slider*

```
> X12(t) := X5(t) + h2_hc·sin(X7(t)) + ((Lsl0 + LslPre-Lsl(t))·sin(X7(t))):
> X13(t) := X6(t) - h2_hc·cos(X7(t)) - ((Lsl0 + LslPre-Lsl(t))·cos(X7(t))):
```

slider **to** *barge + tower*

> $X1(t) := X12(t) + (L10 + Lc1Pre - Lc1(t)) \cdot \sin(X4(t)) + (h_b) \cdot \sin(X3(t))$:

> $X2(t) := X13(t) - ((L10 + Lc1Pre - Lc1(t)) \cdot \cos(X4(t))) - (h_b) \cdot \cos(X3(t))$:

>

Energy balance

> $EB := eval(\dot{E}(t) - \dot{W}(t)) = 0$:

>

> $with(Physics)$:

>

> $EoM1\_full := simplify(factor(diff(EB, \dot{X3})))$:

> $EoM2\_full := simplify(factor(diff(EB, \dot{X4})))$:

> $EoM3\_full := simplify(factor(diff(EB, \dot{X7})))$:

> $EoM4\_full := simplify(factor(diff(EB, \dot{X8})))$:

> $EoM5\_full := simplify(factor(diff(EB, \dot{X11})))$:

> $EoM6\_full := simplify(factor(diff(EB, \dot{Lc1})))$:

> $EoM7\_full := simplify(factor(diff(EB, \dot{Lc2})))$:

> $EoM8\_full := simplify(factor(diff(EB, \dot{Lc3})))$:

> $EoM9\_full := simplify(factor(diff(EB, \dot{Lsl})))$:

>

External forces

> $F_{bhc} := -b_{hc} \cdot \dot{Lsl}(t)$:

> $F_{yw} := H_{sw2} \cdot \zeta_a \cdot \exp(-I\omega \cdot t)$:

> $F_{zw} := H_{sw3} \cdot \zeta_a \cdot \exp(-I\omega \cdot t)$:

> $M_{xw} := H_{sw4} \cdot \zeta_a \cdot \exp(-I\omega \cdot t)$:

>

> $F_{wy} := F_{yw} - a_{b22} \cdot \ddot{X1}(t) - a_{b24} \cdot \ddot{X3}(t) - b_{b22} \cdot \dot{X1}(t) - b_{b24} \cdot \dot{X3}(t)$:

> $F_{wz} := F_{zw} - a_{b33} \cdot \ddot{X2}(t) - b_{b33} \cdot \dot{X2}(t)$:

> $M_{wx} := M_{xw} - a_{b44} \cdot \ddot{X3}(t) - a_{b42} \cdot \ddot{X1}(t) - b_{b44} \cdot \dot{X3}(t) - b_{b42} \cdot \dot{X1}(t)$:

>

Small angle approximation

> $List\_small\_angles := [\cos(X3(t)) = 1, \sin(X3(t)) = X3(t), \cos(X4(t)) = 1, \sin(X4(t)) = X4(t), \cos(X7(t)) = 1, \sin(X7(t)) = X7(t), \cos(X8(t)) = 1, \sin(X8(t)) = X8(t), \cos(X11(t)) = 1, \sin(X11(t)) = X11(t)]$:

> $EoM1\_full$:

> $EoM1\_sa := factor(subs[eval](List\_small\_angles, EoM1\_full))$:

> $EoM2\_sa := factor(subs[eval](List\_small\_angles, EoM2\_full))$:

> $EoM3\_sa := factor(subs[eval](List\_small\_angles, EoM3\_full))$:

> $EoM4\_sa := factor(subs[eval](List\_small\_angles, EoM4\_full))$:

> $EoM5\_sa := factor(subs[eval](List\_small\_angles, EoM5\_full))$:

> $EoM6\_sa := factor(subs[eval](List\_small\_angles, EoM6\_full))$:

```
> EoM7_sa := factor(subs[eval](List_small_angles, EoM7_full)) :
> EoM8_sa := factor(subs[eval](List_small_angles, EoM8_full)) :
> EoM9_sa := factor(subs[eval](List_small_angles, EoM9_full)) :
>
```

Replace for matrix and vector

$$> List\_phys2vec := \left[\ddot{X3}(t) = X3dd, \dot{X3}(t) = X3d, X3(t) = X3, \ddot{X4}(t) = X4dd, \dot{X4}(t) = X4d, X4(t) \right.$$

$$= X4, \ddot{X7}(t) = X7dd, \dot{X7}(t) = X7d, X7(t) = X7, \ddot{X8}(t) = X8dd, \dot{X8}(t) = X8d, X8(t) = X8,$$

$$\ddot{X11}(t) = X11dd, \dot{X11}(t) = X11d, X11(t) = X11, \ddot{Lc1}(t) = Lc1dd, \dot{Lc1}(t) = Lc1d, Lc1(t)$$

$$= Lc1, \ddot{Lc2}(t) = Lc2dd, \dot{Lc2}(t) = Lc2d, Lc2(t) = Lc2\ , \ddot{Lc3}(t) = Lc3dd, \dot{Lc3}(t) = Lc3d,$$

$$\left. Lc3(t) = Lc3, \ddot{Lsl}(t) = Lsldd, \dot{Lsl}(t) = Lsld, Lsl(t) = Lsl, \zeta_a = \frac{zw}{\exp(-I\omega t)} \right] :$$

$$> List\_vec2phys := \left[X3dd = \ddot{\phi}_b, X3d = \dot{\phi}_b, X3 = \phi_b, X4dd = \ddot{\phi}_{c1}, X4d = \dot{\phi}_{c1}, X4 = \phi_{c1}, X7dd = \ddot{\phi}_{hc}, X7d \right.$$

$$= \dot{\phi}_{hc}, X7 = \phi_{hc}, X8dd = \ddot{\phi}_{c2}, X8d = \dot{\phi}_{c2}, X8 = \phi_{c2}, X11dd = \ddot{\phi}_{c3}, X11d = \dot{\phi}_{c3}, X11 = \phi_{c3}, Lc1dd =$$

$$\ddot{L}_{c1},\ Lc1d = \dot{L}_{c1}, Lc1 = L_{c1}, Lc2dd = \ddot{L}_{c2},\ Lc2d = \dot{L}_{c2}, Lc2 = L_{c2}, Lc3dd = \ddot{L}_{c3},\ Lc3d = \dot{L}_{c3}, Lc3$$

$$\left. = L_{c3}, Lsldd = \ddot{L}_{sl},\ Lsld = \dot{L}_{sl}, Lsl = L_{sl}, zw = \zeta_a \cdot \exp(-I\omega t) \right] :$$

```
> EoM1 := factor(subs[eval](List_phys2vec, EoM1_sa)) :
> EoM2 := factor(subs[eval](List_phys2vec, EoM2_sa)) :
> EoM3 := factor(subs[eval](List_phys2vec, EoM3_sa)) :
> EoM4 := factor(subs[eval](List_phys2vec, EoM4_sa)) :
> EoM5 := factor(subs[eval](List_phys2vec, EoM5_sa)) :
> EoM6 := factor(subs[eval](List_phys2vec, EoM6_sa)) :
> EoM7 := factor(subs[eval](List_phys2vec, EoM7_sa)) :
> EoM8 := factor(subs[eval](List_phys2vec, EoM8_sa)) :
> EoM9 := factor(subs[eval](List_phys2vec, EoM9_sa)) :
>
> with(VectorCalculus) :
> list_p := [X3, X4, X7, X8, X11, Lc1, Lc2, Lc3, Lsl] :
> list_pd := [X3d, X4d, X7d, X8d, X11d, Lc1d, Lc2d, Lc3d, Lsld] :
> list_pdd := [X3dd, X4dd, X7dd, X8dd, X11dd, Lc1dd, Lc2dd, Lc3dd, Lsldd] :
> X := vector(9, list_p) :
> Xd := vector(9, list_pd) :
> Xdd := vector(9, list_pdd) :
>
> con0 := [X3 = 0, X4 = 0, X7 = 0, X8 = 0, X11 = 0, Lc1 = 0, Lc2 = 0, Lc3 = 0, Lsl = 0, X3d = 0,
    X4d = 0, X7d = 0, X8d = 0, X11d = 0, Lc1d = 0, Lc2d = 0, Lc3d = 0, Lsld = 0, X3dd = 0,
    X4dd = 0, X7dd = 0, X8dd = 0, X11dd = 0, Lc1dd = 0, Lc2dd = 0, Lc3dd = 0, Lsldd = 0, zw
```

```
        = 0 ] :
>
```

Constant right hand side terms

```
> RHS_EoM1_con := - (eval(lhs(EoM1), con0)) :
> RHS_EoM2_con := - (eval(lhs(EoM2), con0)) :
> RHS_EoM3_con := - (eval(lhs(EoM3), con0)) :
> RHS_EoM4_con := - (eval(lhs(EoM4), con0)) :
> RHS_EoM5_con := - (eval(lhs(EoM5), con0)) :
> RHS_EoM6_con := - (eval(lhs(EoM6), con0)) :
> RHS_EoM7_con := - (eval(lhs(EoM7), con0)) :
> RHS_EoM8_con := - (eval(lhs(EoM8), con0)) :
> RHS_EoM9_con := - (eval(lhs(EoM9), con0)) :
>
```

Wave height dependent right hand side terms

```
>
> RHS_EoM1 := -zw·eval(diff(lhs(EoM1), zw), con0) :
> RHS_EoM2 := -zw·eval(diff(lhs(EoM2), zw), con0) :
> RHS_EoM3 := -zw·eval(diff(lhs(EoM3), zw), con0) :
> RHS_EoM4 := -zw·eval(diff(lhs(EoM4), zw), con0) :
> RHS_EoM5 := -zw·eval(diff(lhs(EoM5), zw), con0) :
> RHS_EoM6 := -zw·eval(diff(lhs(EoM6), zw), con0) :
> RHS_EoM7 := -zw·eval(diff(lhs(EoM7), zw), con0) :
> RHS_EoM8 := -zw·eval(diff(lhs(EoM8), zw), con0) :
> RHS_EoM9 := -zw·eval(diff(lhs(EoM9), zw), con0) :
>
```

Gradient terms

```
> grad_p_EoM1 := eval(Gradient(lhs(EoM1), list_p), con0) :
> grad_p_EoM2 := eval(Gradient(lhs(EoM2), list_p), con0) :
> grad_p_EoM3 := eval(Gradient(lhs(EoM3), list_p), con0) :
> grad_p_EoM4 := eval(Gradient(lhs(EoM4), list_p), con0) :
> grad_p_EoM5 := eval(Gradient(lhs(EoM5), list_p), con0) :
> grad_p_EoM6 := eval(Gradient(lhs(EoM6), list_p), con0) :
> grad_p_EoM7 := eval(Gradient(lhs(EoM7), list_p), con0) :
> grad_p_EoM8 := eval(Gradient(lhs(EoM8), list_p), con0) :
> grad_p_EoM9 := eval(Gradient(lhs(EoM9), list_p), con0) :
>
> grad_pd_EoM1 := eval(Gradient(lhs(EoM1), list_pd), con0) :
> grad_pd_EoM2 := eval(Gradient(lhs(EoM2), list_pd), con0) :
> grad_pd_EoM3 := eval(Gradient(lhs(EoM3), list_pd), con0) :
> grad_pd_EoM4 := eval(Gradient(lhs(EoM4), list_pd), con0) :
> grad_pd_EoM5 := eval(Gradient(lhs(EoM5), list_pd), con0) :
> grad_pd_EoM6 := eval(Gradient(lhs(EoM6), list_pd), con0) :
> grad_pd_EoM7 := eval(Gradient(lhs(EoM7), list_pd), con0) :
```

```
> grad_pd_EoM8 := eval(Gradient(lhs(EoM8), list_pd), con0) :
> grad_pd_EoM9 := eval(Gradient(lhs(EoM9), list_pd), con0) :
>
> grad_pdd_EoM1 := eval(Gradient(lhs(EoM1), list_pdd), con0) :
> grad_pdd_EoM2 := eval(Gradient(lhs(EoM2), list_pdd), con0) :
> grad_pdd_EoM3 := eval(Gradient(lhs(EoM3), list_pdd), con0) :
> grad_pdd_EoM4 := eval(Gradient(lhs(EoM4), list_pdd), con0) :
> grad_pdd_EoM5 := eval(Gradient(lhs(EoM5), list_pdd), con0) :
> grad_pdd_EoM6 := eval(Gradient(lhs(EoM6), list_pdd), con0) :
> grad_pdd_EoM7 := eval(Gradient(lhs(EoM7), list_pdd), con0) :
> grad_pdd_EoM8 := eval(Gradient(lhs(EoM8), list_pdd), con0) :
> grad_pdd_EoM9 := eval(Gradient(lhs(EoM9), list_pdd), con0) :
>
> A := Matrix(9, 9, 0) :
> B := Matrix(9, 9, 0) :
> C := Matrix(9, 9, 0) :
> F := Vector(9, [RHS_EoM1, RHS_EoM2, RHS_EoM3, RHS_EoM4, RHS_EoM5, RHS_EoM6,
      RHS_EoM7, RHS_EoM8, RHS_EoM9 ]) :
>
> for j from 1 to 9 do
  A[1, j] := grad_pdd_EoM1[j] :
  B[1, j] := grad_pd_EoM1[j] :
  C[1, j] := grad_p_EoM1[j] :
  A[2, j] := grad_pdd_EoM2[j] :
  B[2, j] := grad_pd_EoM2[j] :
  C[2, j] := grad_p_EoM2[j] :
  A[3, j] := grad_pdd_EoM3[j] :
  B[3, j] := grad_pd_EoM3[j] :
  C[3, j] := grad_p_EoM3[j] :
  A[4, j] := grad_pdd_EoM4[j] :
  B[4, j] := grad_pd_EoM4[j] :
  C[4, j] := grad_p_EoM4[j] :
  A[5, j] := grad_pdd_EoM5[j] :
  B[5, j] := grad_pd_EoM5[j] :
  C[5, j] := grad_p_EoM5[j] :
  A[6, j] := grad_pdd_EoM6[j] :
  B[6, j] := grad_pd_EoM6[j] :
  C[6, j] := grad_p_EoM6[j] :
  A[7, j] := grad_pdd_EoM7[j] :
  B[7, j] := grad_pd_EoM7[j] :
  C[7, j] := grad_p_EoM7[j] :
  A[8, j] := grad_pdd_EoM8[j] :
  B[8, j] := grad_pd_EoM8[j] :
  C[8, j] := grad_p_EoM8[j] :
  A[9, j] := grad_pdd_EoM9[j] :
  B[9, j] := grad_pd_EoM9[j] :
```

```
    C[9, j] := grad_p_EoM9[j] :
    end do:
>
```

A, B and C matrix

```
> A := simplify(A) :
> B := simplify(B) :
> CC := simplify(C) :
>
>
```

Force vector

```
> FF := Vector(9, [RHS_EoM1, RHS_EoM2, RHS_EoM3, RHS_EoM4, RHS_EoM5,
      RHS_EoM6, RHS_EoM7, RHS_EoM8, RHS_EoM9]) :
> F_disp := convert(FF, Matrix) :

>
> FF_con := Vector(9, [RHS_EoM1_con, RHS_EoM2_con, RHS_EoM3_con, RHS_EoM4_con,
      RHS_EoM5_con, RHS_EoM6_con, RHS_EoM7_con, RHS_EoM8_con, RHS_EoM9_con ])
      :
> F_con := convert(FF_con, Matrix) :
>
```

System matrix (Hsys)

```
> YY := (-ω^2·A + I B·ω + CC) :
>
```

Write to Python

```
> with(CodeGeneration) :
> Python(F_con) :
> Python(F_disp) :
> Python(YY) :
```

D.2 motions, forces and moment Maple script

```
> restart
> with(Physics):
>
```

Motion of the tower

```
>
> Yt(t) := -bl·sin(X3(t)) + X1(t):
> Zt(t) := bl·cos(X3(t)) + X2(t):
```

Kinematic constraints

crane **to** *crane hook*

```
>
> X9(t) := (L30 + Lc3Pre-Lc3(t))·sin(X11(t)):
> X10(t) := h_crane - (L30 + Lc3Pre-Lc3(t))·cos(X11(t)):
```

crane hook **to** *hc*

```
> X5(t) := X9(t) + ((L20 + Lc2Pre-Lc2(t))·sin(X8(t))) + h1_hc·sin(X7(t)):
> X6(t) := X10(t) - ((L20 + Lc2Pre-Lc2(t))·cos(X8(t))) - h1_hc·cos(X7(t)):
```

hc **to** *slider*

```
> X12(t) := X5(t) + h2_hc·sin(X7(t)) + ((Lsl0 + LslPre-Lsl(t))·sin(X7(t))):
> X13(t) := X6(t) - h2_hc·cos(X7(t)) - ((Lsl0 + LslPre-Lsl(t))·cos(X7(t))):
```

slider **to** *barge + tower*

```
> X1(t) := X12(t) + (L10 + Lc1Pre-Lc1(t))·sin(X4(t)) + (h_b)·sin(X3(t)):
> X2(t) := X13(t) - ((L10 + Lc1Pre-Lc1(t))·cos(X4(t))) - (h_b)·cos(X3(t)):
> YY := eval(X1(t)):
> ZZ := eval(X2(t)):
>
```

Cable forces

```
> Fcz(t) := cos(X4(t))·(Lc1Pre-Lc1(t))·c_c1:
> Fcy(t) := sin(X4(t))·(Lc1Pre-Lc1(t))·c_c1:
>
```

Barge forces

```
> Fbz(t) := (Fcz(t) - mt·Zt(t)..-mt·g):
> Fby(t) := (-Fcy(t) - mt·Yt(t)..):
>
```

Vertical barge forces angled

```
> Fbz_angle(t) := cos(X3(t))·Fbz(t) - sin(X3(t))·Fby(t):
> Fbz_angle2 := eval(Fbz_angle(t)):
>
```

Moment between the tower and barge

```
> Mb(t) := -Fcz(t)·h_tower·sin(X3(t)) + Fcy(t)·h_tower·cos(X3(t)) - Jxx·X3(t)..
      + mt·(g + Zt(t)..)·al·sin(X3(t)) + mt·Yt(t)..·al·cos(X3(t)):
> Mb := eval(Mb(t)):
>
```

Smal angle approximation

```
> List_small_angles := [cos(X3(t)) = 1, sin(X3(t)) = X3(t), cos(X4(t)) = 1, sin(X4(t))
      = X4(t), cos(X7(t)) = 1, sin(X7(t)) = X7(t), cos(X8(t)) = 1, sin(X8(t)) = X8(t),
     cos(X11(t)) = 1, sin(X11(t)) = X11(t)] :
> List_phys2vec := [X3(t)(2) = X3dd, X3(t)' = X3d, X3(t) = X3, X4(t)(2) = X4dd, X4(t)' = X4d, X4(t)
      = X4, X7(t)(2) = X7dd, X7(t)' = X7d, X7(t) = X7, X8(t)(2) = X8dd, X8(t)' = X8d, X8(t) = X8,
     X11(t)(2) = X11dd, X11(t)' = X11d, X11(t) = X11, Lc1(t)(2) = Lc1dd, Lc1(t)' = Lc1d, Lc1(t)
      = Lc1, Lc2(t)(2) = Lc2dd, Lc2(t)' = Lc2d, Lc2(t) = Lc2 , Lc3(t)(2) = Lc3dd, Lc3(t)' = Lc3d,
      Lc3(t) = Lc3, Lsl(t)(2) = Lsldd, Lsl(t)' = Lsld, Lsl(t) = Lsl] :
>
> Mb_short := factor(subs[eval](List_small_angles, Mb)) :
> Mb_simple := factor(subs[eval](List_phys2vec, Mb_short)) :
> Fbz_angle3 := factor(subs[eval](List_small_angles, Fbz_angle2)) :
> Fbz_angle4 := factor(subs[eval](List_phys2vec, Fbz_angle3)) :
```

Vertical and horizontal motions feeder and tower

```
> Zt := eval(Zt(t)) :
> Zt_short := factor(subs[eval](List_small_angles, Zt)) :
> Zt_simple := factor(subs[eval](List_phys2vec, Zt_short)) :
> YYY := factor(subs[eval](List_small_angles, YY)) :
> ZZZ := factor(subs[eval](List_small_angles, ZZ)) :
>
> YYYY := factor(subs[eval](List_phys2vec, YYY)) :
> ZZZZ := factor(subs[eval](List_phys2vec, ZZZ)) :
>
```

Write to Python

```
> with(CodeGeneration) :
> Python(Mb_simple) :
> Python(ZZZZ) :
> Python(YYYY) :
> Python(Zt_simple) :
```

Appendix E: Validation plots

E.1 Roll validation plots

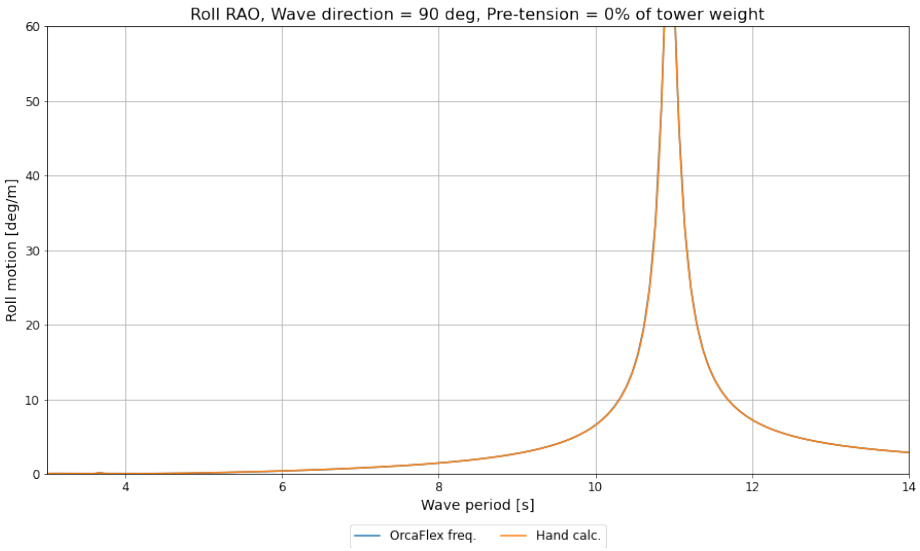

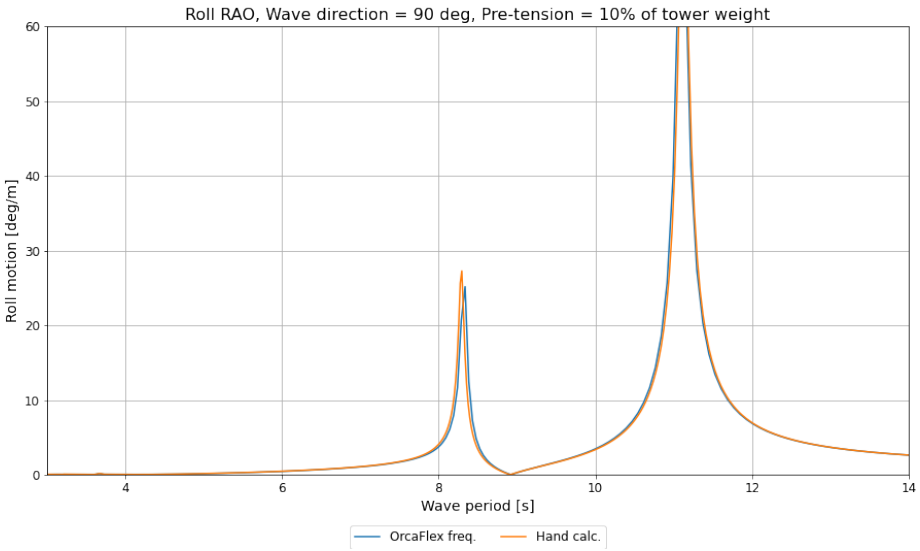

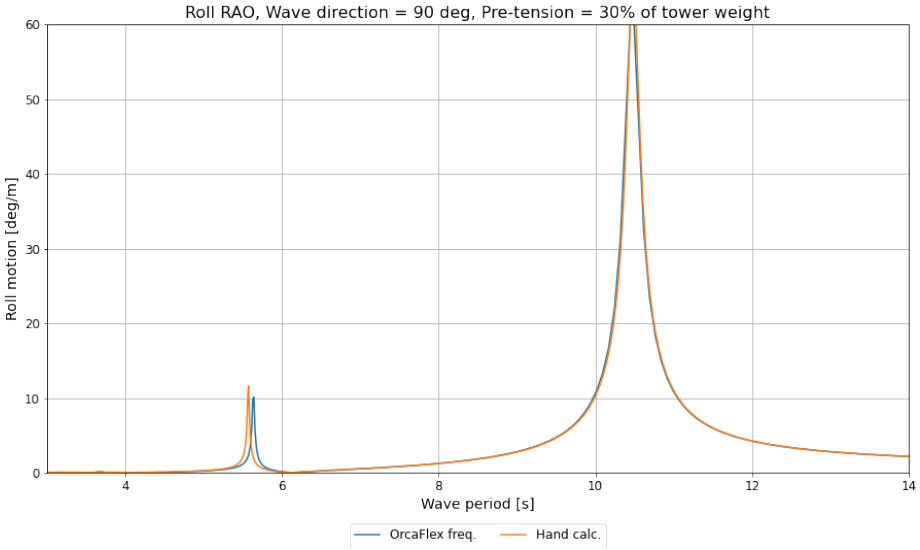
Roll RAO, Wave direction = 90 deg, Pre-tension = 30% of tower weight
Roll motion [deg/m]
Wave period [s]
OrcaFlex freq.
Hand calc.

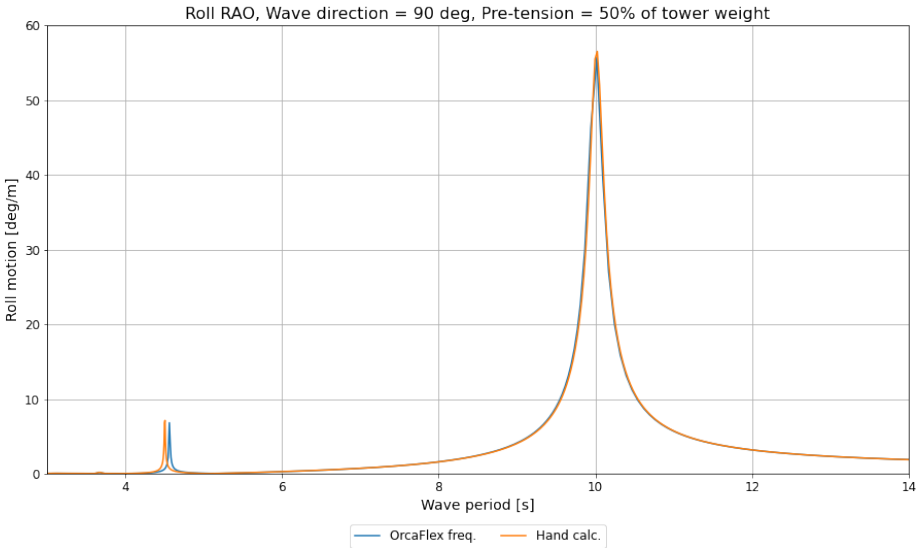
Roll RAO, Wave direction = 90 deg, Pre-tension = 50% of tower weight
Roll motion [deg/m]
Wave period [s]
OrcaFlex freq.
Hand calc.

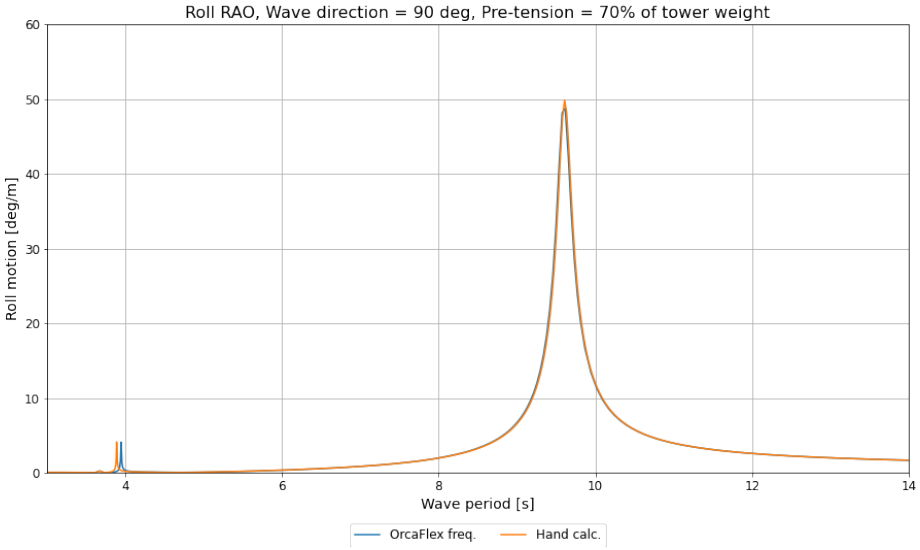
Roll RAO, Wave direction = 90 deg, Pre-tension = 70% of tower weight
Roll motion [deg/m]
Wave period [s]
OrcaFlex freq.
Hand calc.

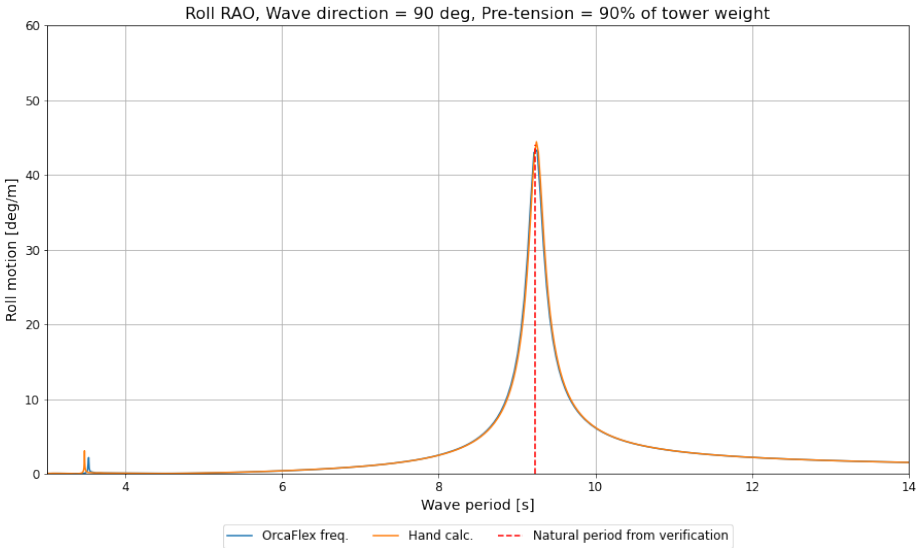
Roll RAO, Wave direction = 90 deg, Pre-tension = 90% of tower weight
Roll motion [deg/m]
Wave period [s]
OrcaFlex freq.
Hand calc.
Natural period from verification

E.2 Heave validation plots

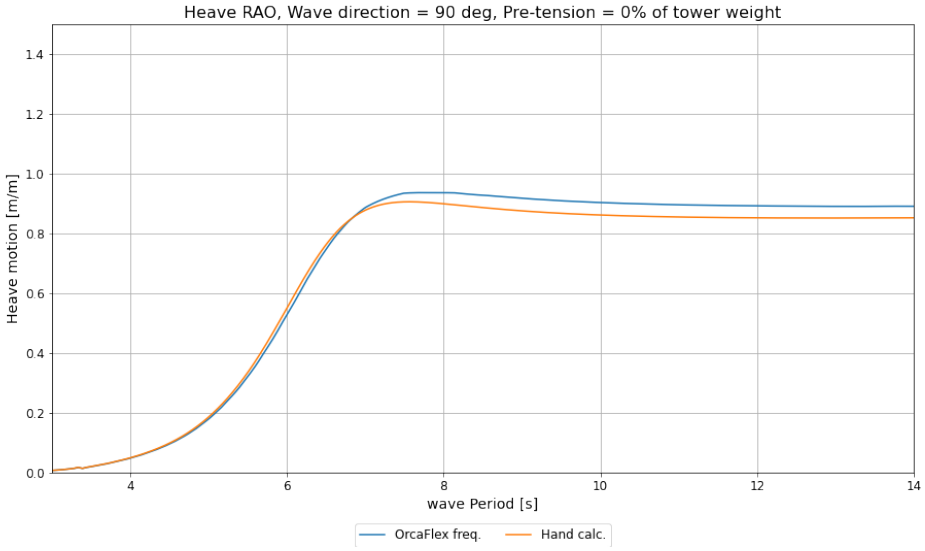

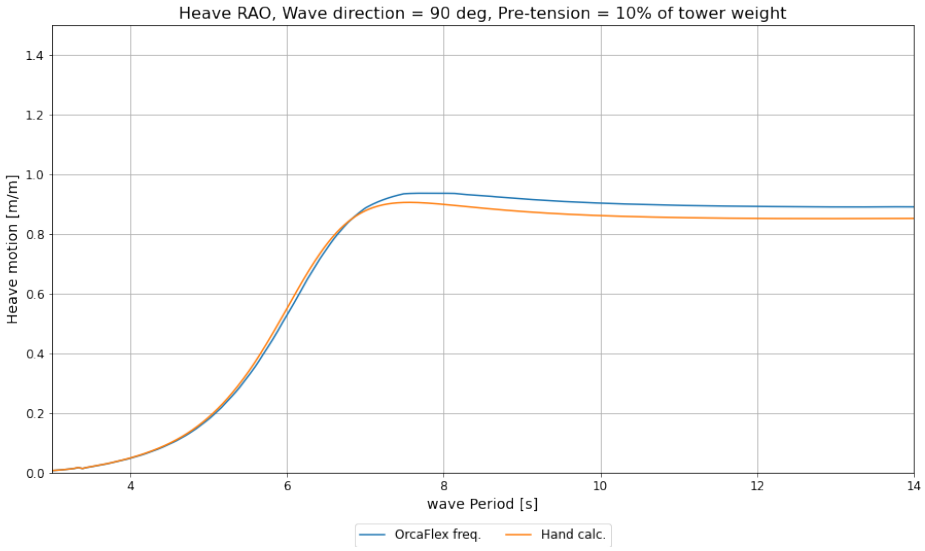

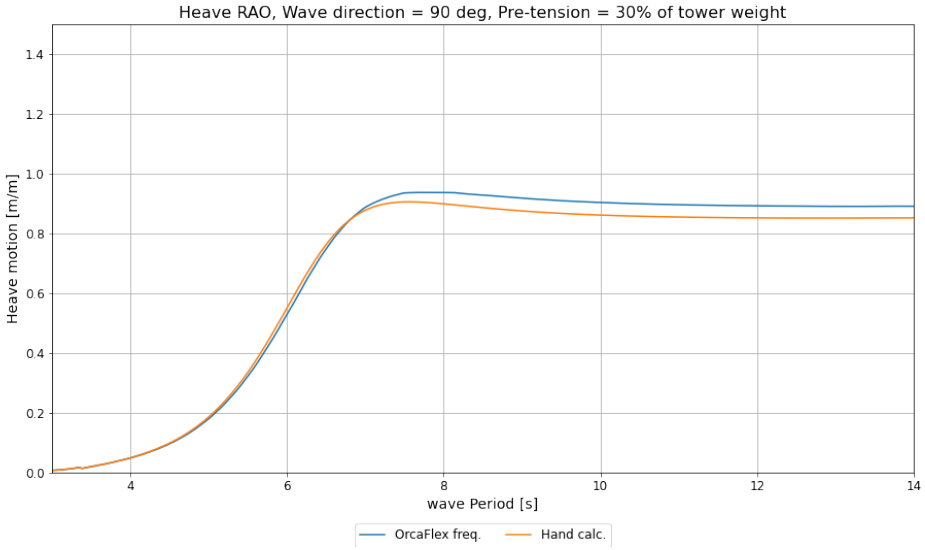
Heave RAO, Wave direction = 90 deg, Pre-tension = 30% of tower weight
Heave motion [m/m]
wave Period [s]
OrcaFlex freq.
Hand calc.

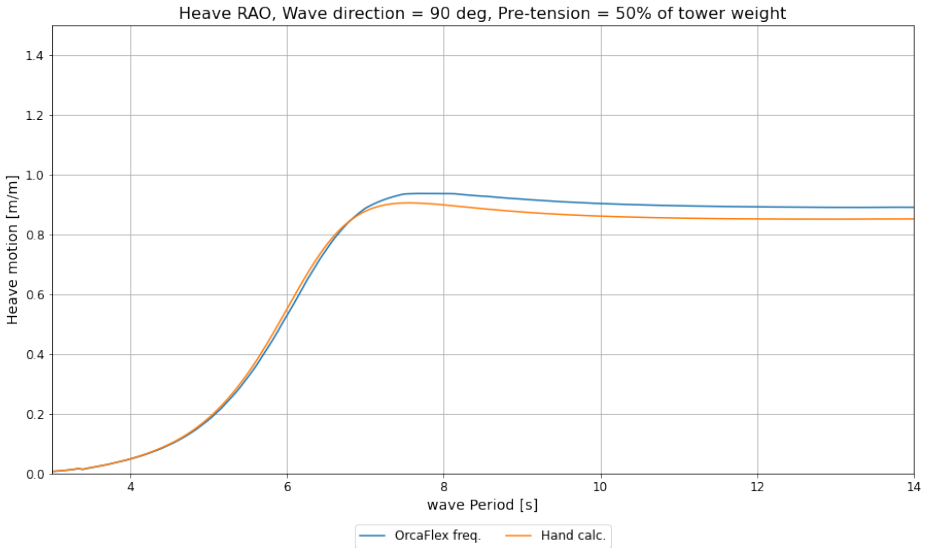
Heave RAO, Wave direction = 90 deg, Pre-tension = 50% of tower weight
Heave motion [m/m]
wave Period [s]
OrcaFlex freq.
Hand calc.

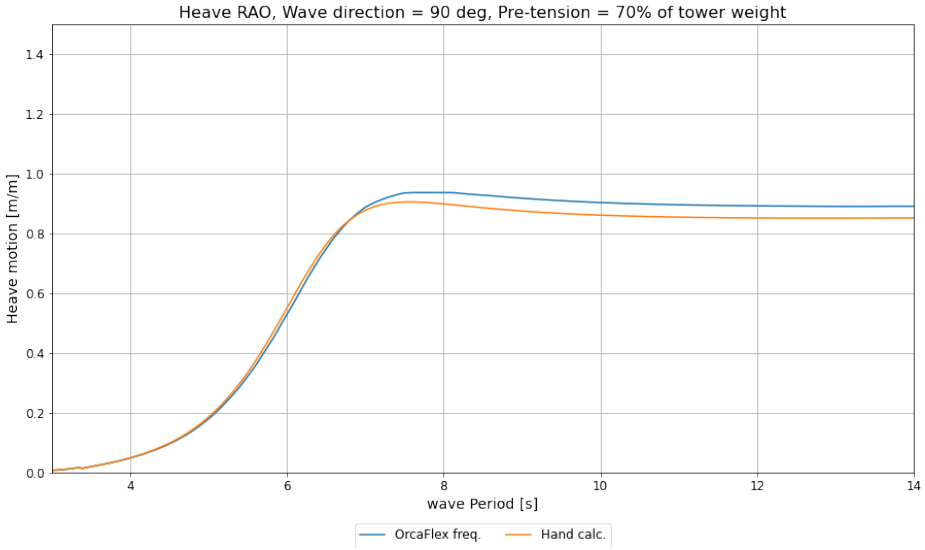
Heave RAO, Wave direction = 90 deg, Pre-tension = 70% of tower weight
Heave motion [m/m]
wave Period [s]
OrcaFlex freq.
Hand calc.

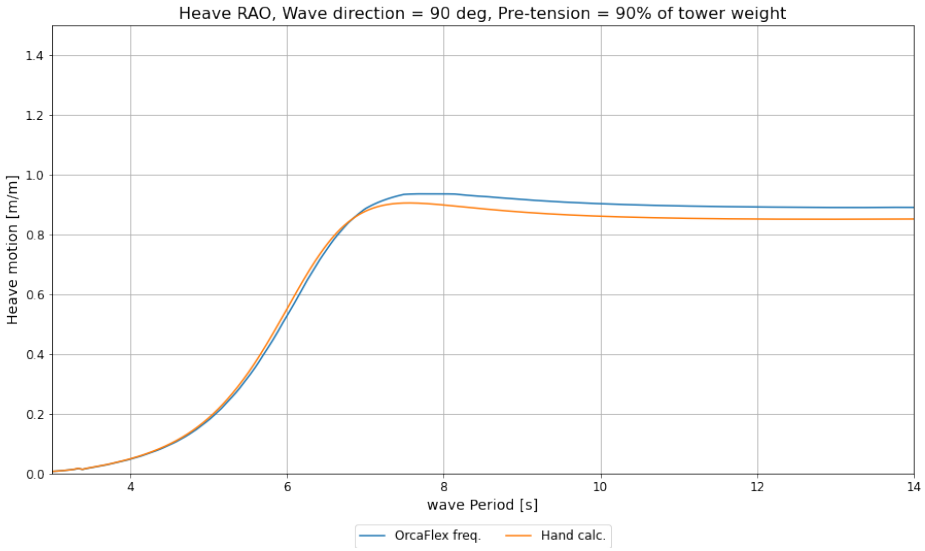
Heave RAO, Wave direction = 90 deg, Pre-tension = 90% of tower weight
Heave motion [m/m]
wave Period [s]
OrcaFlex freq.
Hand calc.

E.3 Sway validation plots

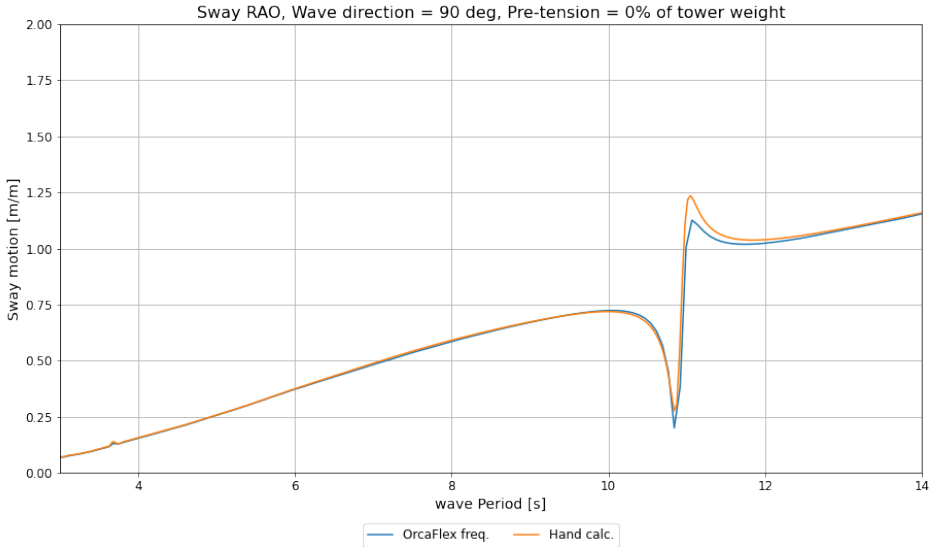

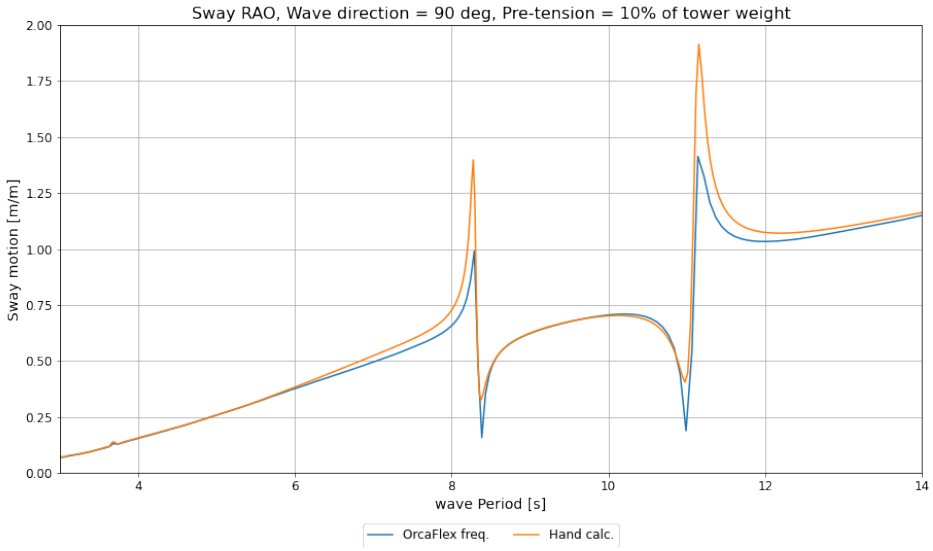

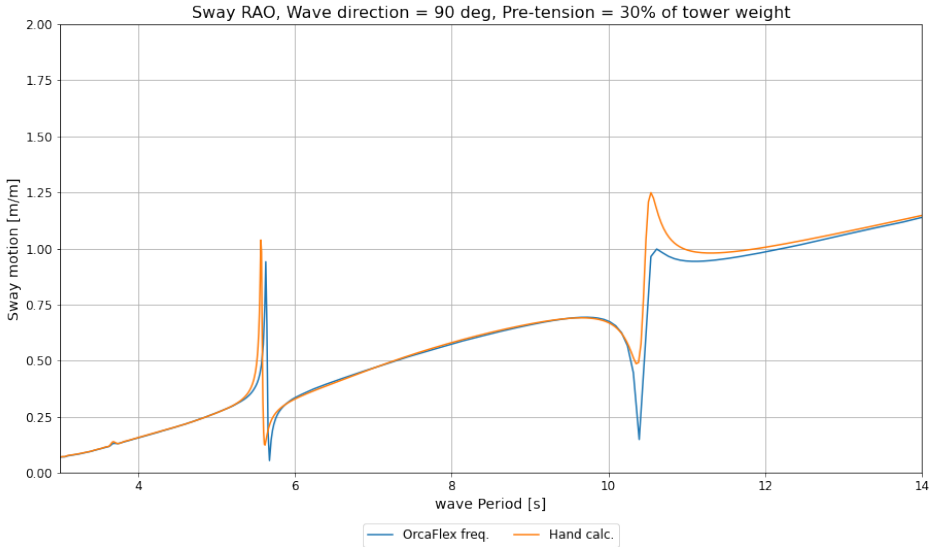
Sway RAO, Wave direction = 90 deg, Pre-tension = 30% of tower weight
Sway motion [m/m]
wave Period [s]
OrcaFlex freq.
Hand calc.

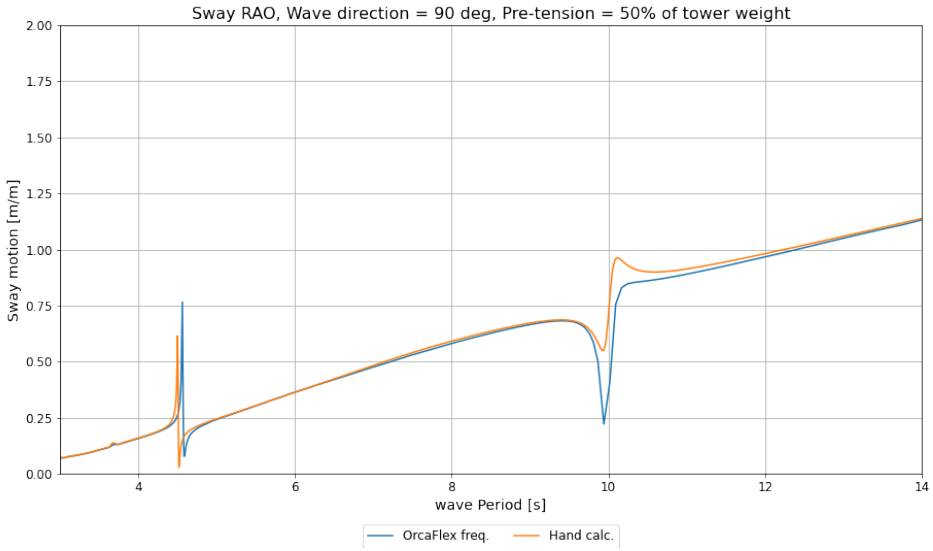
Sway RAO, Wave direction = 90 deg, Pre-tension = 50% of tower weight
Sway motion [m/m]
wave Period [s]
OrcaFlex freq.
Hand calc.

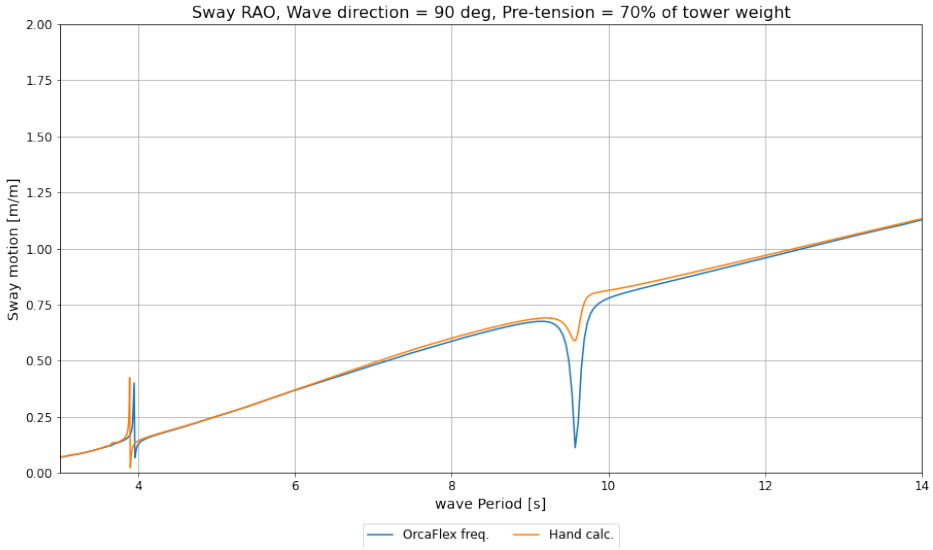
Sway RAO, Wave direction = 90 deg, Pre-tension = 70% of tower weight
Sway motion [m/m]
wave Period [s]
OrcaFlex freq.
Hand calc.

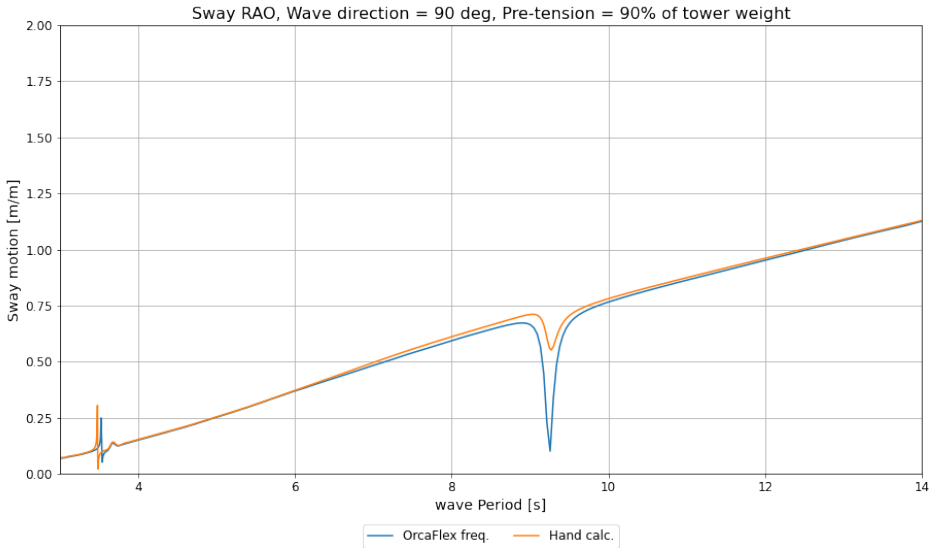
Sway RAO, Wave direction = 90 deg, Pre-tension = 90% of tower weight
Sway motion [m/m]
wave Period [s]
OrcaFlex freq.
Hand calc.

E.4 Moment validation plots

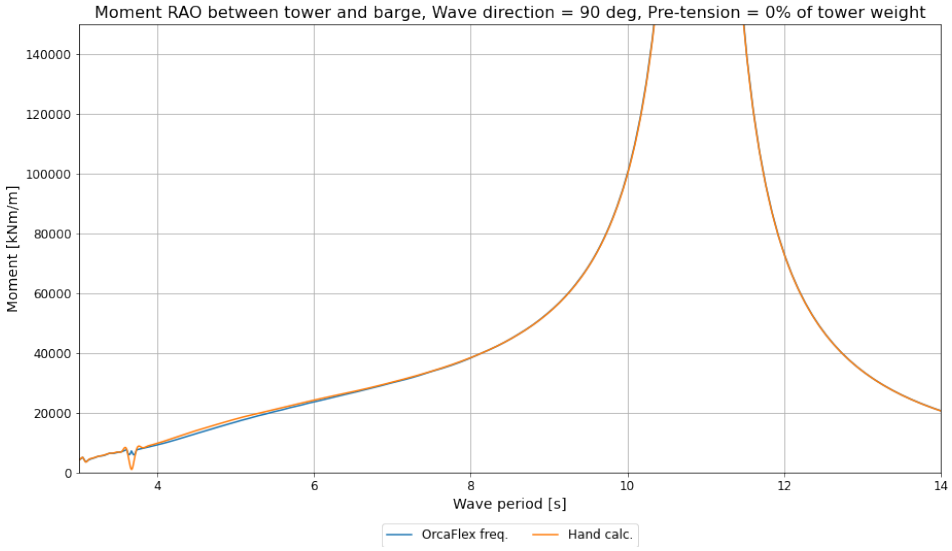

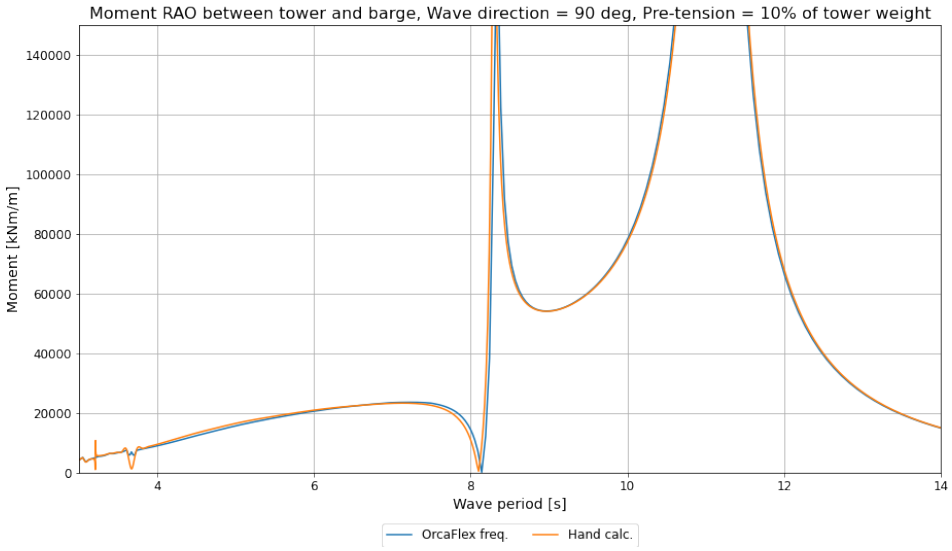

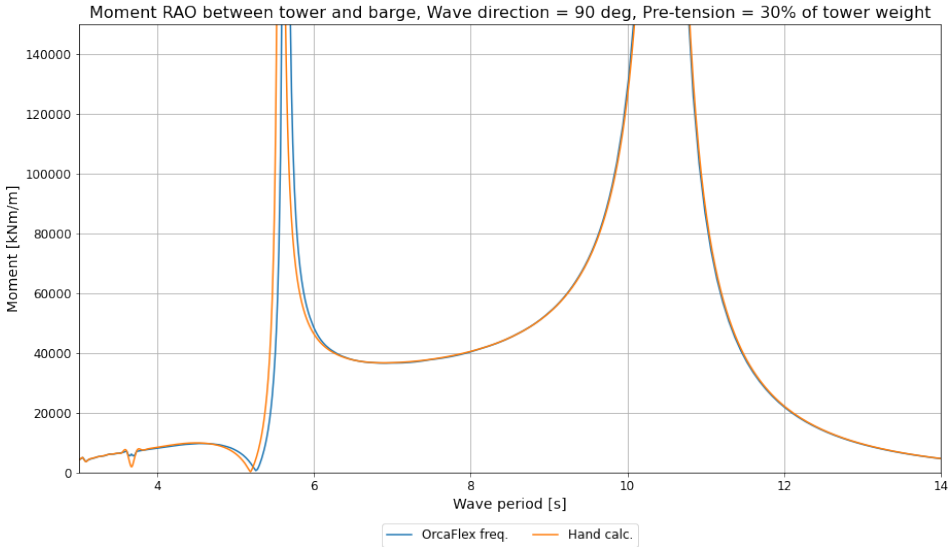
Moment RAO between tower and barge, Wave direction = 90 deg, Pre-tension = 30% of tower weight
Moment [kNm/m]
Wave period [s]
OrcaFlex freq.
Hand calc.

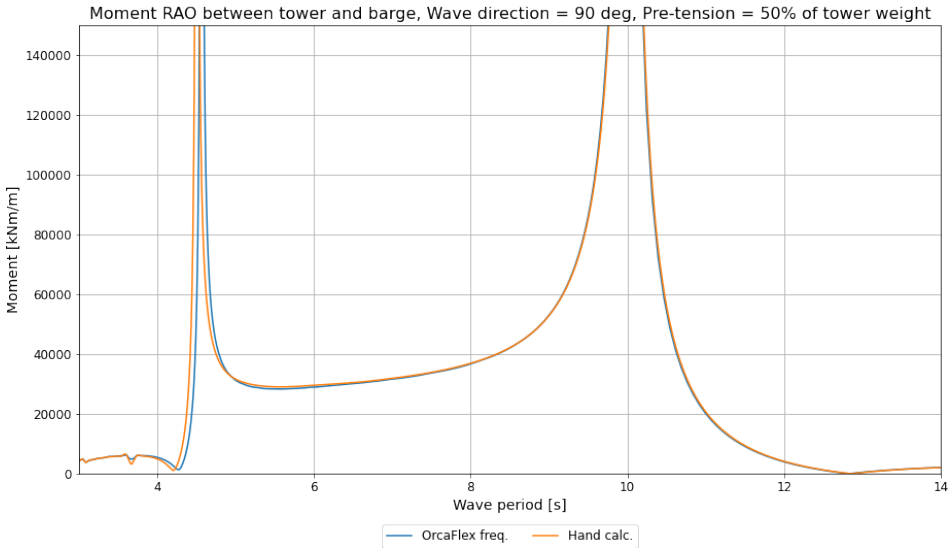
Moment RAO between tower and barge, Wave direction = 90 deg, Pre-tension = 50% of tower weight
Moment [kNm/m]
Wave period [s]
OrcaFlex freq.
Hand calc.

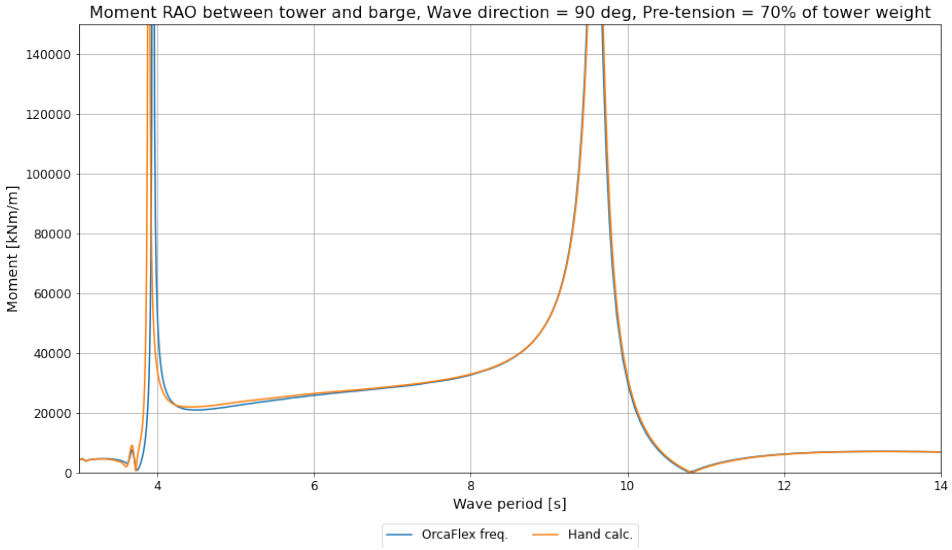
Moment RAO between tower and barge, Wave direction = 90 deg, Pre-tension = 70% of tower weight
Moment [kNm/m]
Wave period [s]
OrcaFlex freq.
Hand calc.

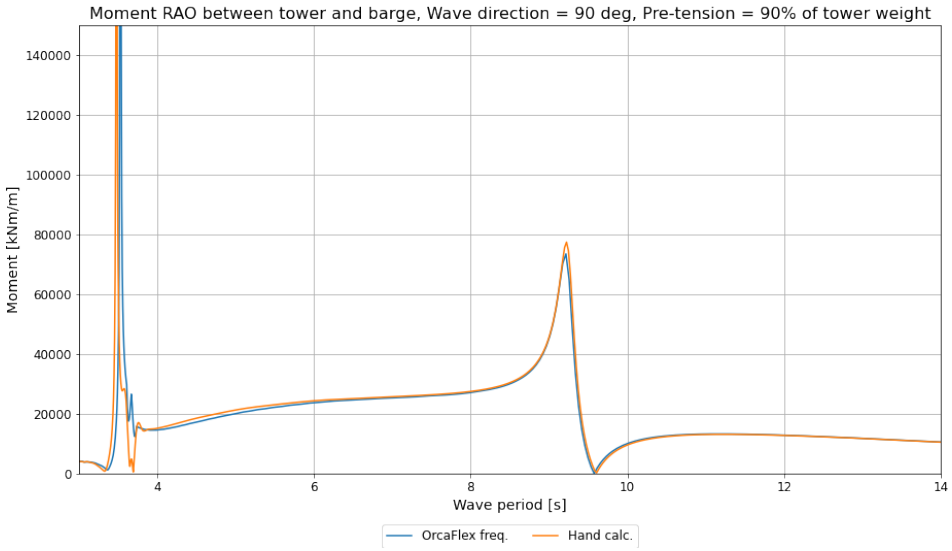
Moment RAO between tower and barge, Wave direction = 90 deg, Pre-tension = 90% of tower weight
Moment [kNm/m]
Wave period [s]
OrcaFlex freq.
Hand calc.

Appendix F: Python codes

This Appendix contains confidential information and is therefore excluded from the public thesis version.

Appendix G: Results plots

G.1 Tension in the HC-tower sling

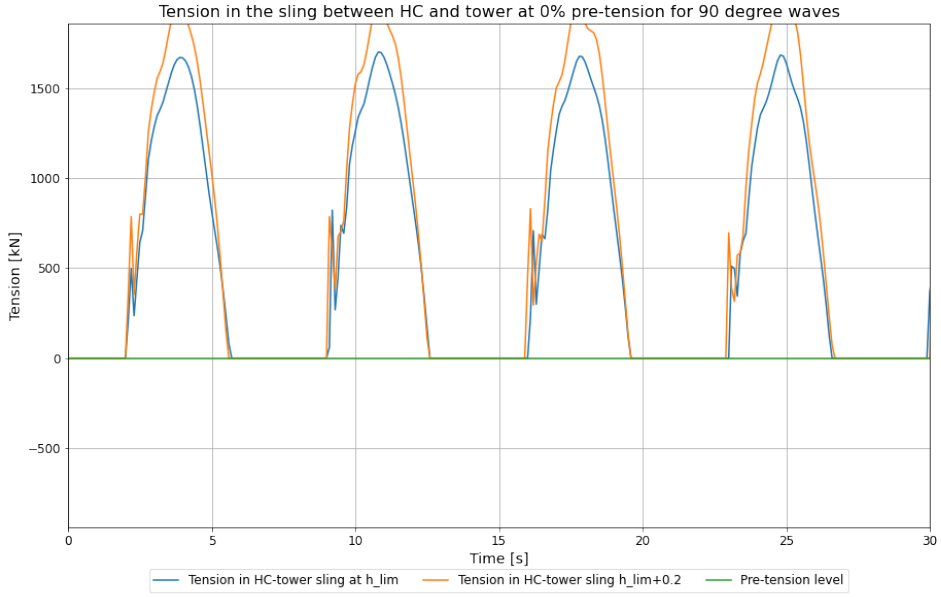

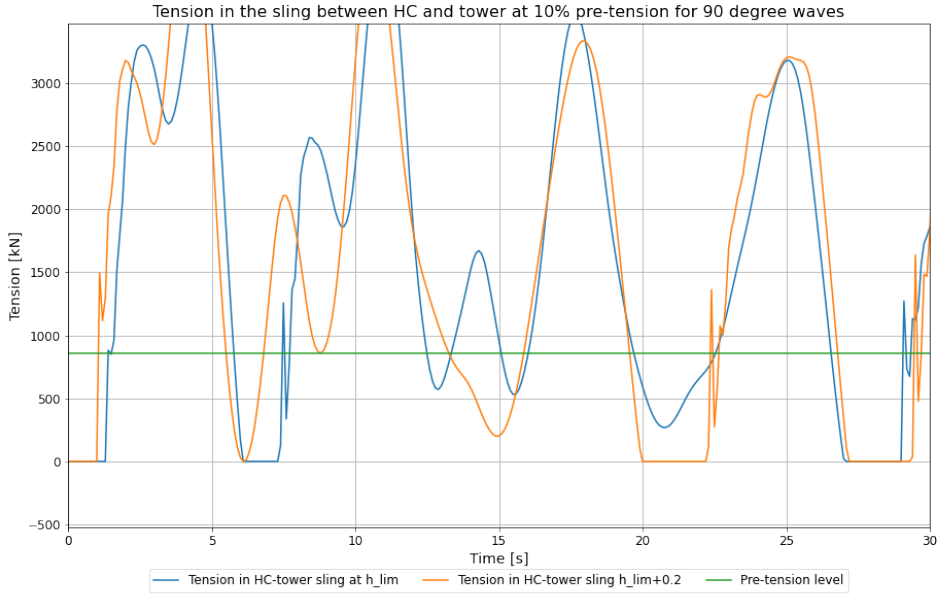

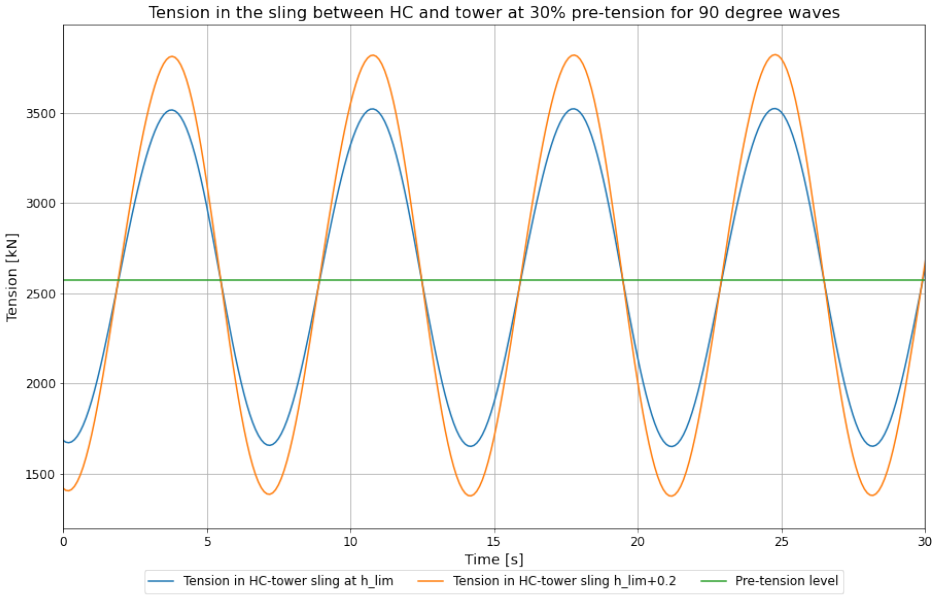
Tension in the sling between HC and tower at 30% pre-tension for 90 degree waves
Tension [kN]
Time [s]
Tension in HC-tower sling at h_lim
Tension in HC-tower sling h_lim+0.2
Pre-tension level

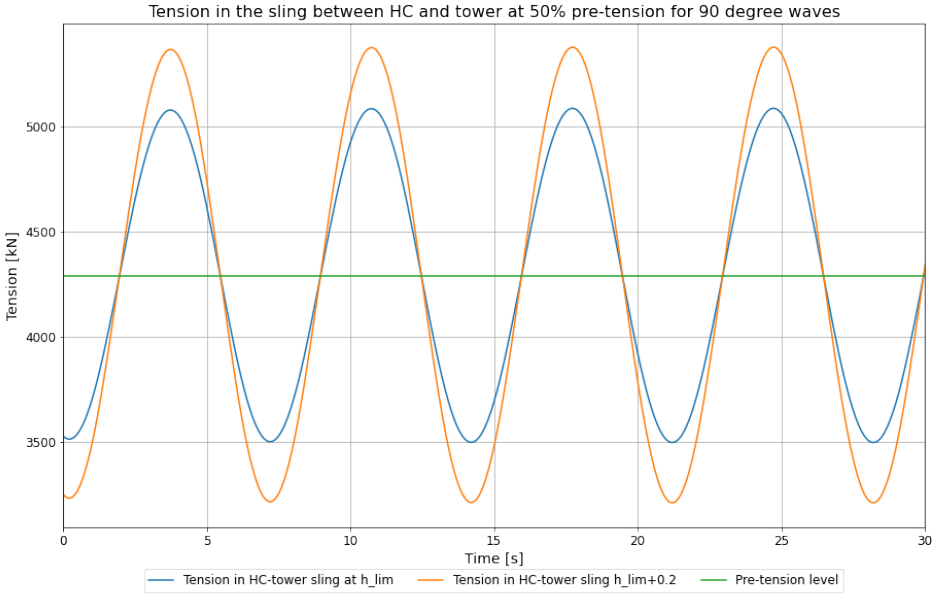
Tension in the sling between HC and tower at 50% pre-tension for 90 degree waves
Tension [kN]
Time [s]
Tension in HC-tower sling at h_lim
Tension in HC-tower sling h_lim+0.2
Pre-tension level

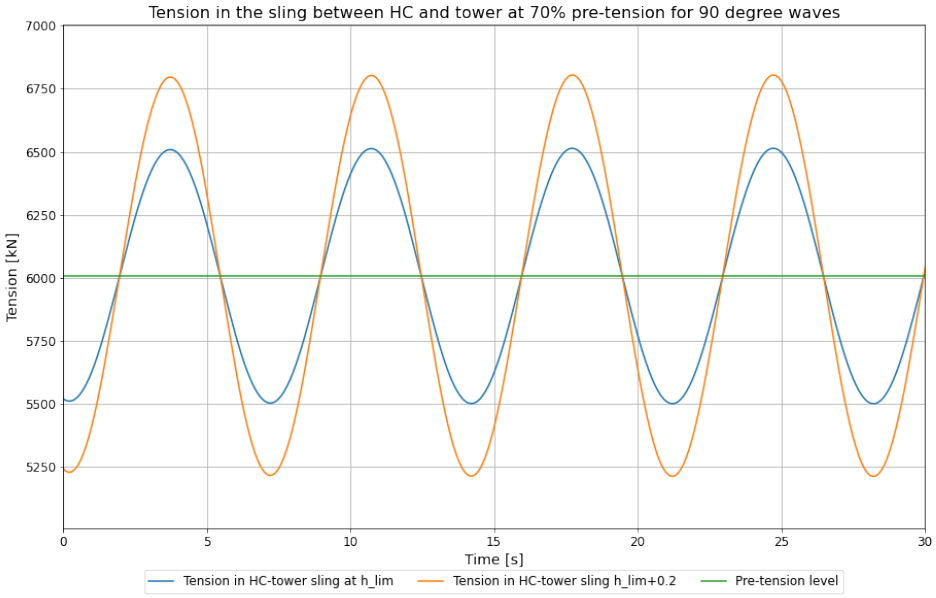
Tension in the sling between HC and tower at 70% pre-tension for 90 degree waves
Tension [kN]
Time [s]
Tension in HC-tower sling at h_lim
Tension in HC-tower sling h_lim+0.2
Pre-tension level

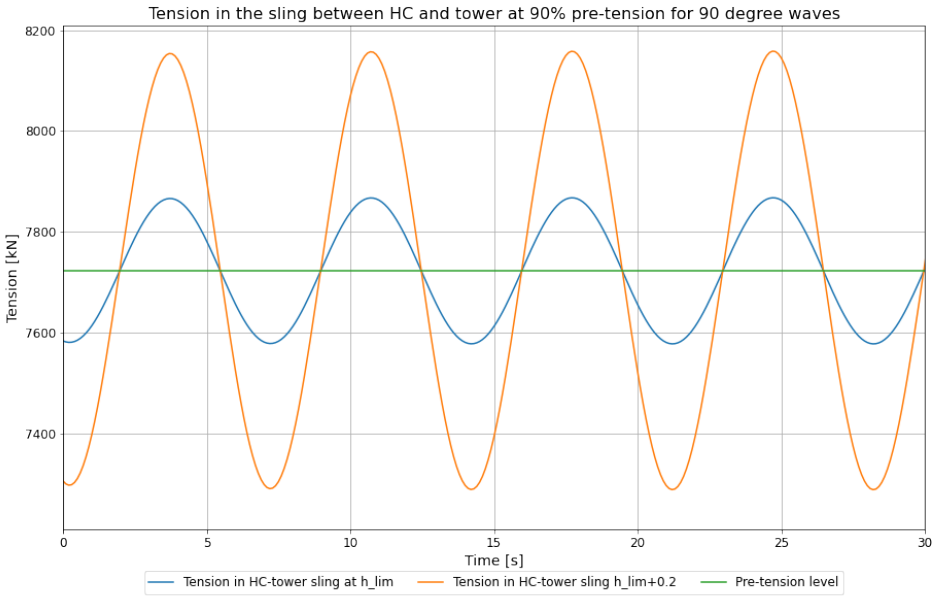
Tension in the sling between HC and tower at 90% pre-tension for 90 degree waves
Tension [kN]
Time [s]
Tension in HC-tower sling at h_lim
Tension in HC-tower sling h_lim+0.2
Pre-tension level

G.2 Heave motion feeder

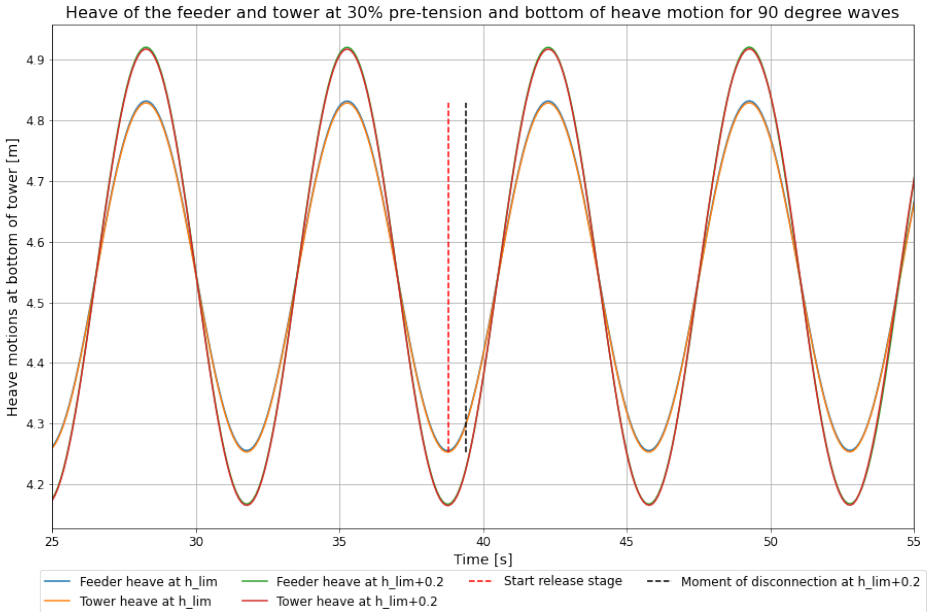

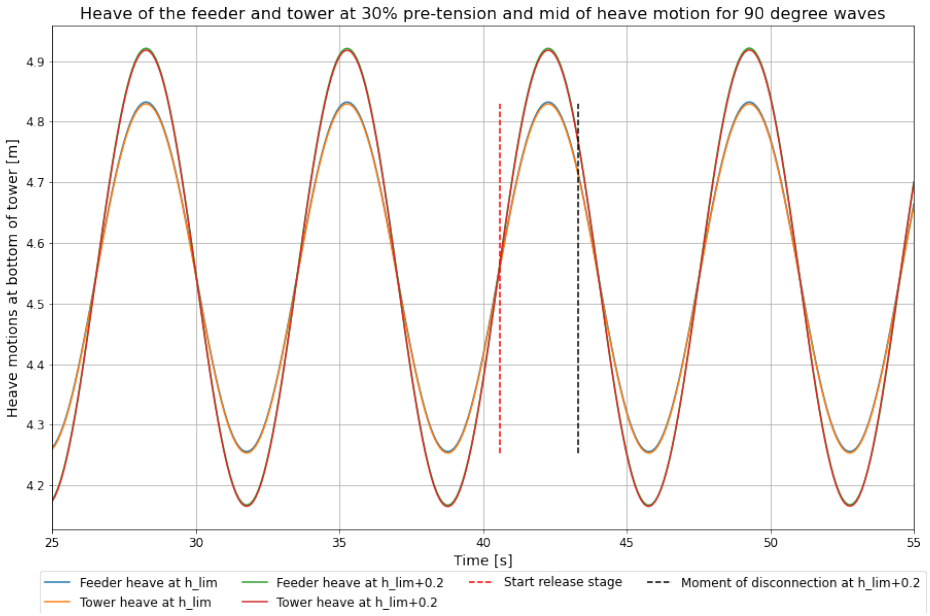

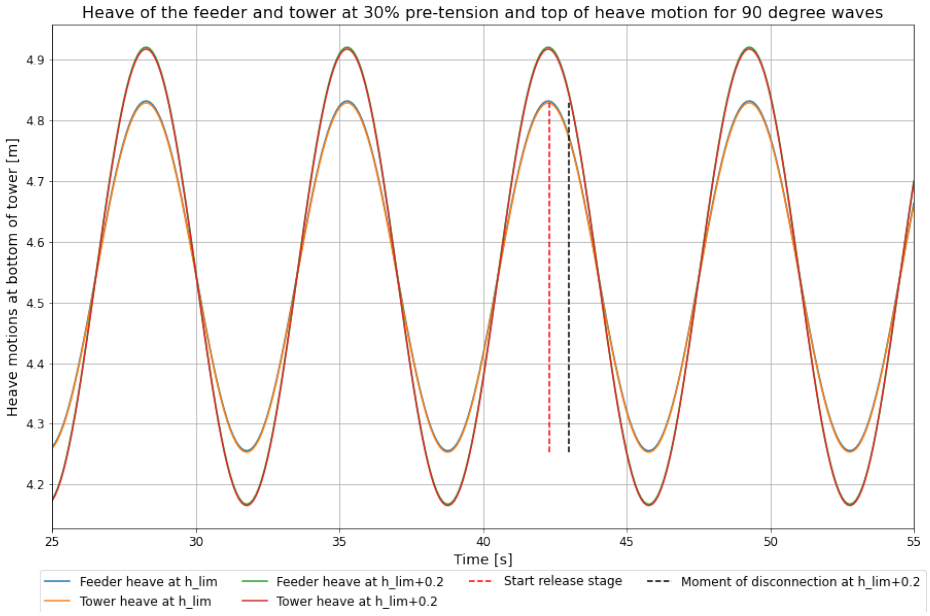
Heave of the feeder and tower at 30% pre-tension and top of heave motion for 90 degree waves
Heave motions at bottom of tower [m]
Time [s]
Feeder heave at h_lim
Tower heave at h_lim
Feeder heave at h_lim+0.2
Tower heave at h_lim+0.2
Start release stage
Moment of disconnection at h_lim+0.2

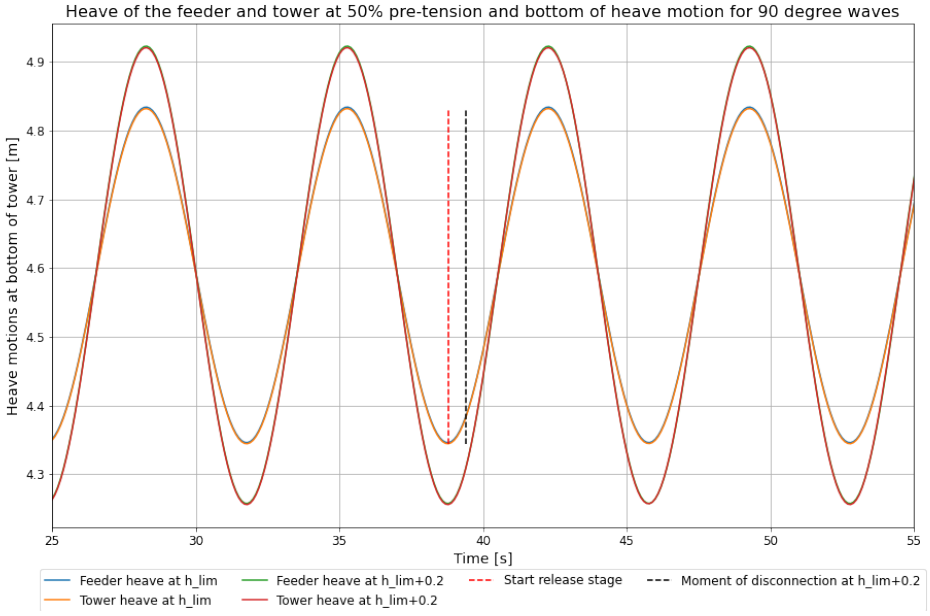
Heave of the feeder and tower at 50% pre-tension and bottom of heave motion for 90 degree waves
Heave motions at bottom of tower [m]
Time [s]
Feeder heave at h_lim
Tower heave at h_lim
Feeder heave at h_lim+0.2
Tower heave at h_lim+0.2
Start release stage
Moment of disconnection at h_lim+0.2

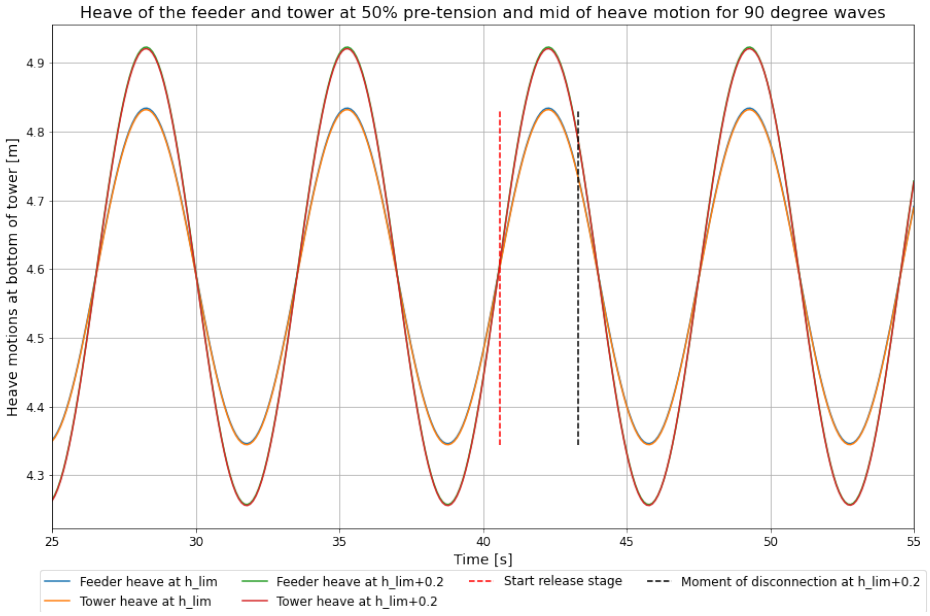
Heave of the feeder and tower at 50% pre-tension and mid of heave motion for 90 degree waves
Heave motions at bottom of tower [m]
Time [s]
Feeder heave at h_lim
Tower heave at h_lim
Feeder heave at h_lim+0.2
Tower heave at h_lim+0.2
Start release stage
Moment of disconnection at h_lim+0.2

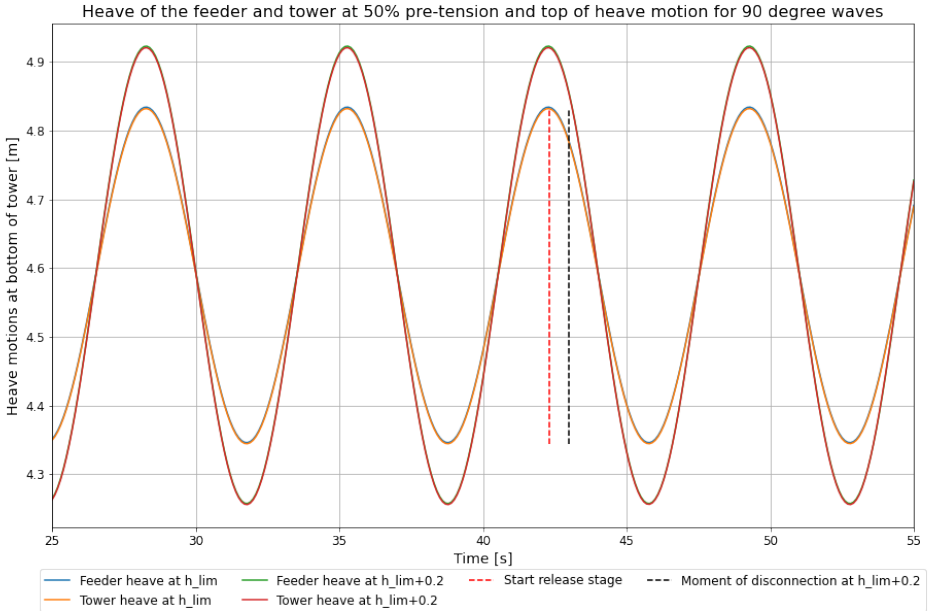
Heave of the feeder and tower at 50% pre-tension and top of heave motion for 90 degree waves
Heave motions at bottom of tower [m]
Time [s]
Feeder heave at h_lim
Tower heave at h_lim
Feeder heave at h_lim+0.2
Tower heave at h_lim+0.2
Start release stage
Moment of disconnection at h_lim+0.2

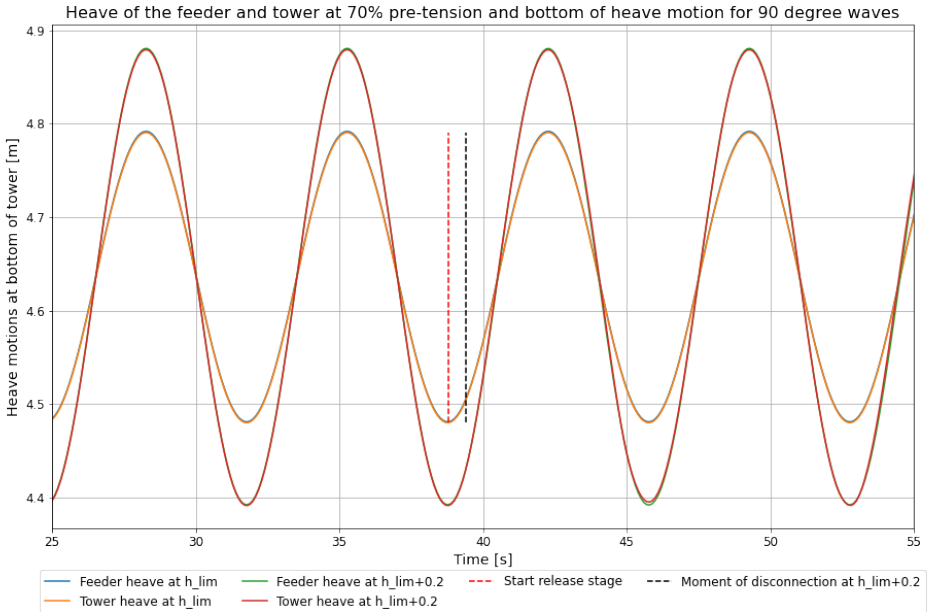
Heave of the feeder and tower at 70% pre-tension and bottom of heave motion for 90 degree waves
Heave motions at bottom of tower [m]
Time [s]
Feeder heave at h_lim
Tower heave at h_lim
Feeder heave at h_lim+0.2
Tower heave at h_lim+0.2
Start release stage
Moment of disconnection at h_lim+0.2

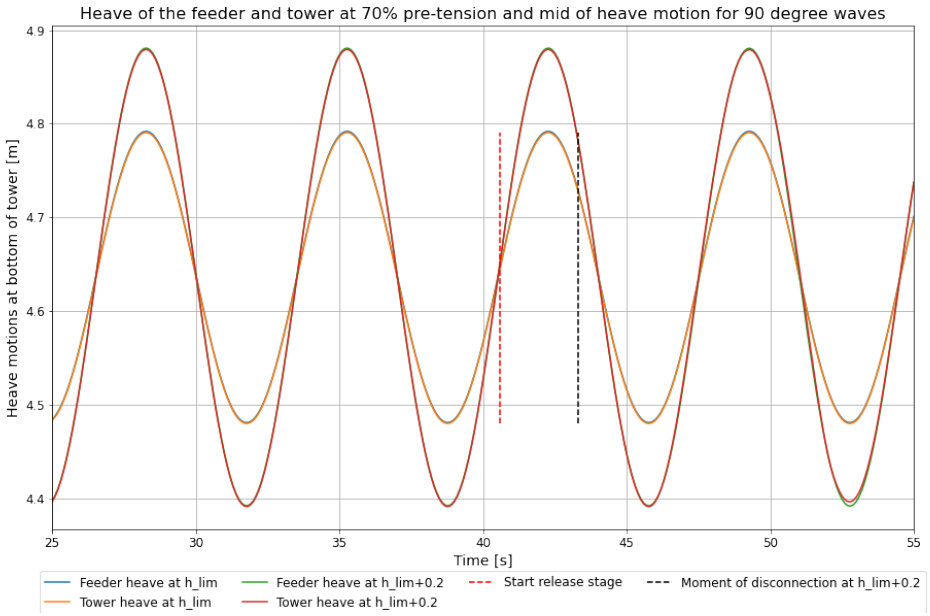
Heave of the feeder and tower at 70% pre-tension and mid of heave motion for 90 degree waves
Heave motions at bottom of tower [m]
Time [s]
Feeder heave at h_lim
Tower heave at h_lim
Feeder heave at h_lim+0.2
Tower heave at h_lim+0.2
Start release stage
Moment of disconnection at h_lim+0.2

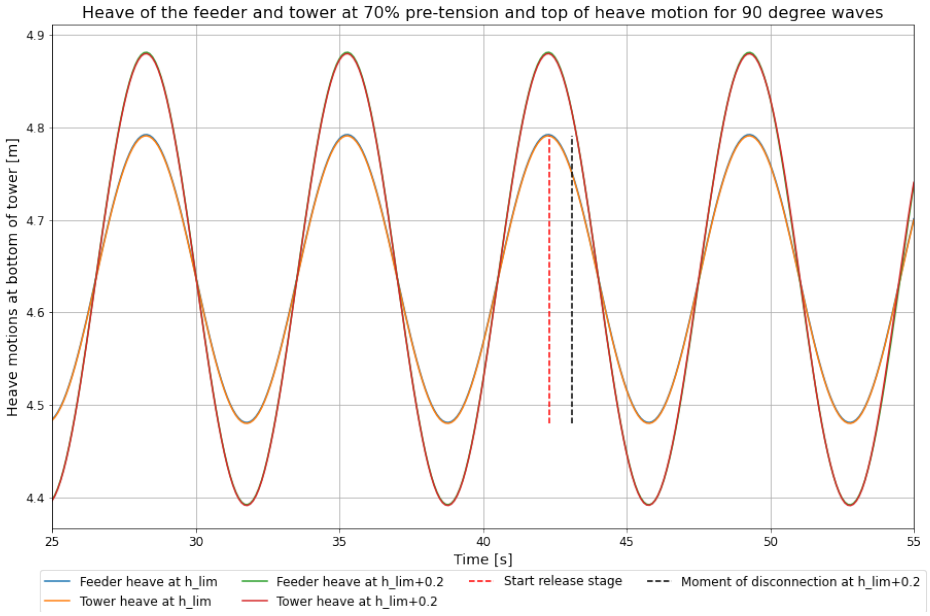
Heave of the feeder and tower at 70% pre-tension and top of heave motion for 90 degree waves
Heave motions at bottom of tower [m]
Time [s]
Feeder heave at h_lim
Tower heave at h_lim
Feeder heave at h_lim+0.2
Tower heave at h_lim+0.2
Start release stage
Moment of disconnection at h_lim+0.2

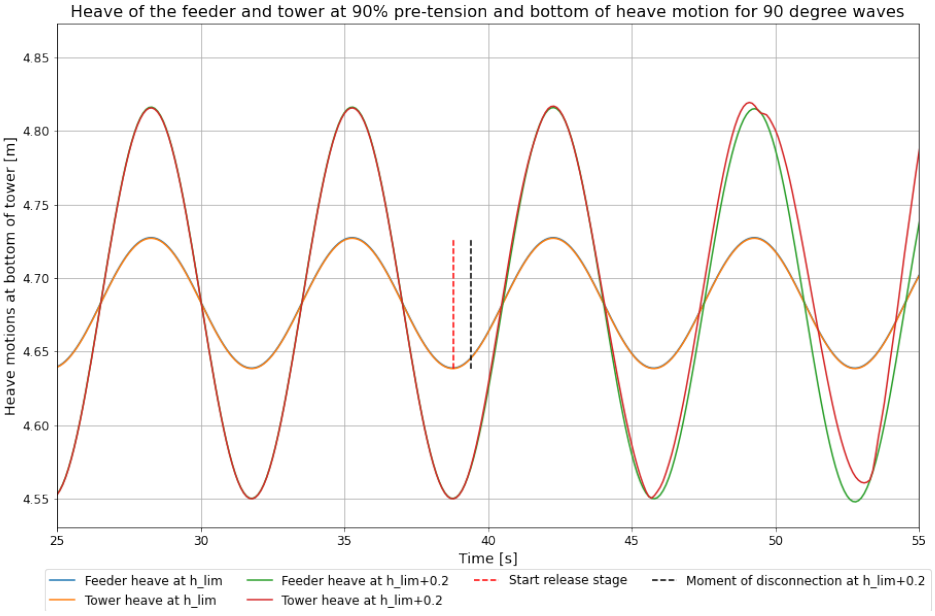
Heave of the feeder and tower at 90% pre-tension and bottom of heave motion for 90 degree waves
Heave motions at bottom of tower [m]
Time [s]
Feeder heave at h_lim
Tower heave at h_lim
Feeder heave at h_lim+0.2
Tower heave at h_lim+0.2
Start release stage
Moment of disconnection at h_lim+0.2

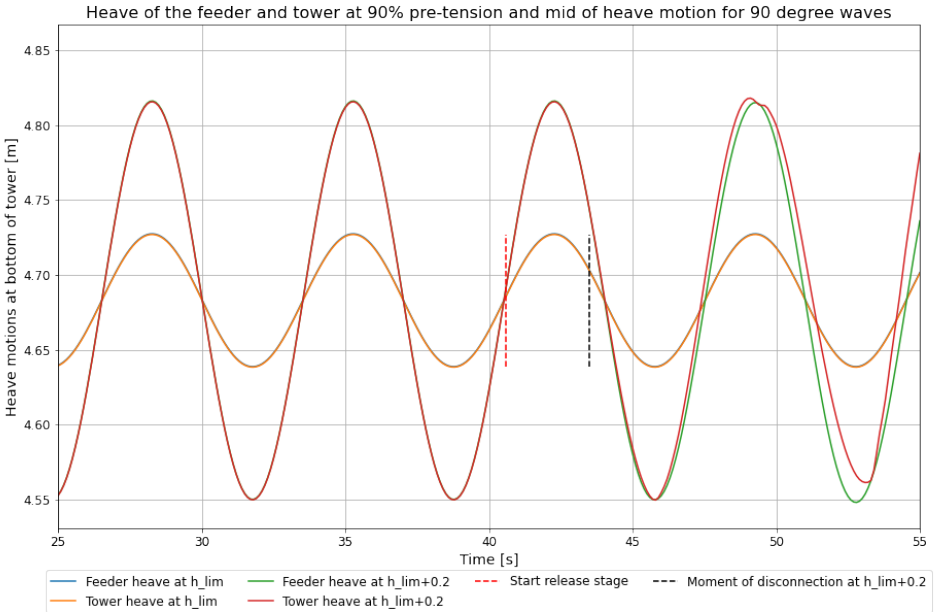
Heave of the feeder and tower at 90% pre-tension and mid of heave motion for 90 degree waves
Heave motions at bottom of tower [m]
Time [s]
Feeder heave at h_lim
Tower heave at h_lim
Feeder heave at h_lim+0.2
Tower heave at h_lim+0.2
Start release stage
Moment of disconnection at h_lim+0.2

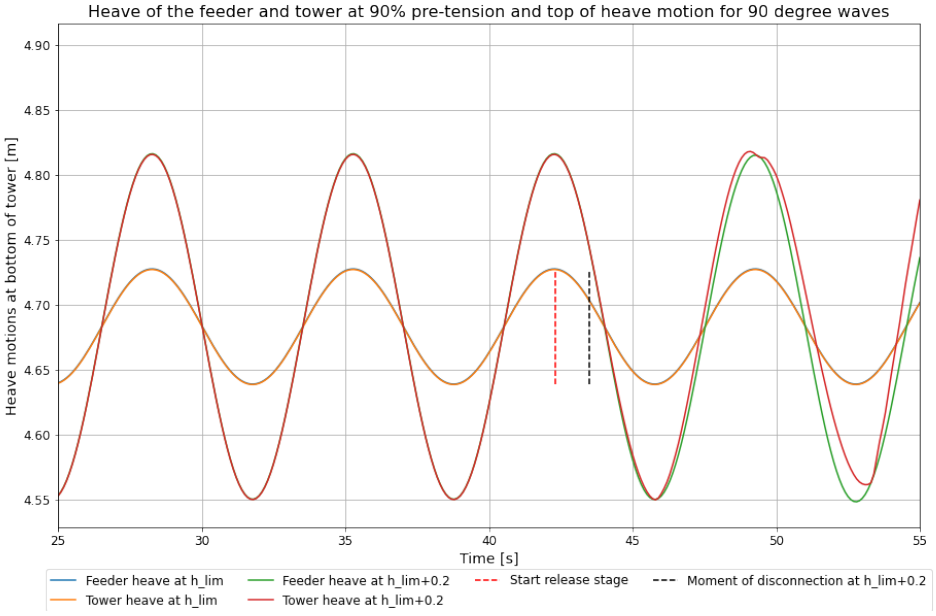
Heave of the feeder and tower at 90% pre-tension and top of heave motion for 90 degree waves
Heave motions at bottom of tower [m]
Time [s]
Feeder heave at h_lim
Tower heave at h_lim
Feeder heave at h_lim+0.2
Tower heave at h_lim+0.2
Start release stage
Moment of disconnection at h_lim+0.2

G.3 X-axis rotations of tower and feeder

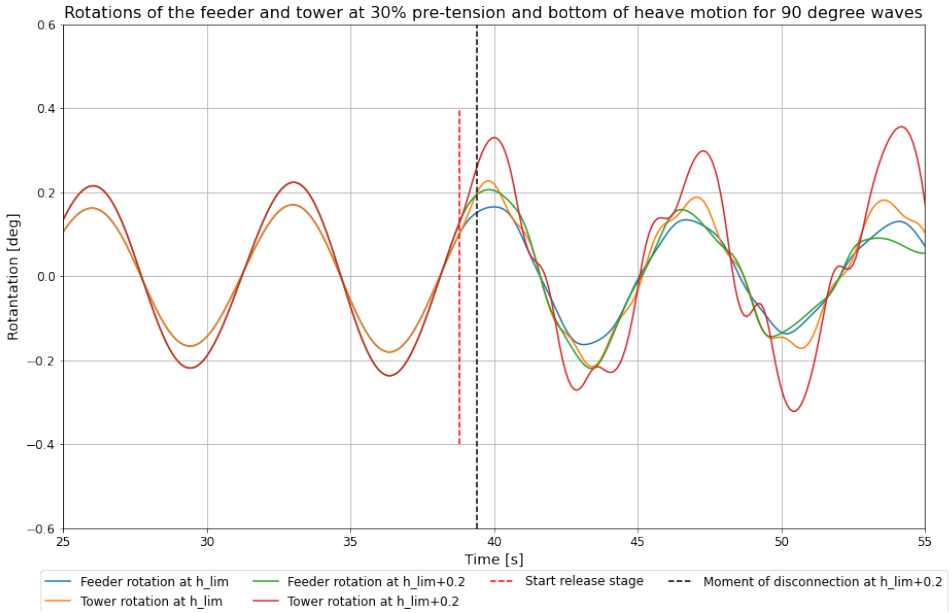

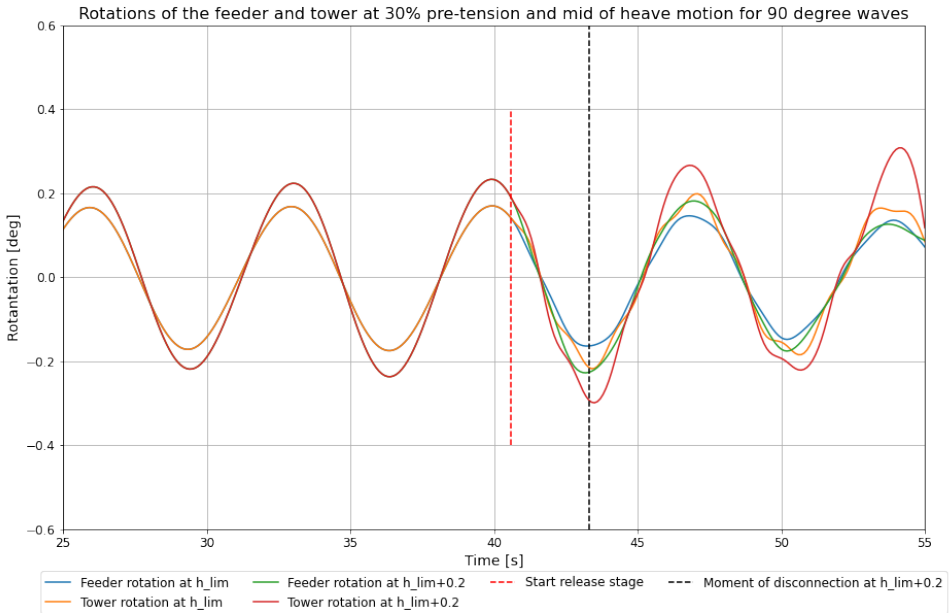

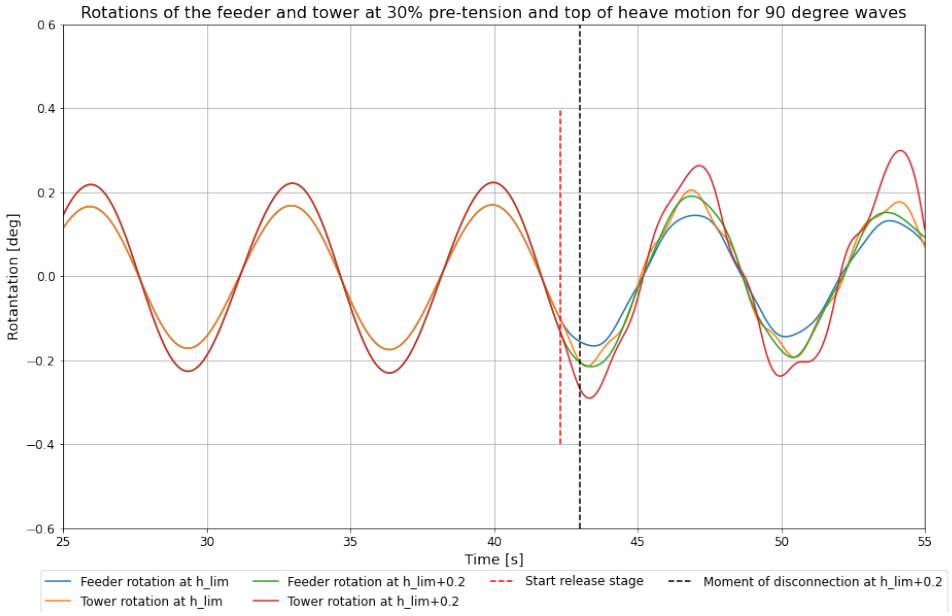
Rotations of the feeder and tower at 30% pre-tension and top of heave motion for 90 degree waves
Rotantation [deg]
Time [s]
Feeder rotation at h_lim
Tower rotation at h_lim
Feeder rotation at h_lim+0.2
Tower rotation at h_lim+0.2
Start release stage
Moment of disconnection at h_lim+0.2

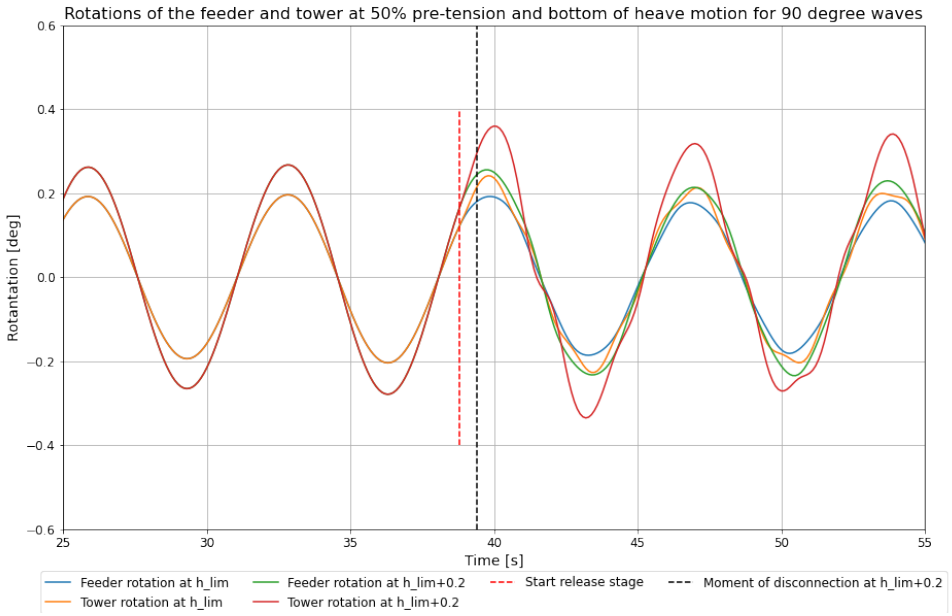
Rotations of the feeder and tower at 50% pre-tension and bottom of heave motion for 90 degree waves
Rotantation [deg]
Time [s]
Feeder rotation at h_lim
Tower rotation at h_lim
Feeder rotation at h_lim+0.2
Tower rotation at h_lim+0.2
Start release stage
Moment of disconnection at h_lim+0.2

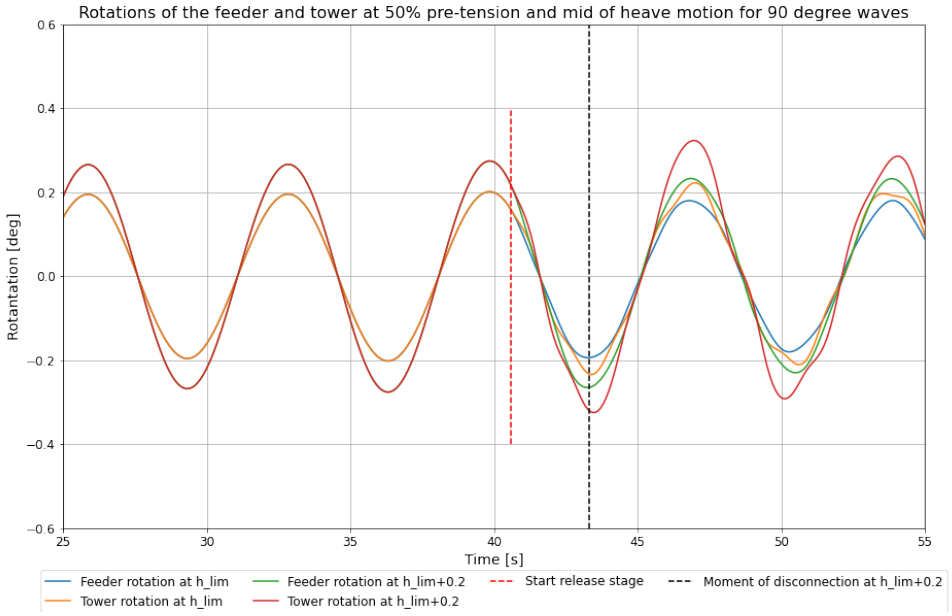
Rotations of the feeder and tower at 50% pre-tension and mid of heave motion for 90 degree waves
Rotantation [deg]
Time [s]
Feeder rotation at h_lim
Tower rotation at h_lim
Feeder rotation at h_lim+0.2
Tower rotation at h_lim+0.2
Start release stage
Moment of disconnection at h_lim+0.2

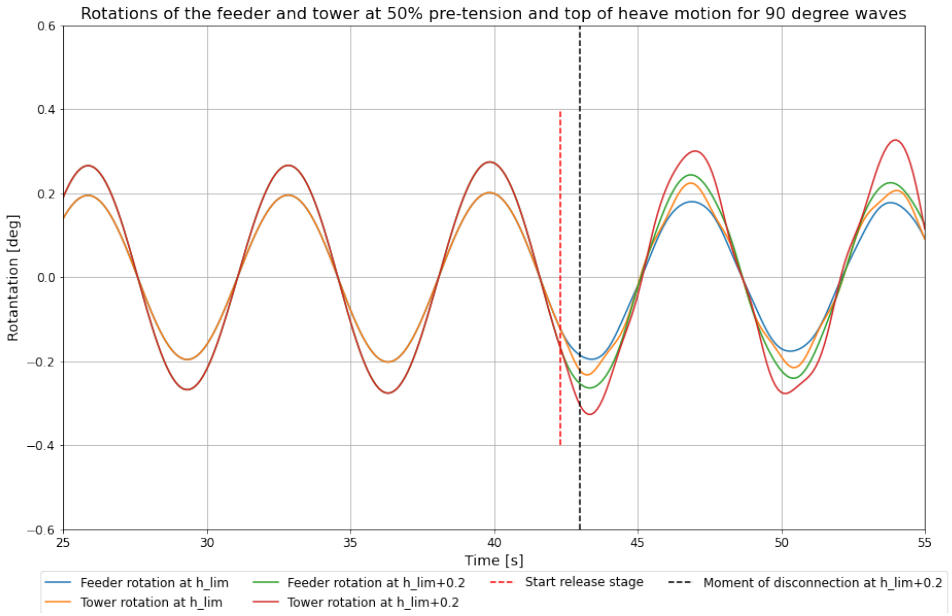
Rotations of the feeder and tower at 50% pre-tension and top of heave motion for 90 degree waves
Rotantation [deg]
Time [s]
Feeder rotation at h_lim
Tower rotation at h_lim
Feeder rotation at h_lim+0.2
Tower rotation at h_lim+0.2
Start release stage
Moment of disconnection at h_lim+0.2

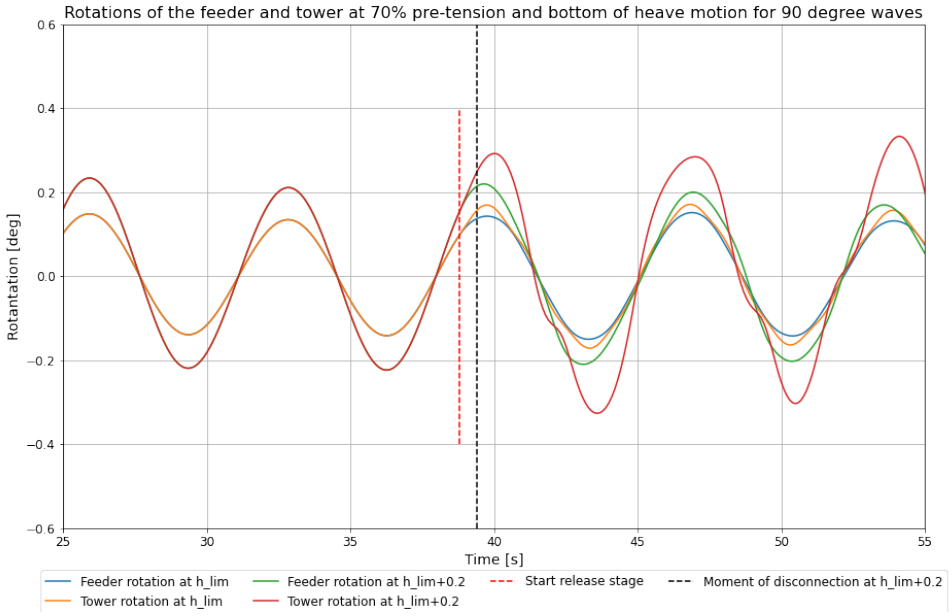
Rotations of the feeder and tower at 70% pre-tension and bottom of heave motion for 90 degree waves
Rotantation [deg]
Time [s]
Feeder rotation at h_lim
Tower rotation at h_lim
Feeder rotation at h_lim+0.2
Tower rotation at h_lim+0.2
Start release stage
Moment of disconnection at h_lim+0.2

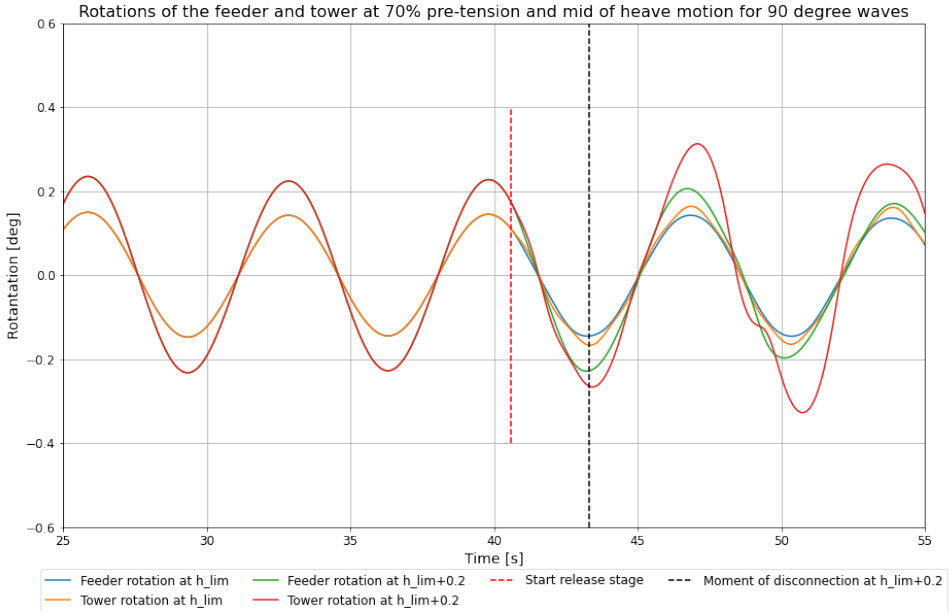
Rotations of the feeder and tower at 70% pre-tension and mid of heave motion for 90 degree waves
Rotantation [deg]
Time [s]
Feeder rotation at h_lim
Tower rotation at h_lim
Feeder rotation at h_lim+0.2
Tower rotation at h_lim+0.2
Start release stage
Moment of disconnection at h_lim+0.2

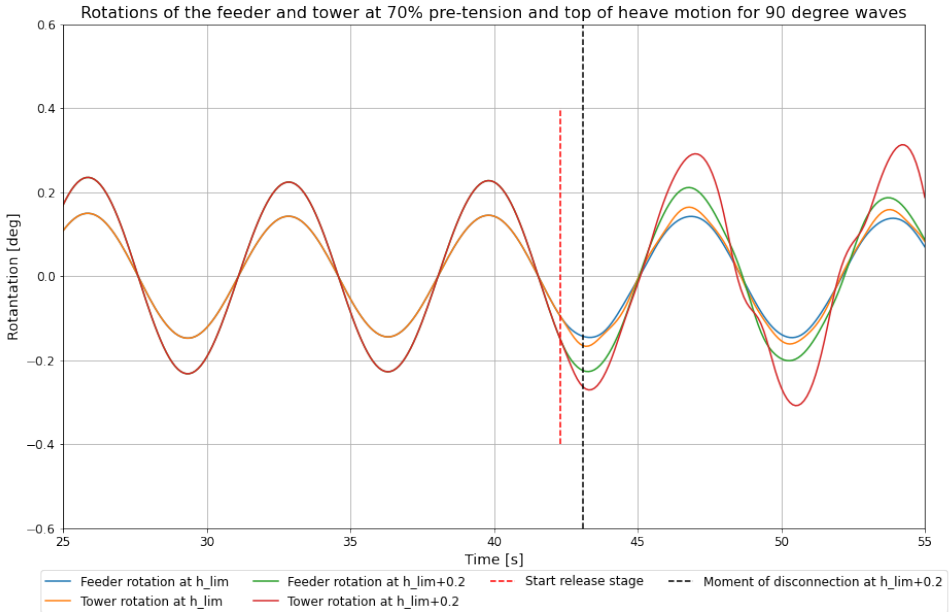
Rotations of the feeder and tower at 70% pre-tension and top of heave motion for 90 degree waves
Rotantation [deg]
Time [s]
Feeder rotation at h_lim
Tower rotation at h_lim
Feeder rotation at h_lim+0.2
Tower rotation at h_lim+0.2
Start release stage
Moment of disconnection at h_lim+0.2

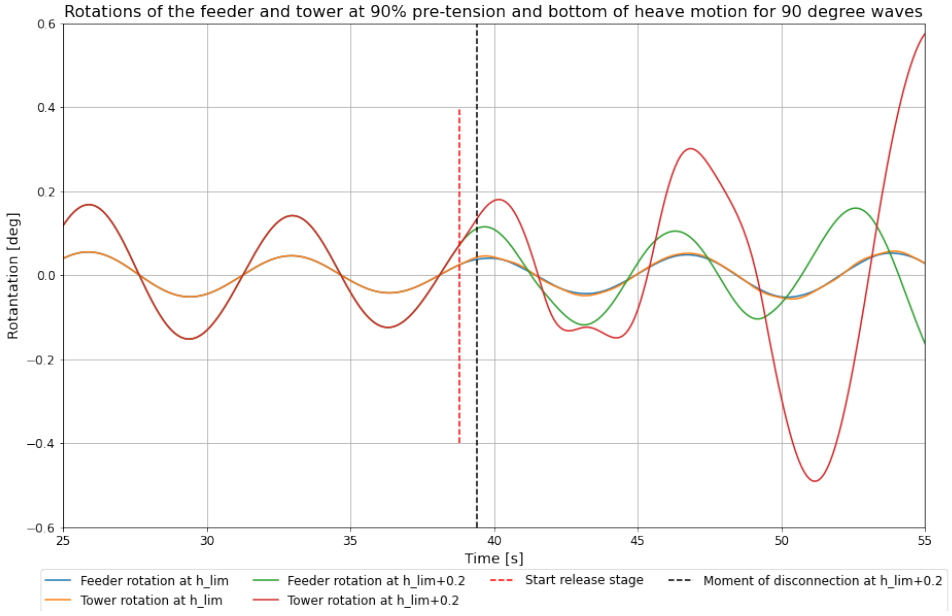
Rotations of the feeder and tower at 90% pre-tension and bottom of heave motion for 90 degree waves
Rotantation [deg]
Time [s]
Feeder rotation at h_lim
Tower rotation at h_lim
Feeder rotation at h_lim+0.2
Tower rotation at h_lim+0.2
Start release stage
Moment of disconnection at h_lim+0.2

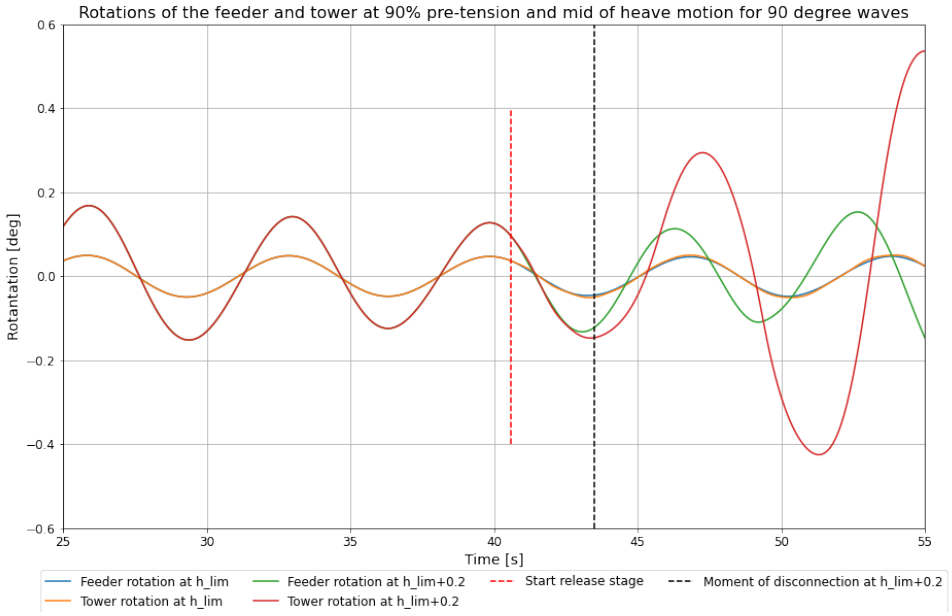
Rotations of the feeder and tower at 90% pre-tension and mid of heave motion for 90 degree waves
Rotantation [deg]
Time [s]
Feeder rotation at h_lim
Tower rotation at h_lim
Feeder rotation at h_lim+0.2
Tower rotation at h_lim+0.2
Start release stage
Moment of disconnection at h_lim+0.2

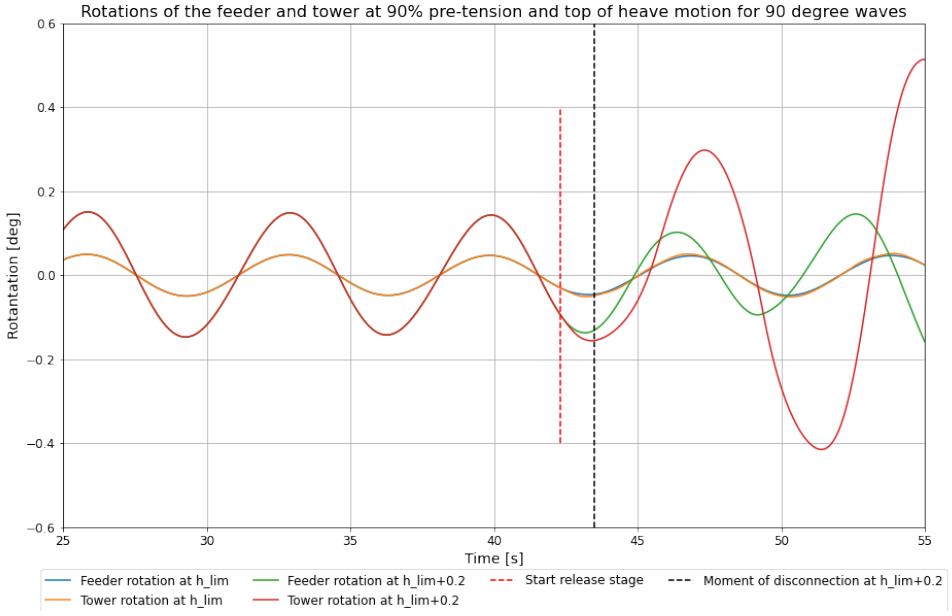
Rotations of the feeder and tower at 90% pre-tension and top of heave motion for 90 degree waves
Rotantation [deg]
Time [s]
Feeder rotation at h_lim
Tower rotation at h_lim
Feeder rotation at h_lim+0.2
Tower rotation at h_lim+0.2
Start release stage
Moment of disconnection at h_lim+0.2

G.4 Clearance between barge and tower

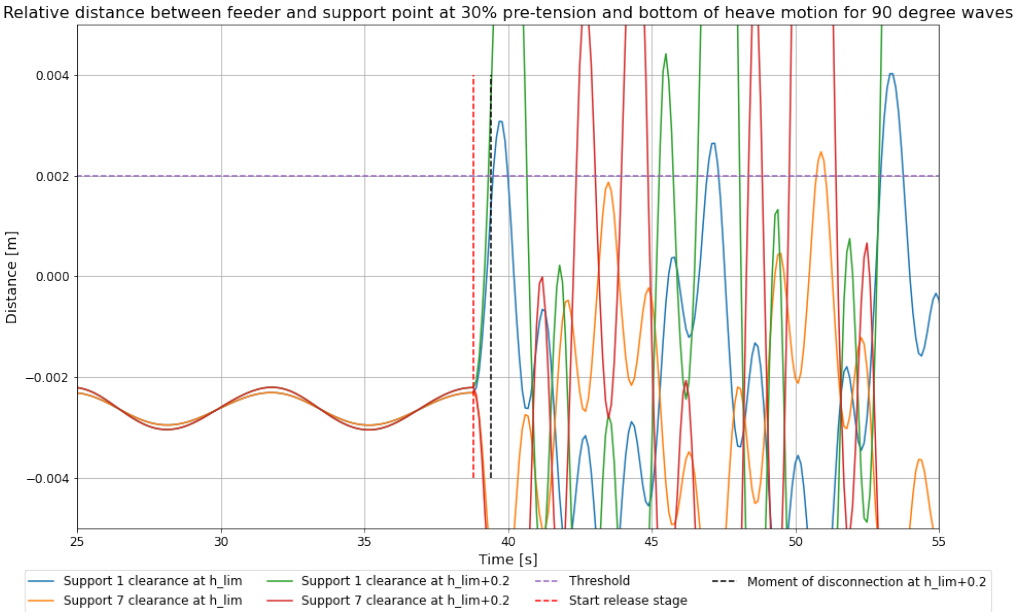

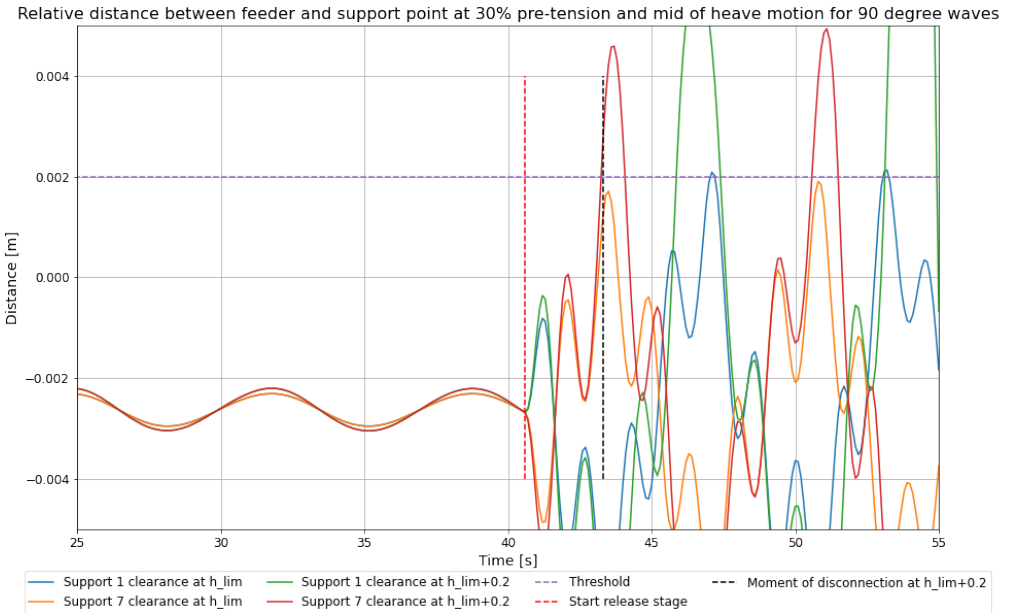

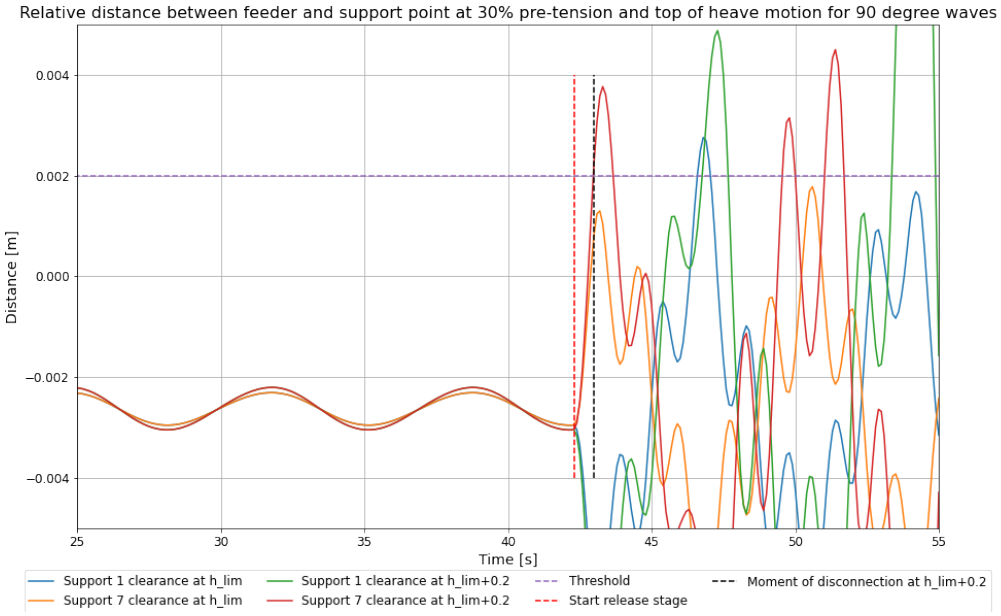
Relative distance between feeder and support point at 30% pre-tension and top of heave motion for 90 degree waves
Distance [m]
0.004
0.002
0.000
−0.002
−0.004
25
30
35
40
45
50
55
Time [s]
Support 1 clearance at h_lim
Support 7 clearance at h_lim
Support 1 clearance at h_lim+0.2
Support 7 clearance at h_lim+0.2
Threshold
Start release stage
Moment of disconnection at h_lim+0.2

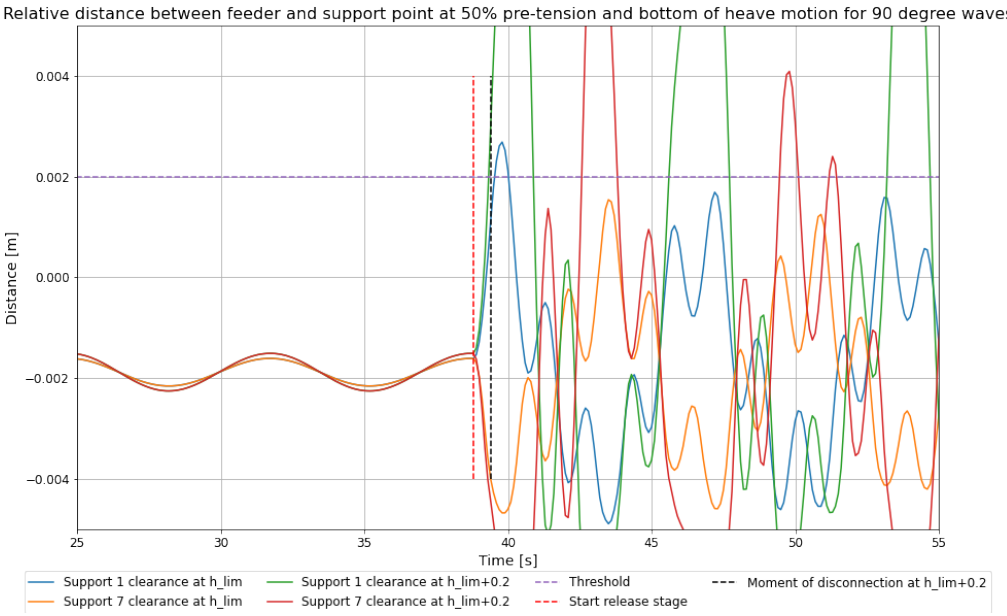
Relative distance between feeder and support point at 50% pre-tension and bottom of heave motion for 90 degree waves
Distance [m]
0.004
0.002
0.000
−0.002
−0.004
25
30
35
40
45
50
55
Time [s]
Support 1 clearance at h_lim
Support 7 clearance at h_lim
Support 1 clearance at h_lim+0.2
Support 7 clearance at h_lim+0.2
Threshold
Start release stage
Moment of disconnection at h_lim+0.2

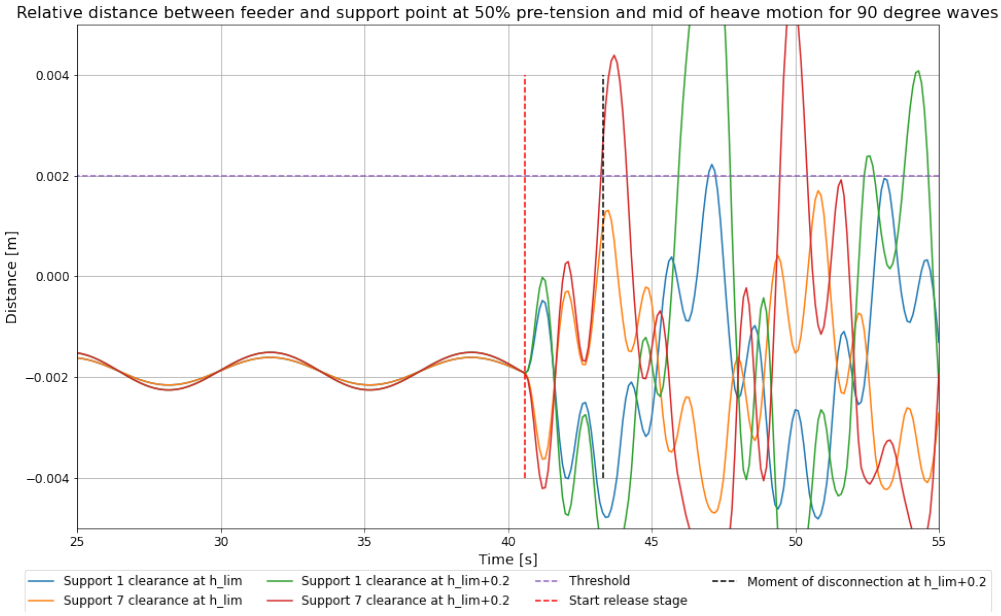
Relative distance between feeder and support point at 50% pre-tension and mid of heave motion for 90 degree waves
Distance [m]
Time [s]
Support 1 clearance at h_lim
Support 7 clearance at h_lim
Support 1 clearance at h_lim+0.2
Support 7 clearance at h_lim+0.2
Threshold
Start release stage
Moment of disconnection at h_lim+0.2

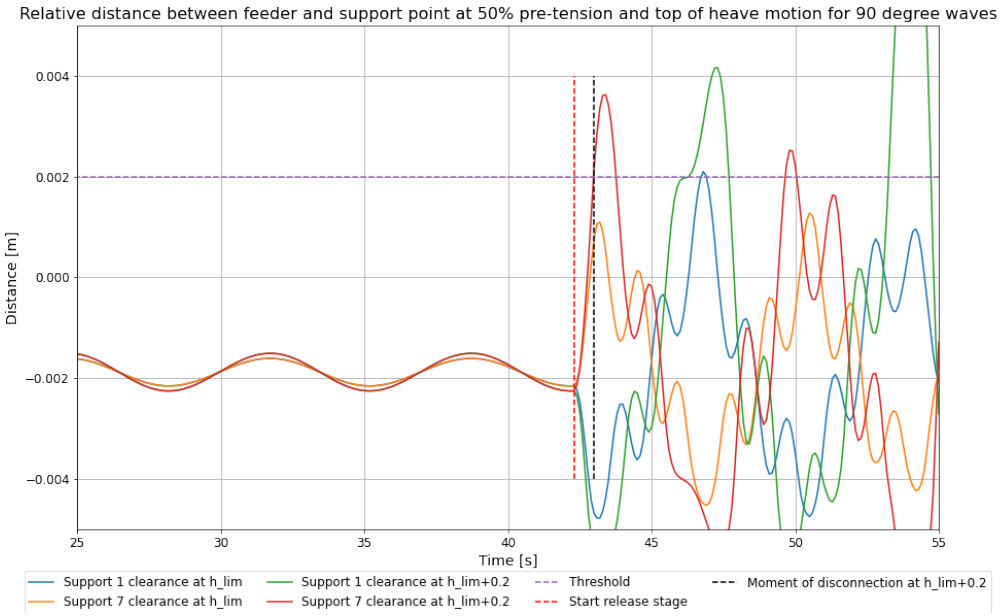
Relative distance between feeder and support point at 50% pre-tension and top of heave motion for 90 degree waves
Distance [m]
Time [s]
Support 1 clearance at h_lim
Support 7 clearance at h_lim
Support 1 clearance at h_lim+0.2
Support 7 clearance at h_lim+0.2
Threshold
Start release stage
Moment of disconnection at h_lim+0.2

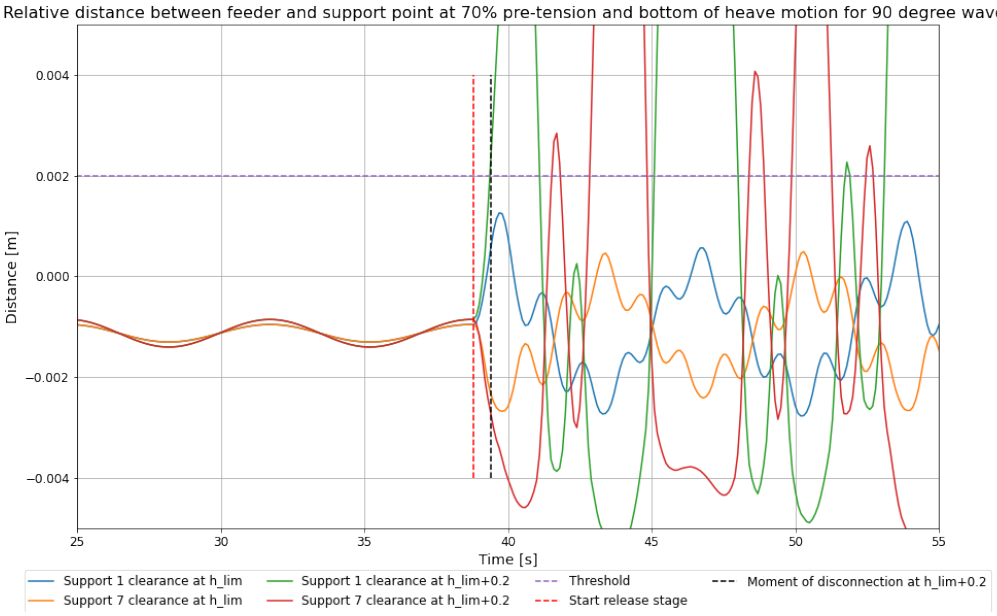
Relative distance between feeder and support point at 70% pre-tension and bottom of heave motion for 90 degree waves
Distance [m]
Time [s]
Support 1 clearance at h_lim
Support 7 clearance at h_lim
Support 1 clearance at h_lim+0.2
Support 7 clearance at h_lim+0.2
Threshold
Start release stage
Moment of disconnection at h_lim+0.2

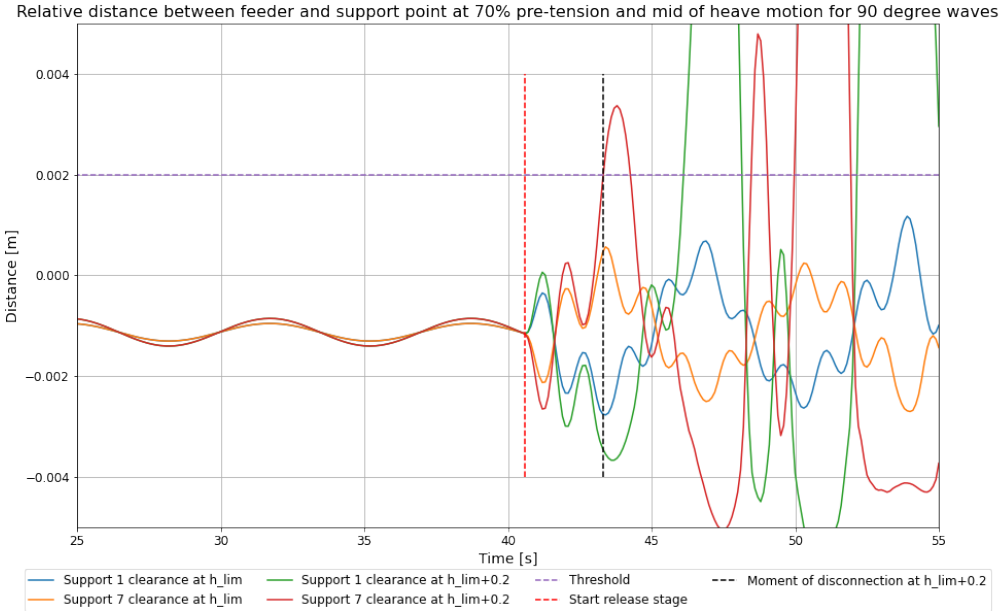
Relative distance between feeder and support point at 70% pre-tension and mid of heave motion for 90 degree waves
Distance [m]
Time [s]
Support 1 clearance at h_lim
Support 7 clearance at h_lim
Support 1 clearance at h_lim+0.2
Support 7 clearance at h_lim+0.2
Threshold
Start release stage
Moment of disconnection at h_lim+0.2

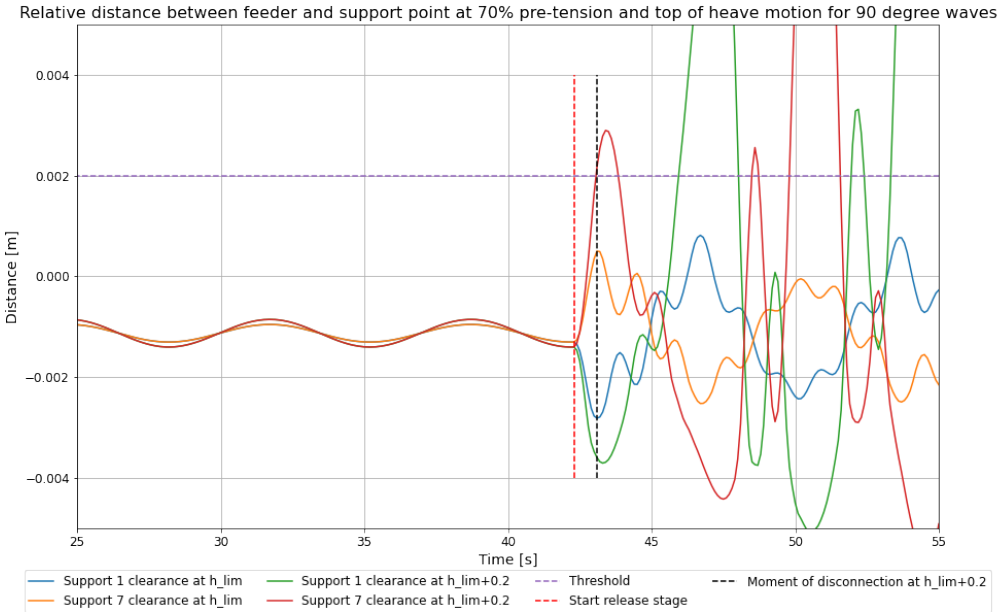
Relative distance between feeder and support point at 70% pre-tension and top of heave motion for 90 degree waves
Distance [m]
Time [s]
Support 1 clearance at h_lim
Support 7 clearance at h_lim
Support 1 clearance at h_lim+0.2
Support 7 clearance at h_lim+0.2
Threshold
Start release stage
Moment of disconnection at h_lim+0.2

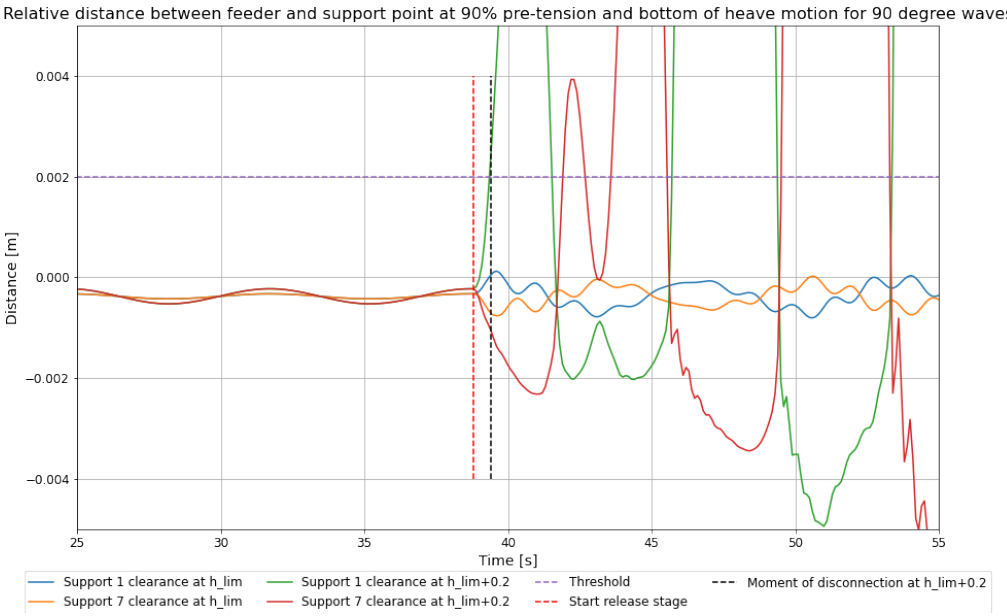
Relative distance between feeder and support point at 90% pre-tension and bottom of heave motion for 90 degree waves
Distance [m]
Time [s]
Support 1 clearance at h_lim
Support 7 clearance at h_lim
Support 1 clearance at h_lim+0.2
Support 7 clearance at h_lim+0.2
Threshold
Start release stage
Moment of disconnection at h_lim+0.2

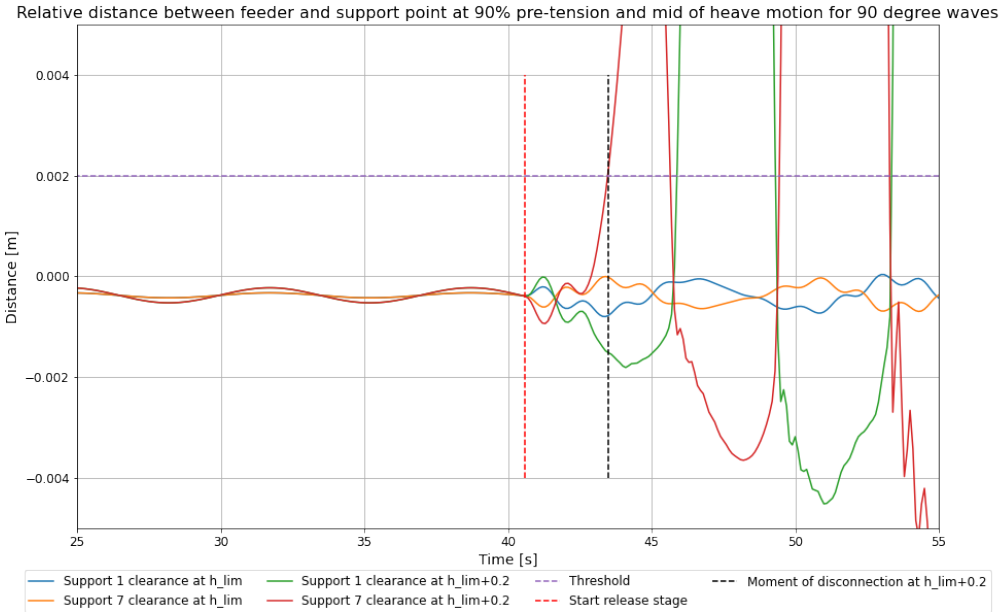
Relative distance between feeder and support point at 90% pre-tension and mid of heave motion for 90 degree waves
Distance [m]
Time [s]
Support 1 clearance at h_lim
Support 7 clearance at h_lim
Support 1 clearance at h_lim+0.2
Support 7 clearance at h_lim+0.2
Threshold
Start release stage
Moment of disconnection at h_lim+0.2

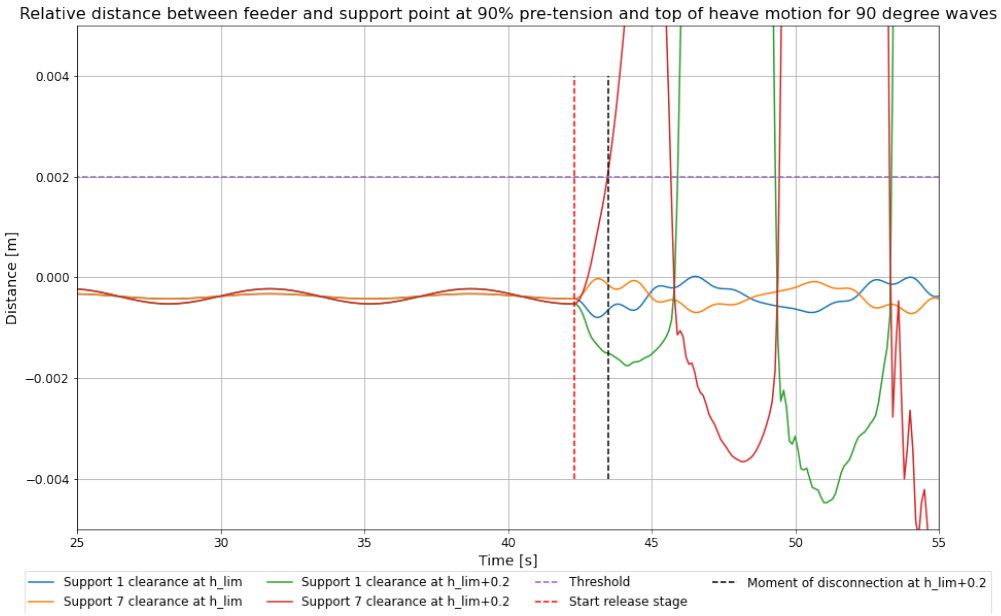
Relative distance between feeder and support point at 90% pre-tension and top of heave motion for 90 degree waves
Distance [m]
Time [s]
Support 1 clearance at h_lim
Support 7 clearance at h_lim
Support 1 clearance at h_lim+0.2
Support 7 clearance at h_lim+0.2
Threshold
Start release stage
Moment of disconnection at h_lim+0.2

G.5 Loads on support points

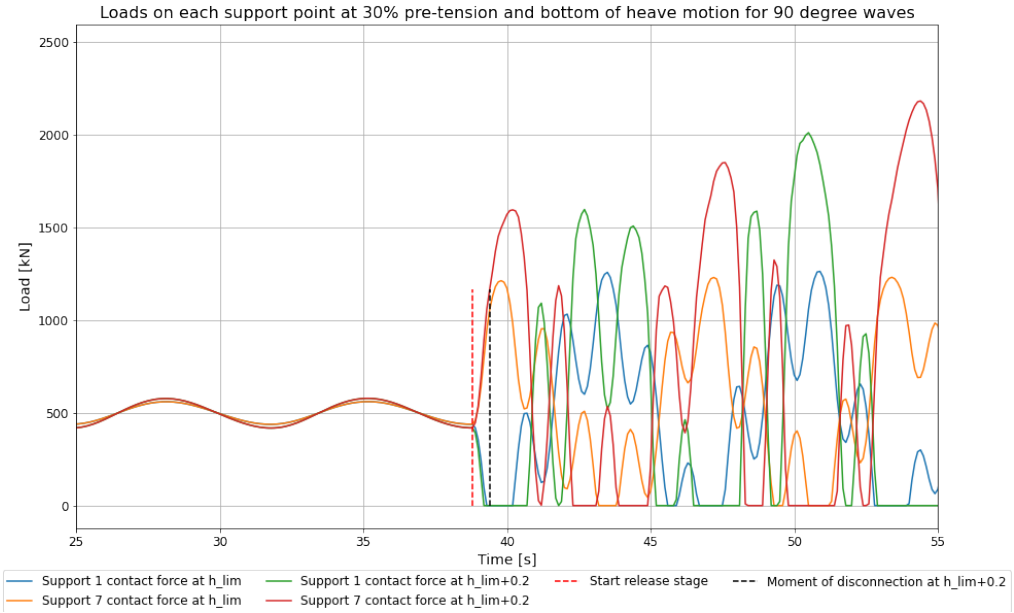

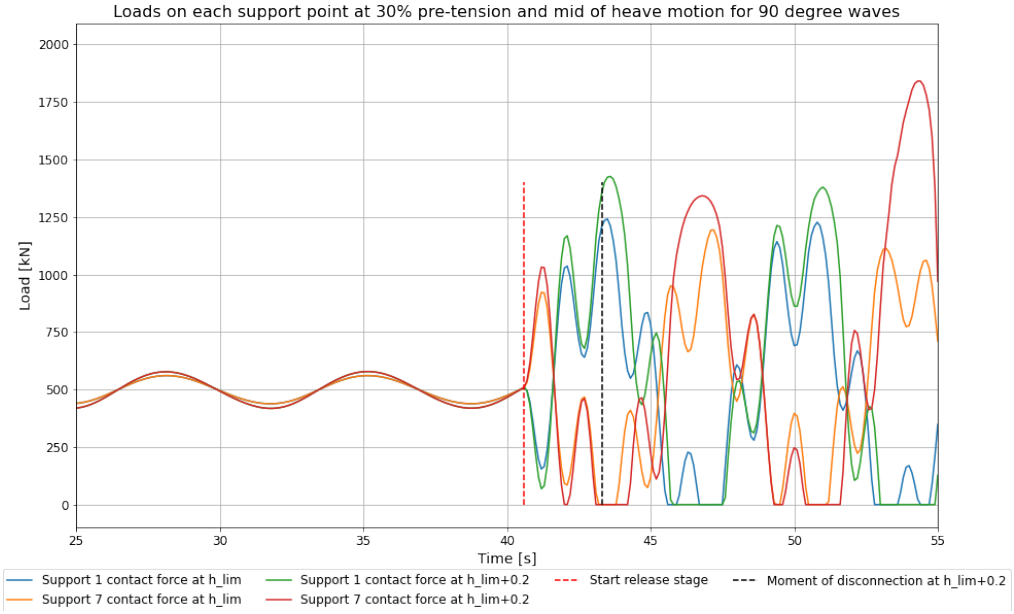

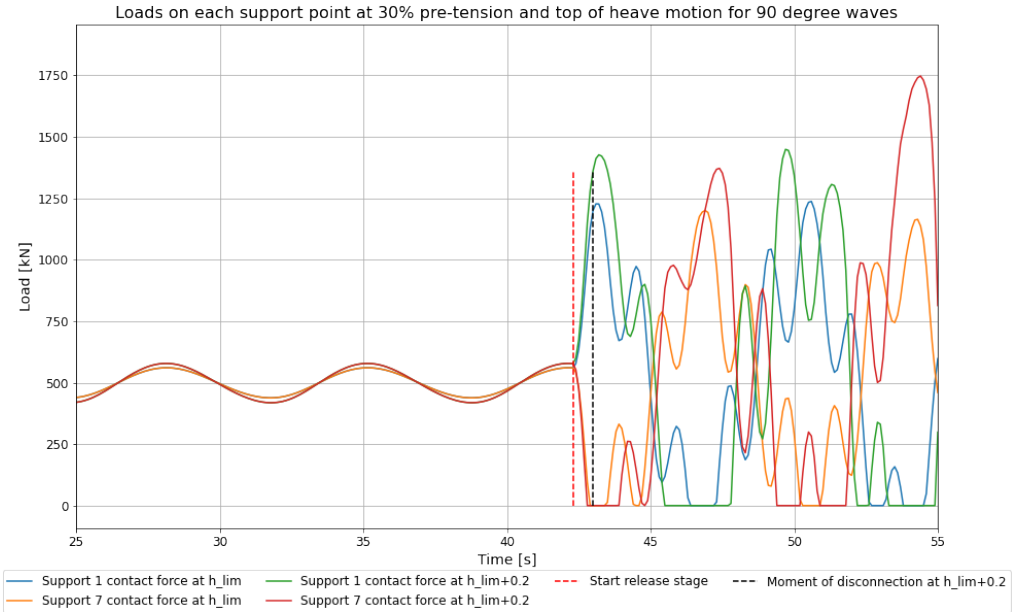
Loads on each support point at 30% pre-tension and top of heave motion for 90 degree waves
Load [kN]
Time [s]
Support 1 contact force at h_lim
Support 7 contact force at h_lim
Support 1 contact force at h_lim+0.2
Support 7 contact force at h_lim+0.2
Start release stage
Moment of disconnection at h_lim+0.2

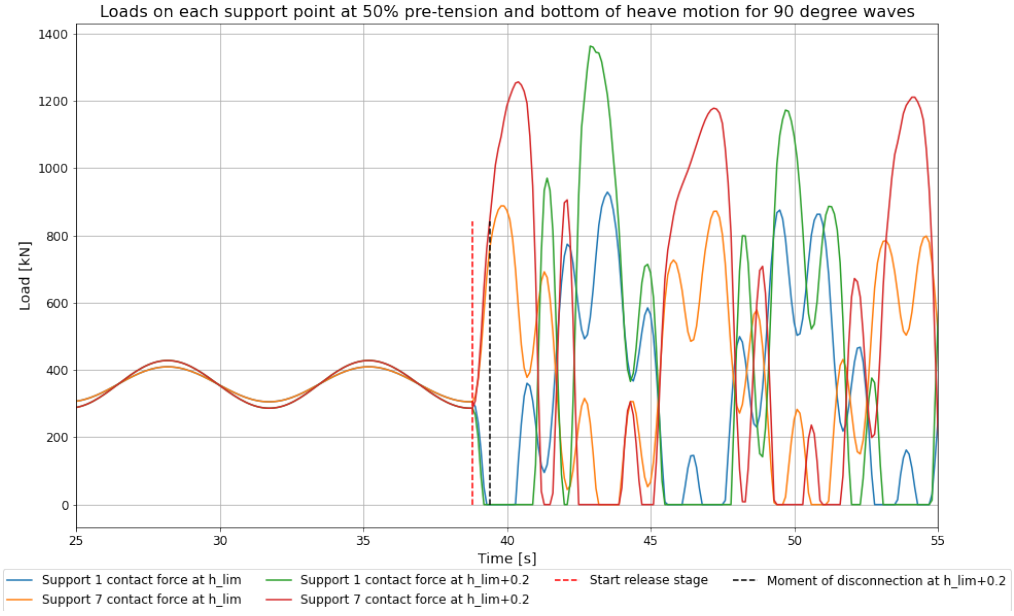
Loads on each support point at 50% pre-tension and bottom of heave motion for 90 degree waves
Load [kN]
Time [s]
Support 1 contact force at h_lim
Support 7 contact force at h_lim
Support 1 contact force at h_lim+0.2
Support 7 contact force at h_lim+0.2
Start release stage
Moment of disconnection at h_lim+0.2

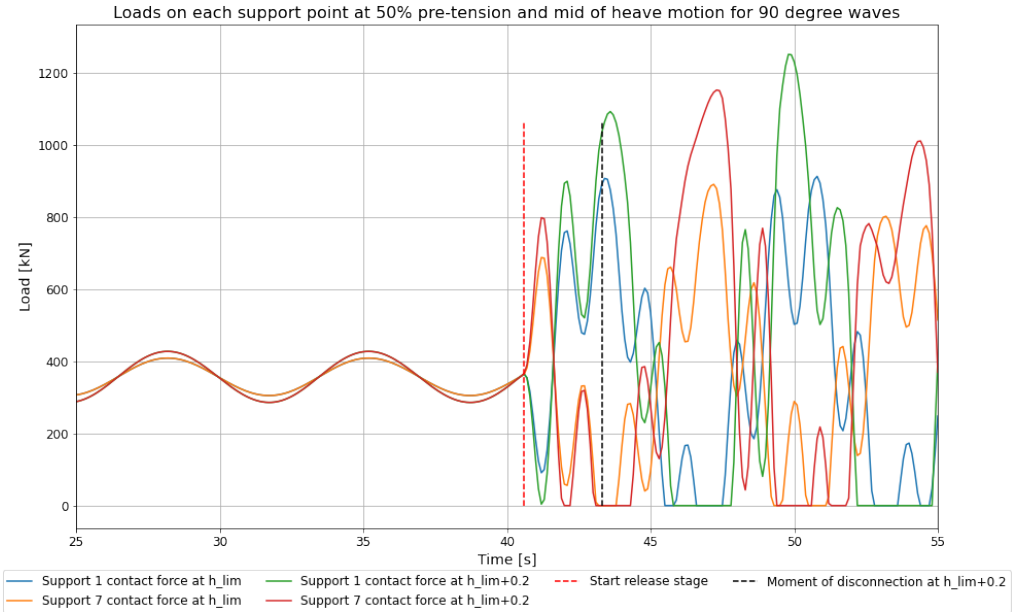
Loads on each support point at 50% pre-tension and mid of heave motion for 90 degree waves
Load [kN]
Time [s]
Support 1 contact force at h_lim
Support 7 contact force at h_lim
Support 1 contact force at h_lim+0.2
Support 7 contact force at h_lim+0.2
Start release stage
Moment of disconnection at h_lim+0.2

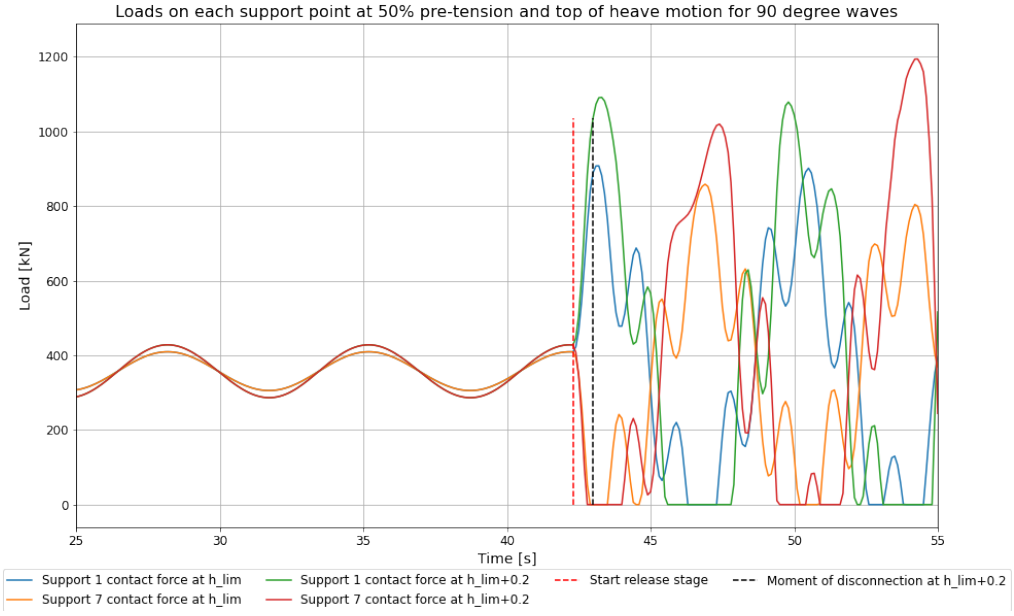
Loads on each support point at 50% pre-tension and top of heave motion for 90 degree waves
Load [kN]
Time [s]
Support 1 contact force at h_lim
Support 7 contact force at h_lim
Support 1 contact force at h_lim+0.2
Support 7 contact force at h_lim+0.2
Start release stage
Moment of disconnection at h_lim+0.2

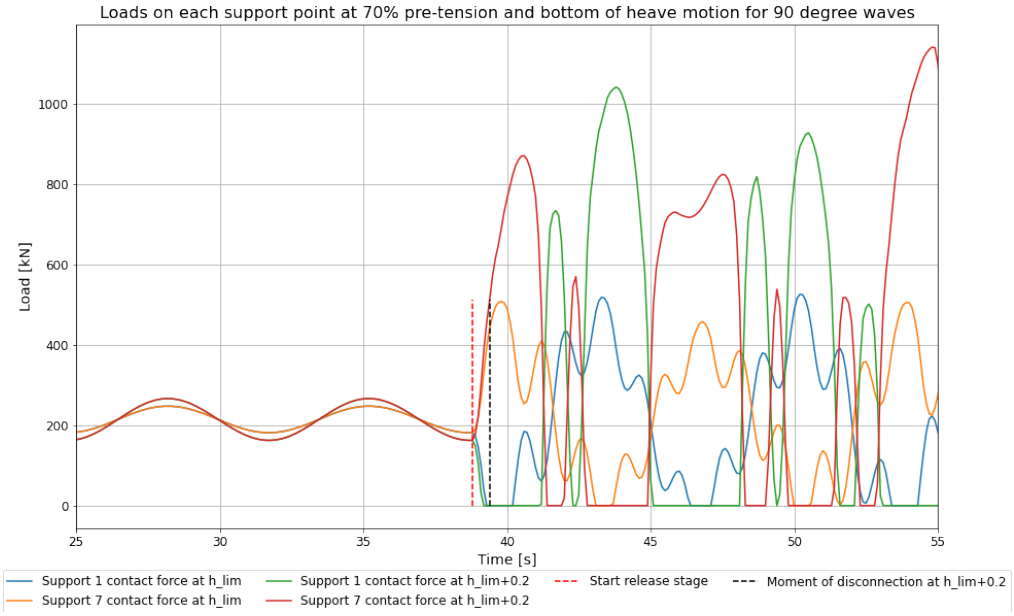
Loads on each support point at 70% pre-tension and bottom of heave motion for 90 degree waves
Load [kN]
Time [s]
Support 1 contact force at h_lim
Support 7 contact force at h_lim
Support 1 contact force at h_lim+0.2
Support 7 contact force at h_lim+0.2
Start release stage
Moment of disconnection at h_lim+0.2

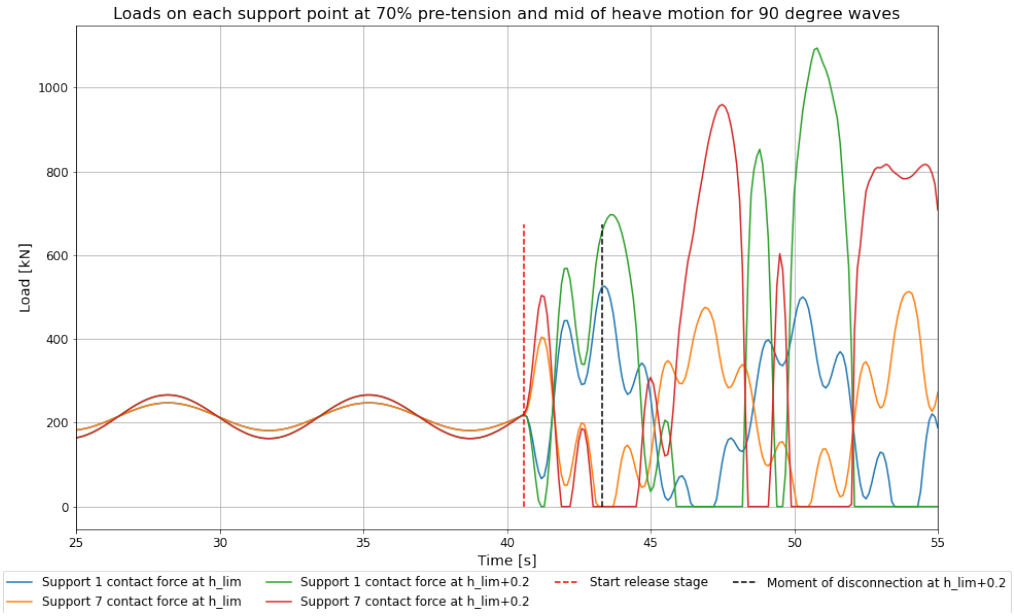
Loads on each support point at 70% pre-tension and mid of heave motion for 90 degree waves
Load [kN]
Time [s]
Support 1 contact force at h_lim
Support 7 contact force at h_lim
Support 1 contact force at h_lim+0.2
Support 7 contact force at h_lim+0.2
Start release stage
Moment of disconnection at h_lim+0.2

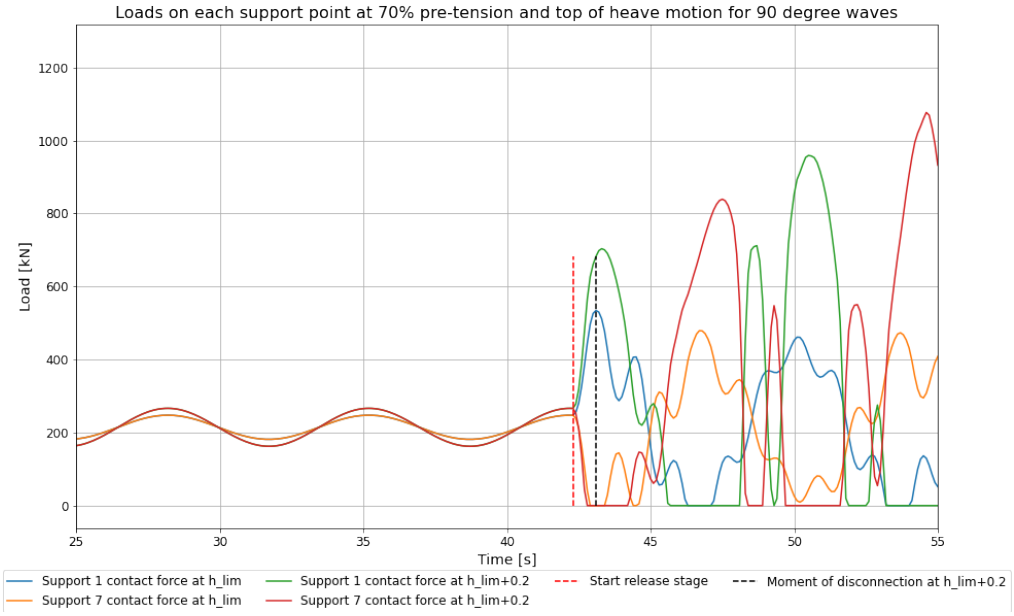
Loads on each support point at 70% pre-tension and top of heave motion for 90 degree waves
Load [kN]
Time [s]
Support 1 contact force at h_lim
Support 7 contact force at h_lim
Support 1 contact force at h_lim+0.2
Support 7 contact force at h_lim+0.2
Start release stage
Moment of disconnection at h_lim+0.2

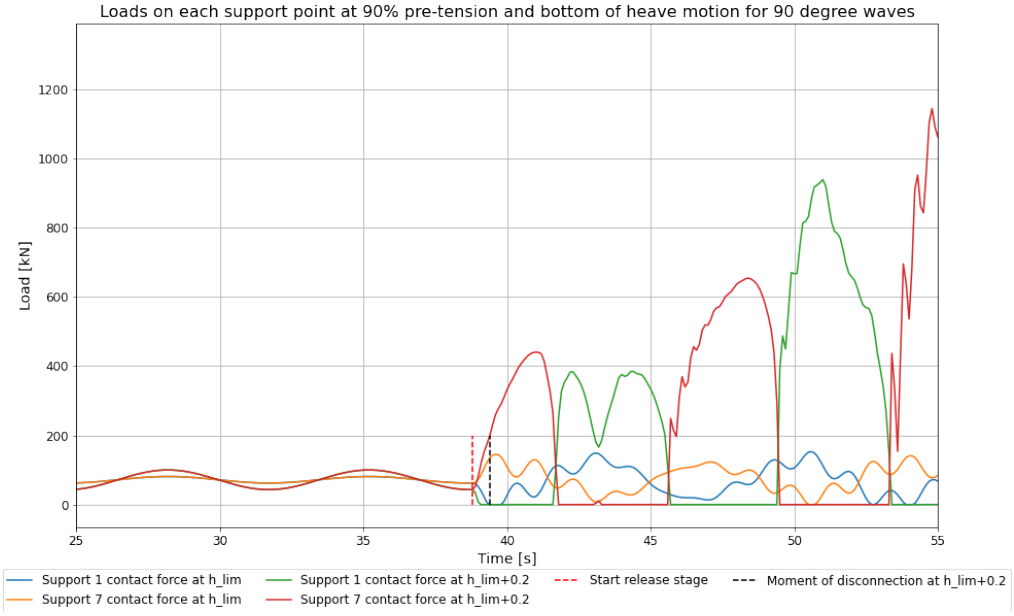
Loads on each support point at 90% pre-tension and bottom of heave motion for 90 degree waves
Load [kN]
Time [s]
Support 1 contact force at h_lim
Support 7 contact force at h_lim
Support 1 contact force at h_lim+0.2
Support 7 contact force at h_lim+0.2
Start release stage
Moment of disconnection at h_lim+0.2

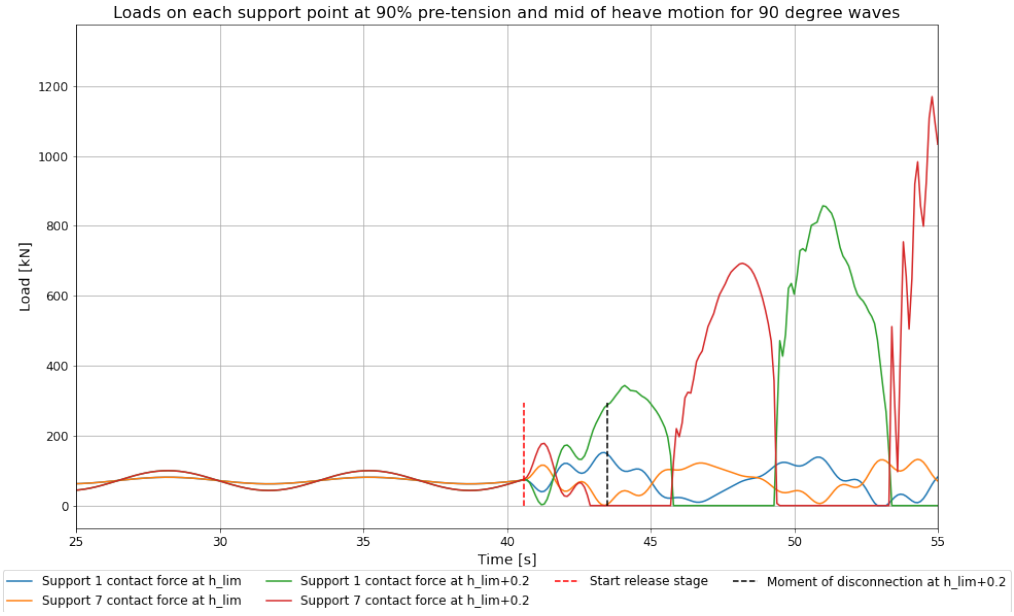
Loads on each support point at 90% pre-tension and mid of heave motion for 90 degree waves
Load [kN]
Time [s]
Support 1 contact force at h_lim
Support 7 contact force at h_lim
Support 1 contact force at h_lim+0.2
Support 7 contact force at h_lim+0.2
Start release stage
Moment of disconnection at h_lim+0.2

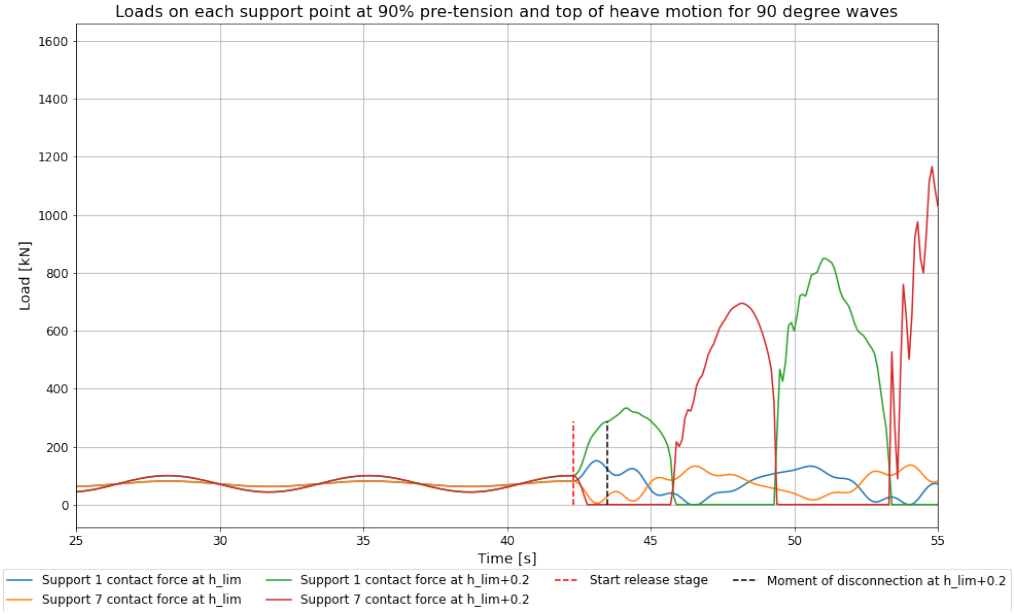
Loads on each support point at 90% pre-tension and top of heave motion for 90 degree waves
Load [kN]
Time [s]
Support 1 contact force at h_lim
Support 7 contact force at h_lim
Support 1 contact force at h_lim+0.2
Support 7 contact force at h_lim+0.2
Start release stage
Moment of disconnection at h_lim+0.2